Space–charge limited current in nanodiodes: Ballistic, collisional, and dynamical effects F

(iD) **Peng Zhang,** (iD) **Yee Sin Ang,** (iD) **Allen L. Garner, et al.**

COLLECTIONS

F   This paper was selected as Featured

View Online   Export Citation   CrossMark

ARTICLES YOU MAY BE INTERESTED IN

100 years of the physics of diodes
Applied Physics Reviews **4**, 011304 (2017); https://doi.org/10.1063/1.4978231

Next generation ferroelectric materials for semiconductor process integration and their applications
Journal of Applied Physics **129**, 100901 (2021); https://doi.org/10.1063/5.0037617

Transitions between electron emission and gas breakdown mechanisms across length and pressure scales
Journal of Applied Physics **128**, 210903 (2020); https://doi.org/10.1063/5.0030220

129, 100902

Space–charge limited current in nanodiodes: Ballistic, collisional, and dynamical effects Ⓕ

Peng Zhang,[1,a] ⓘD Yee Sin Ang,[2,a] ⓘD Allen L. Garner,[3,4,5,a] ⓘD Ágúst Valfells,[6,a] ⓘD J. W. Luginsland,[7,a] ⓘD
and L. K. Ang[2,a] ⓘD

AFFILIATIONS

[1]Department of Electrical and Computer Engineering, Michigan State University, East Lansing, Michigan 48824-1226, USA
[2]Science, Mathematics and Technology, Singapore University of Technology and Design, Singapore 487372, Singapore
[3]School of Nuclear Engineering, Purdue University, West Lafayette, Indiana 47906, USA
[4]School of Electrical and Computer Engineering, Purdue University, West Lafayette, Indiana 47907, USA
[5]Department of Agricultural and Biological Engineering, Purdue University, West Lafayette, Indiana 47907, USA
[6]Department of Engineering, Reykjavík University, Menntavegi 1, 101 Reykjavík, Iceland
[7]Confluent Sciences, LLC, 3124 Camino Real Court NE, Albuquerque, New Mexico 87111, USA

[a]**Authors to whom correspondence should be addressed:** pz@egr.msu.edu; yeesin_ang@sutd.edu.sg; algarner@purdue.edu;
av@ru.is; john.luginsland@confluentsciences.com; and ricky_ang@sutd.edu.sg

ABSTRACT

This Perspective reviews the fundamental physics of space–charge interactions that are important in various media: vacuum gap, air gap, liquids, and solids including quantum materials. It outlines the critical and recent developments since a previous review paper on diode physics [Zhang *et al.* Appl. Phys. Rev. **4**, 011304 (2017)] with particular emphasis on various theoretical aspects of the space–charge limited current (SCLC) model: physics at the nano-scale, time-dependent, and transient behaviors; higher-dimensional models; and transitions between electron emission mechanisms and material properties. While many studies focus on steady-state SCLC, the increasing importance of fast-rise time electric pulses, high frequency microwave and terahertz sources, and ultrafast lasers has motivated theoretical investigations in time-dependent SCLC. We particularly focus on recent studies in discrete particle effects, temporal phenomena, time-dependent photoemission to SCLC, and AC beam loading. Due to the reduction in the physical size and complicated geometries, we report recent studies in multi-dimensional SCLC, including finite particle effects, protrusive SCLC, novel techniques for exotic geometries, and fractional models. Due to the importance of using SCLC models in determining the mobility of organic materials, this paper shows the transition of the SCLC model between classical bulk solids and recent two-dimensional (2D) Dirac materials. Next, we describe some selected applications of SCLC in nanodiodes, including nanoscale vacuum-channel transistors, micro-plasma transistors, thermionic energy converters, and multipactor. Finally, we conclude by highlighting future directions in theoretical modeling and applications of SCLC.

I. INTRODUCTION

In physics and engineering, space–charge effects generally refer to the phenomenon when the dynamics of the charge particle flow (like an electron beam) is strongly influenced by electromagnetic interactions between the flow and its surrounding structures. For example, the space–charge limited current (SCLC) is defined as the maximum steady-state current density that can be transported in a one-dimensional (1D) gap of spacing D, under a DC bias of V. The classical SCLC model for a vacuum gap, known as the 1D Child–Langmuir (CL) law,[1,2] is given by

$$J_{CL} = \frac{4\sqrt{2}}{9} \varepsilon_o \sqrt{\frac{e}{m}} \frac{V^{3/2}}{D^2},$$ (1)

where e is the electron charge, m is the free-electron mass, and ε_0 is the free-space permittivity. For a trap-free solid (or dielectric) of mobility μ and dielectric constant ε, the corresponding SCLC model is known as the 1D Mott–Gurney (MG) law[3,4] given by

$$J_{MG} = \frac{9}{8}\mu\varepsilon\frac{V^2}{D^3}. \tag{2}$$

The underlying scaling of the CL law and MG law shown in Eqs. (1) and (2) can be understood by using a capacitance model under the transit time approximation. The concept is simple. The maximal charge that can be held by a gap or a diode (e.g., a planar capacitor) is proportional to $C \times V$, where C is the capacitance of the gap. The amount of current that can be transported across the gap is $I = Q/T = CV/T$, where T is the electron transit time. To first order approximation, considering T as the transit time (without the space–charge field), yields the scaling laws in Eqs. (1) and (2), where the numerical values can be obtained by using the electric field condition at the cathode surface. Such an approach has been used to derive the CL law for planar[5] and cylindrical[6] gaps and to obtain the MG law.[7]

In 1996, Luginsland et al.[8] extended Eq. (1) to two dimensions (2D) for a uniform SCLC emission over a finite strip of width W by fitting particle-in-cell (PIC) simulations to obtain (for $W/D > 0.1$),

$$\frac{J_{CL}(2D)}{J_{CL}} = 1 + \frac{0.3145D}{W} - 0.0004\left(\frac{D}{W}\right)^2. \tag{3}$$

This 2D classical CL law was later analytically derived and proved by Lau[9] to be

$$\frac{J_{CL}(2D)}{J_{CL}} \cong 1 + \frac{D}{\pi W} \ . \tag{4}$$

An earlier review of the multi-dimensional CL law can be found elsewhere.[10] Similarly, other forms of the 2D and 3D classical CL laws for different emitting areas and operating regimes were also formulated.[11] Further extensions included edge SCLC emission for a 2D non-uniform CL law[12] and sharp tip SCLC emission for a protrusive CL law.[13,14] Recent works on such higher-dimensional CL laws for inhomogeneous thermionic cathodes and others will be discussed later (Sec. IV). Experimental verification of these multi-dimensional features and potential experimental solutions to control these effects was found shortly after these theoretical efforts (see, e.g., Refs. 15 and 16).

It is important to note that the 1D CL law is only valid for a classical large gap where the quantum effects are ignored. In 1991, Lau et al. derived the 1D quantum CL law[17] to include the tunneling of the SCLC through the space–charge potential barrier near the cathode, which will yield a higher value of SCLC as compared to the 1D classical CL law. Using this concept, quantum scaling was calculated explicitly[18] by including the exchange–correlation effects and also by simple dimensional analysis,[19]

$$J_{QCL} \propto V^{1/2}/D^4. \tag{5}$$

The change in voltage scaling from the classical 1D CL law to the quantum CL law ($V^{3/2} \rightarrow V^{1/2}$) was also reported experimentally.[20,21]

By using the transit time model, the quantum CL law was extended to the ultrafast short pulse limit.[22] The transition of the field emission in a gap to the quantum CL law was also calculated.[23,24] An earlier review of the quantum CL law can be found elsewhere.[25] A general scaling law for quantum tunneling current in a nanodiode spanning the direct tunneling regime to field emission to the space–charge limited (SCL) regime has been constructed,[26,27] which was recently extended to dissimilar metal–insulator–metal (MIM) junctions.[28] Recent works on SCLC models in nano-diodes will be discussed in Sec. II.

Most studies of the CL law have focused on the steady-state condition, while transient or time-dependent behavior remains relatively less explored. SCLC obtained from the electrostatic approximation is valid only in the deeply nonrelativistic regime such that its transient behavior for injected current (at energy as low as 30 keV) may produce an inductive voltage that can significantly lower the limiting current from that predicted by the CL law.[29] The roles played by the convection current and by the displacement current, as well as the modification in the transit time due to the intense space charge within the gap, have been simulated by particle in cell (PIC) codes.[30] The steady-state 1D CL law was extended to include the short pulse effects,[31] where the critical SCLC (at short pulse limit) is enhanced by

$$J_{crit}/J_{CL} = 2\left[1 - \sqrt{1 - 3X_{CL}^2/4}\right]\Big/X_{CL}^3, \tag{6}$$

where $X_{CL} = \tau_{\mathrm{p}}/T_{CL} < 1$ is the ratio of the normalized pulse duration to the transit time for the CL law. The breakup of a single short pulse injected with a current density beyond the Child–Langmuir limit, and its dynamics (in THz frequency), was studied by using molecular dynamics (MD) simulation.[32,33] The space–charge modulation of the current in a vacuum diode under photoemission was also studied.[34] For time-varying current injection, it has been studied if the time-averaged SCLC can be higher than the 1D CL law.[35–37] Considering the Coulomb blockade of a few electrons at low voltage shows that the time-average SCLC can exceed the 1D CL law.[38] A 2D and short pulse CL law was also determined by PIC full electromagnetic simulation.[39] These dynamical aspects of SCLC models will be further discussed in Sec. III.

One of the key applications of the SCLC model in solids is to characterize the properties of traps and to estimate the mobility of charge carriers in solids such as trap-filled dielectrics and organics materials. Such trap-filled SCLC models are discussed in pioneering papers from the 1950s.[40,41] In 1971, Goodman and Rose predicted the occurrence of a fundamental electrostatic limit for the photo-current in solid.[42] The model was later extended to the SCL photo-current model[43] applicable for organic semiconductors, which gives a one-half power dependence on applied DC voltage and a three-quarter power dependence (G) on light-induced electron–hole pairs, given by

$$J_{photo\text{-}SCL} \propto V^{1/2} \times G^{3/4}. \tag{7}$$

A smooth transition between the 1D CL law and 1D MG law was developed in 1981.[44] Inspired by the 2D CL law, similar

enhancement of the 2D MG law (over the 1D limit)[45] was developed for both trap-free and trap-filled dielectrics and its transition from Ohm's law.[46] Such enhancement was also shown experimentally in a nanowire.[47] A hybrid model[48] combining the 1D CL and 1D MG laws to describe the SCLC current transport from free space into a high k-dielectric was formulated showing a voltage scaling law V^β between $\beta = 3/2$ (CL law) and $\beta = 2$ (MG law). The extension of the classical 1D MG law to novel quantum materials will be discussed in Secs. II E and II F.

Electron emission in non-vacuum gas environments, particularly, atmospheric pressure, has become of greater importance recently due to the contribution of field emission to gas breakdown for microscale gaps.[49–51] Traditionally, the gas breakdown is driven mechanistically by the Townsend avalanche and predicted mathematically by Paschen's law;[51–53] however, reducing gap distances below approximately 10 μm makes the electric field at the cathode necessary to induce breakdown sufficiently strong to induce field emission.[49–51] This strips additional electrons from the cathode, which ionize more gas near the cathode to create a positive space–charge electric field that contributes to additional field emission.[51,54] Moreover, these ions subsequently collide with the cathode to create additional secondary emission of electrons that feedback into the Townsend avalanche.[51,54] Because previous studies showed that electron emission transitions from field emission to SCL emission with decreasing the gap distance in vacuum,[55] this motivated analytic studies to explore this phenomenon by including the collisional effect as a mobility term in the electron force balance.[56] In the limits of low mobility, electron emission generally transitioned to the MG law; at high mobility and voltage, electron emission transitioned to the CL law. In all cases, taking the limit of the gap distance $D \to 0$ yielded the CL law or essentially vacuum. A third order nexus existed where both MG and CL laws matched the Fowler–Nordheim (FN) law.[54] At this point, the MG regime disappeared for gap distances below this critical point, causing electron emission to transition directly from the FN law to the CL law as in vacuum. While not physical since this point automatically fails to satisfy the asymptotic conditions, it serves as a signpost for when the more exact theory must be used rather than any of the individual asymptotic solutions.[57] This approach has been extended to include an external series resistor[58] and thermo-field emission.[59] More details are provided in another recent Perspective paper[57] and in Secs. II B and II C.

It is important to note that $J_{SCL} \propto V^\beta$ with $\beta = 3/2$ (for the CL law) and $\beta = 2$ (MG law) is pervasive in many applications, such as high current cathodes and intense electron beams required for high-power microwaves generation,[60–67] and organic materials and devices[68,69] required for high current injection from electrodes into solids. It is not our intention to provide a comprehensive overview, which can be found in a recent review paper in 2017.[70] The introduction above serves to provide an overview of the key background necessary for the subsequent discussions in the Perspective. This Perspective will focus on providing some highlights on recent works published after 2017, advancing the current understandings of SCLC, suggesting some unsolved problems, and exploring novel applications. We will provide some insights into SCLC models for different media inside a diode, such as vacuum, gas, plasma, liquid, and solid. The objective is to report new phenomena when the size of the medium (diode) is reduced to sub-micrometer dimensions

and to use novel materials and to understand dynamical and transient behaviors far from the steady state.

Figure 1 illustrates the scope of this Perspective: the SCLC in various media and surrounding structures, the manifestation of SCLC in various dynamical and steady-state conditions, and some representative applications of SCLC. SCLC occurs in a broad spectrum of media, covering nearly all states of matter, including vacuum, gas, plasma, liquid, solids in both crystalline and amorphous states, and 2D layered nanomaterials. In both steady-state and dynamical regimes, SCLC has played a pivotal role in governing the operations of a large variety of applications and devices, ranging from vacuum nanoelectronics, space application, material characterizations, high-power microwave generations, fundamental physics of light-matter interactions, thermionic energy converters (TECs), and many others. These discussions should also provide insights into other applications such as coherent radiation sources, non-neutral charged particle beams, accelerators, and electric propulsion, where space–charge effects on the electron beam are critical.

II. STEADY-STATE BALLISTIC TO COLLISIONAL SCLC IN VACUUM, GAS, LIQUID, AND SOLID

A. Transition to space–charge limited current in nanodiodes

When the diode gap size shrinks below 10 nm, collisions during electron transport become less frequent, since the electron mean free path is typically comparable to or larger than the gap size, regardless of the gap medium.[71–73] The possibility for the presence of material defects, such as charge trapping sites,[40,74] is also reduced in sub-10 nm gaps. In gaps that are free of defects and collisions, the gap current is either source-limited or space–charge limited (SCL). The source-limited current is determined by the supply of electrons from the electrodes or the electrical contacts formed between the electrodes and the gap material,[74] which depends on material properties, including the work function, Fermi level, and density of states (DOS) of electrode material, and properties of the gap medium, including the bandgap, electron affinity, and permittivity (through image charge potential for electron emission).[26,28,75,76] The SCL current is determined by the electric potential due to the presence of the electron space charge inside the gap.[18,26,28] From Poisson's equation, it is clear that the space–charge effect depends strongly on the permittivity of the gap medium.

Previous models of SCL current[17,18,26] were recently extended to obtain a generalized self-consistent model for quantum tunneling current in dissimilar metal–insulator–metal (MIM) junctions,[28] by solving the coupled Schrödinger and Poisson equations self-consistently. The results showed that the current density-voltage (J–V) curves span three regimes: direct tunneling, field emission, and SCL regime. For dissimilar MIM junctions, the J–V curves are generally polarity dependent (Fig. 2). Also, as the gap voltage increases, the forward and reverse bias J–V curves exhibit a crossover behavior in the field emission regime because of the different potential barriers for electrons from the two electrodes.

While this self-consistent model is valid for arbitrary gap voltage, it neglects collisional effects and material defects inside the
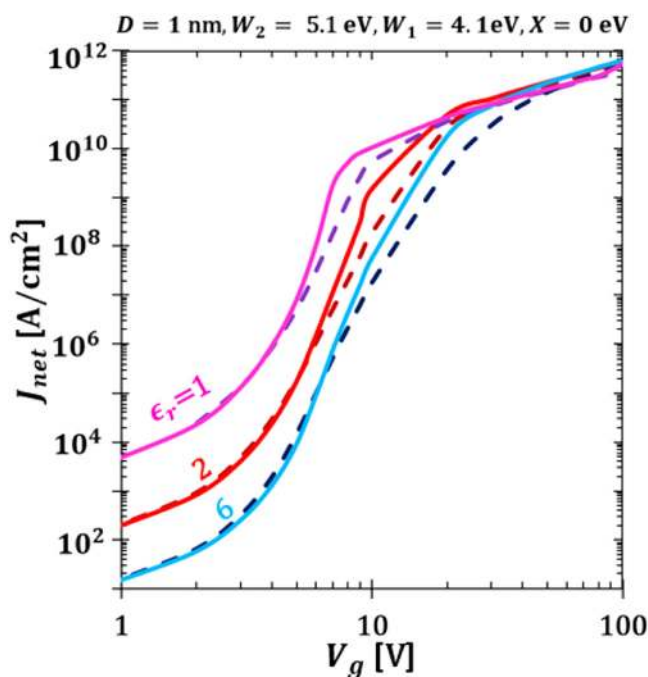
FIG. 1. Schematic overview of space charge limited current (SCLC) in various media, steady-state and dynamical regimes, and several representative applications. SCLC occurs in vacuum, gas, liquid, and solid diodes. SCLC underlies the operations of a large variety of applications, including material characterizations, probing fundamental light-matter interactions, microwave generation, vacuum nanoelectronics, high-power microwave generation, energy conversion, and space technology.

gap. This may be a good approximation for gaps with extremely small thickness in the nanometer scale or sub-nanometer scale;[26,27,77] however, it requires further research to verify if such a model is applicable to sub-10 nm gaps, where scarce collisions and charge trapping are still possible.[50] In addition, the presence of even a small number of charge traps or ions (due to possible ionization events) is expected to dramatically change the electron emission probability from the electrodes, e.g., ion-enhanced field emission.[49] The impact of these effects on SCL current is not well understood and requires systematic evaluation. It would be of interest to see if a universal model similar to that in the collisional regime (discussed in Sec. II B) can be developed to describe the SCL current in the sub-10 nm gaps, thus showing the transition from the collisional regime to the quantum

tunneling regime.[26,28] The effects of temperature-dependent electron transport[78,79] may also be taken into account to study the transition to SCLC in nanodiodes.

Another open question is the high dimensional effects in nanoscale gaps. As the gap distance decreases, the dimension of surface roughness would necessarily become comparable to or even larger than the gap size, where the effects of the electrode surface geometry and physical or chemical morphology,[79–89] along with the nonuniform current distribution due to higher-dimensional gaps or contact junctions,[90–95] require substantial future studies. More discussions on the high dimensional effects can be found in Sec. IV. In addition, when the electron mean free path is comparable to or longer than the device dimension, it is possible to realize

FIG. 2. J–V characteristics of a dissimilar MIM junction. In the calculation, the work function of the two electrodes are $W_2 = 5.1$ eV and $W_1 = 4.1$ eV, electron affinity of the insulator is $X = 0$ eV with gap distance $D = 1$ nm and permittivity ε_r. Solid and dashed lines represent reverse bias (higher work function metal is positively biased) and forward bias (higher work function metal is negatively biased) conditions, respectively. Reproduced with the permission from Banerjee and Zhang, AIP Adv. **9**, 085302 (2019). Copyright 2019 AIP Publishing LLC.

current rectification based solely on geometric effects. Geometrical diodes[96] based on asymmetric geometry of the conducting channel have recently been demonstrated to ratchet quasi-ballistic electrons in silicon nanowires at room temperature.[97] It would be very interesting to examine if such ballistic geometric diodes can be operated in the SCL condition.

B. Space–charge limited current in air gaps

Paschen's law is well known for describing gas breakdown by the Townsend avalanche and is characterized by the breakdown voltage's dependence on the product of the pressure and gap distance, or pD, rather than by either term individually.[51–53] Of particular note, gas breakdown due to the Townsend avalanche is characterized by the presence of a minimum breakdown voltage as a function of pD. In the mid-1950s, Boyle and Kisliuk observed that this minimum vanished at atmospheric pressure and postulated that this occurred due to ion-enhanced field emission.[98] The required stronger electric field at this length scale causes the release of more electrons from the cathode that subsequently ionize more gas molecules near the cathode.[54] This creates positive space–charge that adds to the surface electric field in the Fowler–Nordheim equation. Moreover, the resulting ions add a component

to the secondary emission coefficient that further amplifies the avalanche mechanism. This modifies Paschen's law, eliminating the standard Paschen minimum and causing a continued decrease in the breakdown voltage with decreasing the gap distance. Recent theoretical work using a matched asymptotic analysis has demonstrated that the breakdown voltage scales approximately linearly with field emission in the limit of no ionization.[51,99–101] Detailed reviews on ongoing experimental, theoretical, and simulation studies of these phenomena are presented elsewhere.[49–51,102]

Characterizing this behavior is important for numerous applications.[102] Device miniaturization for microelectromechanical and nanoelectromechanical systems requires accurately predicting gas breakdown at small length scales.[103–107] Conversely, other applications as diverse as electric propulsion for satellites,[108,109] with projections for increased growth in micro-electric propulsion systems due to the increasing number of small satellites requiring technological development to continuously compensate for drag,[108] combustion,[110,111] nanomaterial fabrication[112] environmental remediation,[102] and medicine motivates improved characterization of gas breakdown at micro- and nanoscales for microplasma formation.[113,114]

Another recent Perspective focused on linking electron emission mechanisms, microscale, and nanoscale gas breakdown.[57] Briefly, one may start from the force law for an emitted electron into a gas medium and use electron mobility, which is a function of the electric field and pressure, to account for the collisions of the electron as it traverses the gap.[56] In the limits of the high mobility, small gap distance, and/or high voltage, one recovers the Child–Langmuir law for SCLC in a vacuum diode [Eq. (1)]. In the limit of low mobility (corresponding to high pressure), one recovers the Mott–Gurney law for SCLC with collisions [Eq. (2)]. Prior studies on sheath formation in a gap using a similar assessment of the single-particle motion recovered similar asymptotic behavior.[115] Combining this approach with a prior vacuum diode study using the Fowler–Nordheim equation for field emission as the canonical relationship for applied current[55] permitted the extension of this analysis to include transitions between both space-charge limited conditions and field emission.[56] Subsequent theoretical extensions of this approach to include external resistance,[58] thermo-field emission,[59] and quantum effects[116] have led to what is referred to as nexus theory and reviewed in more detail elsewhere.[57]

C. Space–charge limited current in liquid

Since one may consider the electron motion through a liquid similar to that through a gas with collisions, a recent study applied theory from Ref. 56 to liquids.[117] The majority of this Perspective demonstrates the importance of space–charge effects in vacuum, gases, and solids; however, fewer studies have examined the electron emission mechanism in liquids and most of those are over three to four decades old.[118–124] Characterizing electron processes in dielectric liquids has broad implications in multiple areas, including radiation physics/chemistry, field induced polymerization, nuclear radiation detection, medical imaging, insulator physics, composite insulation, high-power capacitors, pulsed power systems, and electrostatics generators.[123] The characterization of electron processes in liquids includes understanding electron emission (field emission, in particular) as of the initial phases in the

development of electronic breakdown;[125–127] electron emission at the cathode initiates the release of electrons that leads to breakdown.[126,127] Recent applications involving intense electric fields for generating electric discharges for water purification[128] and for cold atmospheric pressure plasmas for treating liquids[129] demonstrate the importance of characterizing the effects of electron emission and breakdown in liquids. One may also have phase changes from liquid to gas at high temperatures and strong electric fields for combustion applications,[130] motivating characterization of electron emission under potentially broad ranges of electron mobility, which may vary dramatically during phase changes.[131–134]

Applying the theory unifying electron emission mechanisms to liquids demonstrated that electron emission was primarily driven by field emission with space–charge beginning to contribute at the highest voltages and currents for the liquids studied.[117] Changing the mobility in accordance with measured values expected for phase changes demonstrated that it was feasible for space–charge to become relevant for the gap distances used for liquids if the phase changed to gas. As such, electron emission may transition from field emission to MG to CL with increasing mobility or decreasing gap distance. This would have important implications for combustion applications, where heating and phase changes may occur. It may also become critical for applications at low temperatures for liquid gases, such as argon or nitrogen, where slight changes in temperature that may arise due to changes in voltage that may ordinarily be neglected may potentially lead to phase changes. For instance, ongoing studies at the Spallation Neutron Source (SNS) at Oak Ridge National Laboratory for studies searching for the permanent electric dipole moment of a neutron require experiments inside a bath of liquid helium at approximately 0.4 K with electric fields up to ∼75 kV/cm, motivating characterization of liquid breakdown mechanisms under this extreme conditions.[126]

D. Space–charge limited current for traditional bulk solids

The SCLC J_{SCL}, the maximum current density that can be transported across a diode of gap distance D with a bias voltage V, may be generally expressed by the scaling law $J_{SCL} \propto V^\beta/D^\gamma$. This limitation is due to the electrostatic repulsion generated by the unscreened charge carriers injected into the solid, which are in excess of the thermodynamically permitted equilibrium condition. For a traditional trap-free bulk solid, the scaling is $(\beta,\gamma) = (2, 3)$, also known as the Mott–Gurney law,[3,4] which is the solid-state counterpart of the Child–Langmuir (CL) law for a vacuum diode, which has a classical scaling of $(\beta, \gamma) = (3/2, 2)$[1,2] and a quantum scaling of $(\beta, \gamma) = (1/2, 4)$.[18] For a trap-filled solid, the MG law becomes the Mark–Helfrich (MH) law[135] with a scaling of $(\beta, \gamma) = (l + 1, 2l + 1)$, where $l = T_c/T \geq 1$, T is the temperature and T_c is a parameter characterizing the exponential spread in the energy of the traps. Beyond the MG and MH laws, field-dependent and carrier-density-dependent mobility transport models are also commonly used to describe SCLC in solids, particularly in organic materials.[136–139] The characterization of mobility by using SCLC models will be discussed below.

The key difference between the vacuum SCLC (CL law) and solid-state SCLC (MG law) lies in two aspects: (a) the transport of

the electrons in the solid follow the mobility equation and (b) the Poisson equation must include the traps carrier density. Here, the presence of mobility $\mu(F, T, n)$ and traps carrier density n_{trap} immediately reveals that the SCLC model for solid is inherently linked to the electronic properties, charge traps and dopants of the solids[140,141] and it is a function of the applied field (F), of temperature (T), and carrier density (n). Thus, despite being a semi-classical transport model first derived as early as the 1930s for a solid diode, SCLC remains an actively studied topic for *material scientists and device engineers*, especially, for experimental characterization of charge transport and trapping mechanisms in organic materials.[68,69,142–145] Fitting the experimentally measured current–voltage (J–V) characteristics with various SCLC models has become one of the standard tools in probing charge transport mechanisms[146] to determine the concentration and the energy distribution of charge traps, and mobility of the solid, especially organic semiconductors.[147]

The classic MG model describes the SCLC when the solid has negligible traps. In this case, the SCLC is caused solely due to the electrostatic potential generated by an "in-transit" carrier when traversing between the injecting and the collecting electrodes. In this trap-free limit, the SCLC is governed by the MG law as shown in Eq. (2). In the presence of a single level of shallow localized trap state in the bandgap [see Fig. 3(a)], the SCLC model retains the same scaling of the trap-free MG law, but the magnitude of the SCLC is significantly reduced due to the trapping of the transport carriers.[40,148] In this case, the SCLC model in the presence of a shallow trap with energy level E_0 below the conduction band, Eq. (2) becomes

$$J_{SL}(V) = \frac{9}{8}\epsilon\mu\theta\frac{V^2}{D^3},$$ (8)

where

$$\theta = \frac{n}{n_{trap}}\exp\left(-\frac{E_0}{k_B T}\right),$$ (9)

where k_B is Botzmann's constant, and $\theta \ll 1$ at room temperature. Interestingly, when the bias voltage is raised to a critical threshold value, the injected carriers are just sufficient to fully fill the trap states, which learns to a rapid increment following a power law,[41,] i.e.,

$$J_{TFL}(V) \propto V^\beta,$$ (10)

with $\beta > 2$. This power law rise of SCLC is commonly known as the *trap-filled limit* (TFL). At higher voltages, the SCLC eventually saturates at the trap-free MG limit [Eq. (2)] when the trap states are filled and have no further effect on the carrier conduction.

Beyond the single-level trap model, Mark and Helfrich[135] also developed an SCLC model that assumed that the trap states are energetically distributed according to an exponential function [see Fig. 3(b)] of

$$n_{trap}(E) = \frac{N_{trap}}{k_B T_c}\exp\left(-\frac{E}{k_B T_c}\right),$$ (11)
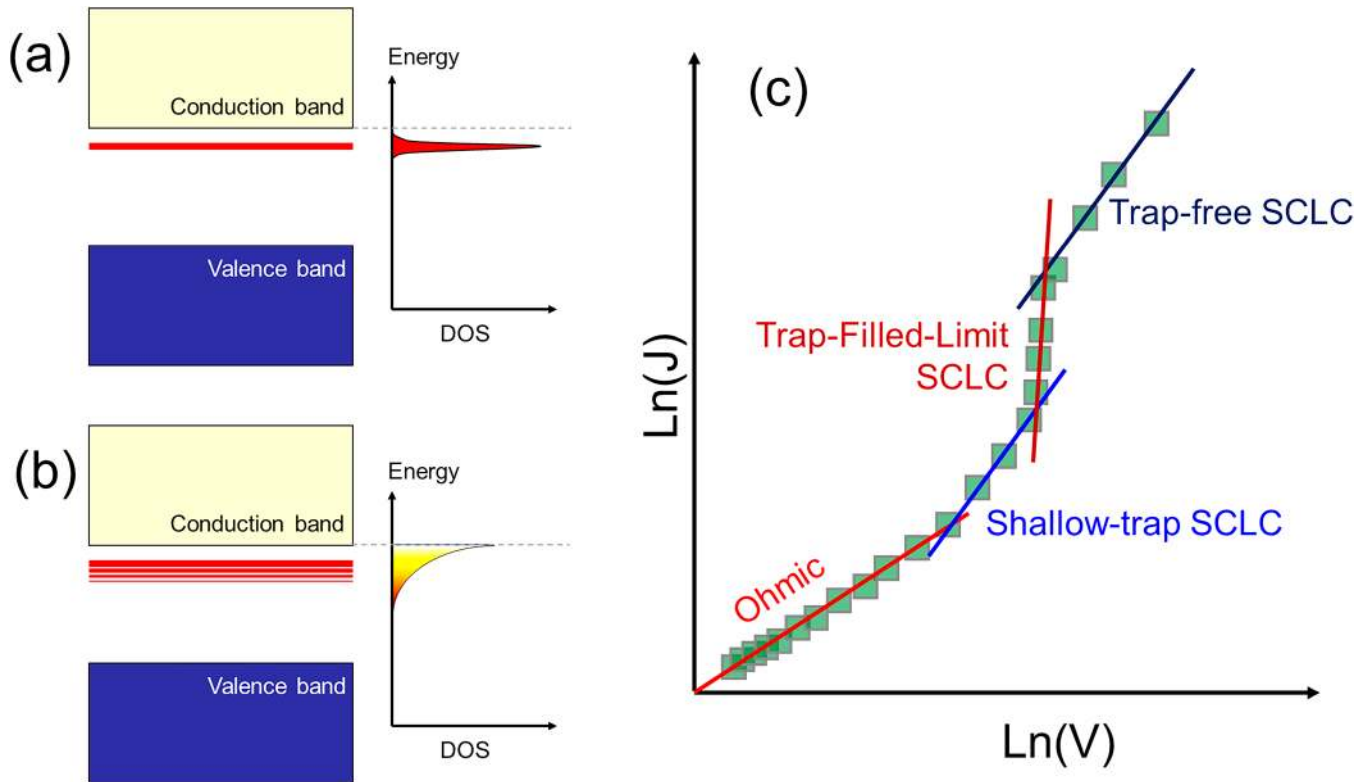
FIG. 3. Schematic illustrations of SCLC in solids under the influence of trap and defect states. Energy band diagram and density of states (DOS) of (a) single-level shallow-trap states and (b) exponential trap states. (c) Typical current–voltage scaling of SCLC in solids. The current–voltage scaling transitions from the low-bias Ohmic regime, shallow-trap SCLC, trap-filled-limit SCLC, and finally, trap-free MG SCLC at sufficiently high bias voltage such that the trap states are completely filled and no longer affect the current conduction. Note that the scale is the logarithm of current density vs the logarithm of the voltage.

where N_{trap} is the total trap density and T_c is a characteristic temperature. For $T < T_c$, the SCLC predicted by the Mark–Helfrich (MH) law is

$$J_{exp}(V,\ T) = N_0 \mu e^{1-l} \left(\frac{\epsilon}{N_{trap}} \frac{l}{l+1} \right)^l \left(\frac{2l+1}{l+1} \right)^{l+1} \frac{V^{l+1}}{D^{2l+1}}, \qquad (12)$$

where N_0 is the effective density of states at the conduction band edge and $l \equiv T_c/T > 1$. The SCLC–voltage scaling is thus always higher than a quadratic scaling for exponentially distributed trap states. Figure 3(c) shows a typical transition of the current–voltage scaling from low-bias Ohmic regime to shallow-trap SCLC to trap-filled limited SCLC and the recovery of the trap-free MG regime at high bias.

Instead of considering a specific energetic distribution of traps or localized defect states in the solid slab, the effect of localized trap and defect states can be collectively included in the carrier mobility. In this case, the carrier mobility becomes *carrier-density-dependent* and/or *electric-field-dependent*, where the SCLC models must be modified accordingly. Vissenberg and Matters[149] proposed that the

charge conduction in organic thin films, such as pentacene and polythienylene vinylene, can be accurately captured by a hopping percolation model in which the injected carriers "hop" between localized defect states. Based on an exponential density of states (DOS) of localized states, the carrier mobility takes the power-law *carrier-density-dependent* form of

$$\mu(n) = \mu_{0n} + a \left[\frac{\left(\frac{T_c}{T} \right)^4 \sin\left(\pi \frac{T}{T_c} \right)}{b} \right]^{\frac{T_c}{T}} n^{\frac{T_c}{T}-1}, \qquad (13)$$

where μ_{0n} is the low-density carrier mobility and a and b are material-dependent parameters. Correspondingly, the SCLC of solids with carrier-density-dependent mobility can be approximately solved as[136,137]

$$J_{carrier}(V) = J_{MG}(V) + c \frac{V^{\frac{T_c}{T}+1}}{D^{2\left(\frac{T_c}{T} \right)+1}}, \qquad (14)$$

where $J_{MG}(V)$ is the MG SCLC with $\mu = \mu_{0n}$ and c is another material-dependent parameter.

For solids that exhibit field-dependent mobility, such as poly (dialkoxy p-phenylene vinylene),[138] the carrier mobility takes the electric-field-dependent[139] form of

$$\mu(F) = \mu_{0F} \exp\left(\gamma \sqrt{F}\right), \qquad (15)$$

where μ_{0F} is the low-field carrier mobility and γ is a material-dependent parameter. The *field-dependent* SCLC can be approximated by[150]

$$J_{field}(V) = \frac{9}{8}\epsilon\mu\frac{V^2}{D^3}\exp\left(0.89 \times \delta \times \sqrt{\frac{V}{D}}\right), \qquad (16)$$

which reduces to the MG law [Eq. (2)] when setting $\delta = 0$, i.e., when the field-dependence is absent. Note, we only introduce the above-selected mobility models in Eqs. (13) and (15) as the representative examples of carrier-density-dependent and field-dependent SCLC models of Eqs. (14) and (16). Due to the enormous complexity of amorphous, polycrystalline, and crystalline nature of bulk organic and inorganic solids, myriads of field-dependent, carrier-density-dependent, and field-and-carrier-density-dependent mobility models are available for different solids (for example, Refs. 151–153). Their corresponding SCLC models can be similarly obtained by solving the drift or drift-diffusion transport model with the Poisson equation. Such SCL models provide useful tools to extract the electrical mobility and to understand the nature of defects of various solids by fitting the experimental current–voltage data with a suitable SCLC model.

E. Space–charge limited current for two-dimensional (2D) Dirac materials

With the advances in fabricating novel two-dimensional (2D) materials,[154–158] the validity of traditional SCLC models for atomically thin monolayers and few-layer materials has been scrutinized. The electronic transport properties of 2D Dirac materials are distinctive of the traditional bulk materials in two aspects: (i) electrostatics and electrodynamics due to reduced dimensionality and (ii) nonparabolic energy–momentum dispersion relation of the transport carriers. Aspect (i) arises because a 2D Dirac material has an atomic-scale thickness of only a few nanometers. The ultrathin-body nature of 2D materials appreciably modifies the electrodynamics and electrostatics of carriers and electrodes. Furthermore, because of such ultra-thin geometry, quantum mechanical effects can also be important. Aspect (ii) originates from the energy band structures of isotropic 2D Dirac materials, such as hBN, MoS₂, and WS₂ monolayers, which follows the relativistic Dirac *linear* energy–momentum dispersion relation,[159,160]

$$\varepsilon_{\boldsymbol{k},s} = s\sqrt{\hbar v_F^2|\boldsymbol{k}|^2 + (\Delta/2)^2} \; , \qquad (17)$$

where $\boldsymbol{k}$ is the carrier wave vector, v_F is a material-dependent parameter commonly known as the Fermi velocity, Δ is the energy

bandgap, and $s = \pm 1$ denotes the conduction and valence bands. The Dirac energy dispersion is in stark contrast to the "effective mass" approximation widely used for common metals and insulators, which follows a *non-relativistic* and *parabolic* energy-momentum dispersion relation of $\varepsilon_k = \hbar|\boldsymbol{k}|^2/2m^*$, where m^* is the electron effective mass. In terms of the carrier transport, the single-particle transport current can be generally described by a Boltzmann-type transport equation, given by

$$\boldsymbol{J}(\boldsymbol{F}, T) = e\int\rho(\varepsilon_k)v_k f(\boldsymbol{F}, T)d\varepsilon_k, \qquad (18)$$

where $\rho(\varepsilon_k)$ is the density of states (DOS) of the carriers, which is intimately linked to the dimensionality and the energy–momentum dispersion of the material, $\boldsymbol{v_k} = \partial\varepsilon_k/\partial\boldsymbol{k}$ is the carrier velocity, and $f(\boldsymbol{F}, T)$ is the carrier distribution function which is dependent on the electric field ($\boldsymbol{F}$) and temperature consistent with a given material's transport properties. This shows that aspect (i) influences $f(\boldsymbol{F}, T)$, while aspect (ii) influences both $\rho(\varepsilon_k)$ and $\boldsymbol{v_k}$. Thus, it is expected that the carrier transport in 2D Dirac materials will exhibit completely different current–voltage characteristics compared to common bulk materials.

By explicitly taking into account the reduced dimensionality, Dirac energy-momentum dispersion, and the 2D ultrathin-body geometry of 2D Dirac semiconductors, such as hBN and MoS₂, a new SCLC model[161] was developed to study the SCLC for 2D Dirac materials (see Fig. 4). The model provides a universal transition of the SCLC scaling law, i.e., $J_{SCL} \propto V^\beta/D^\gamma$, with (β, γ) continuously changing from (2, 3) for common bulk solids (with semiclassical parabolic energy dispersion) to (3/2, 2) for the fully massless (or ultra-relativistic) Dirac quasiparticles in 2D Dirac materials (see Ref. 161 for the detailed analysis of the SCLC in 2D Dirac materials). It is important to note that while this *new* limit of $(\beta, \gamma) = (3/2, 2)$ is identical to the CL law [Eq. (1)], the underlying physical origin of such scaling in 2D Dirac materials is completely different. In the classic CL law, the scaling originates from the *ballistic* transport of *semiclassical* carriers across the vacuum gap. In contrast, the same scaling in the 2D Dirac materials originates from the transport of *ultra-relativistic* quasiparticles in the *collisional* transport regime. For 2D Dirac materials with a finite bandgap, the modified SCLC model indicates a voltage scaling between $\beta = 3/2$ and 2, which agrees well with prior experimental observations of $1.7 < \beta < 2.5$ in monolayer MoS₂[162] and $1.75 < \beta < 2.5$ in monolayer hBN.[163] Note the sub-quadratic scaling of $\beta < 2$, as observed in experiments,[162,163] contradicts the key assumption of $\beta \equiv T_c/T > 2$ as used in the formulation of the MH law. Thus, using the MH law to explain and to fit the experimental measured SCLC for 2D Dirac materials[162,163] is no longer valid. In this case, the experimentally observed anomalous sub-quadratic scaling is successfully resolved by this newly proposed SCLC model.[161] It should be emphasized that the predicted SCLC-voltage scaling of $3/2 < \beta < 2$[161] represents a distinct "smoking gun" signature for distinguishing Dirac materials from the traditional 3D bulk materials, which follows a super-quadratic voltage scaling of $\beta \geq 2$.

Finally, we remark that, with the recent discoveries of a large variety of 2D materials—many of them possess non-parabolic energy-momentum dispersion at the conduction and valence band
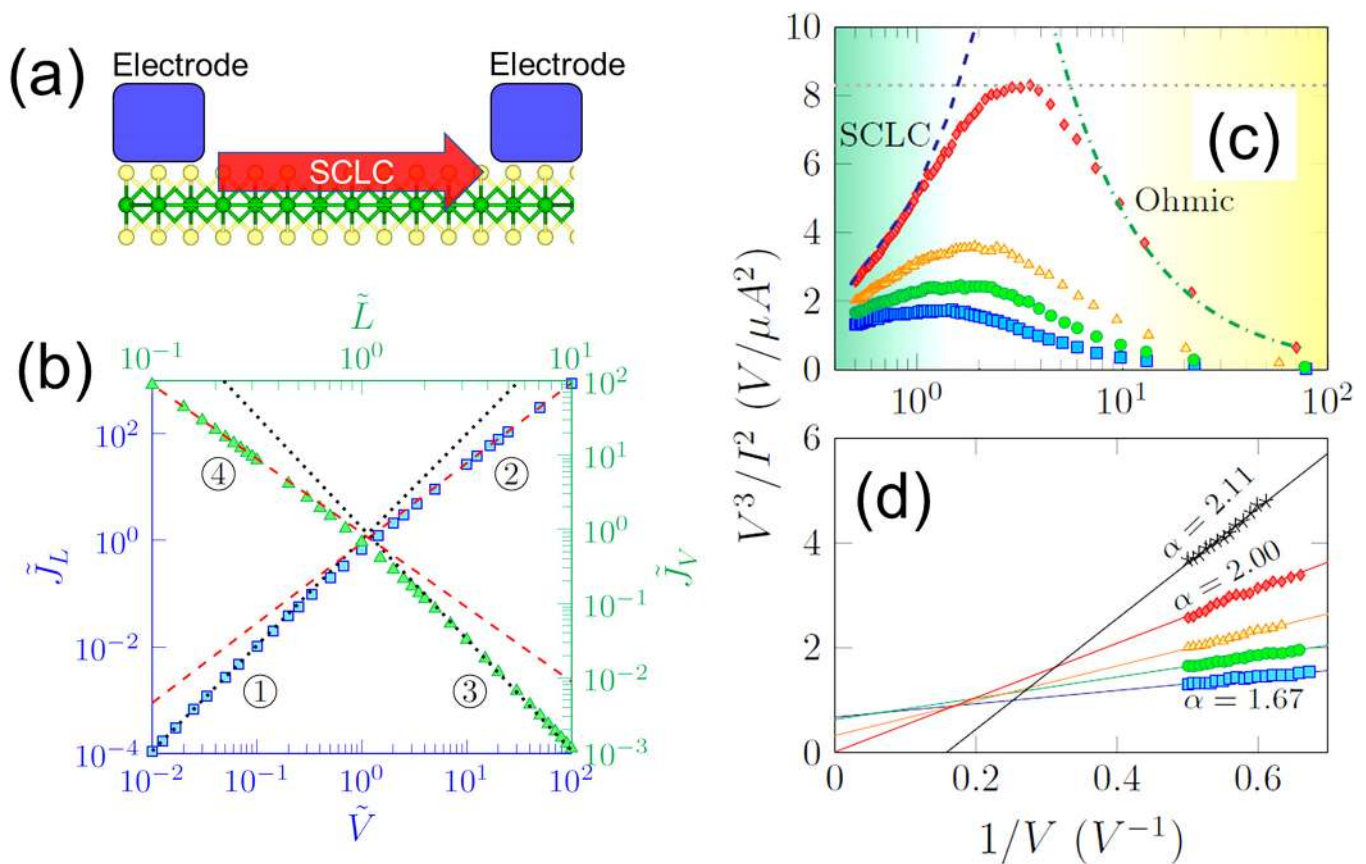
FIG. 4. SCLC model in 2D Dirac materials. (a) Schematic drawing of the 2D-material-based diode. The SCLC flows laterally in the plane of the 2D-material. (b) The current–voltage and current–length scaling of the modified SCLC for 2D Dirac materials. (c) and (d) The modified SCLC model[161] exhibits good agreement with experimental data obtained from Refs. 162 and 163. Reproduced with permission from Ang et al., Phys. Rev. B **95**, 165409 (2017). Copyright 2017 American Physical Society.

edges, the modified SCLC model for 2D Dirac materials[158] highlights the importance of properly taking into account the reduced dimensionality and the actual energy-momentum dispersion of the materials when analyzing the carrier trapping effect using the SCLC method. While the SCLC along the lateral in-plane direction of 2D materials has been studied and discussed above,[161] the SCLC transport vertically out of the 2D plane of 2D-material-based heterostructures remains largely unexplored. A recent experiment[164] demonstrated vertical SCLC flow through a stack of multilayer WSe$_2$ vertical tunneling diodes [see Figs. 5(a) and 5(b)]. Interestingly, despite the layered nature of the WSe$_2$ stack where long-range crystal order is absent, the current–voltage characteristics exhibit the classic Ohmic, TFL, and trap-free SCLC akin to the classical SCLC in a bulk solid [see Fig. 5(c)]. It should be noted that the WSe$_2$ stack reported in Ref. 164 has a thickness of about 20 nm, which is in the thin-film regime rather than in the few-atoms-thick 2D limit. The observation of classic trap-limited and trap-free SCLC is thus expected. We expect unusual SCLC behavior, distinctive from classic SCLC scaling laws of bulk materials as reviewed above,

to arise when the tunneling layer is replaced by *vertical* heterostructures composed of only a few 2D monolayers [see Fig. 5(d)]—a nanostructure is commonly known as the van der Waals (VDW) heterostructure.[165] Understanding the physics of SCLC in VDW heterostructures shall shed new light on the following open questions: What is the interplay between direct quantum mechanical tunneling and SCLC? Can a transitional model between the two different mechanisms be constructed? How does quantum SCLC models developed for vacuum nanodiode[18,19,24,26] and new MG law for 2D Dirac materials[161] manifest in layered VDW heterostructures? Can such vertical SCLC be harnessed to generate new device functionality in VDW heterostructures apart from serving as a transport measurement tool? The recent advancement of experimental fabrication techniques of VDW heterostructures[166] and first-principles density functional theory simulations combined with quantum mechanical nonequilibrium Green's function (NEGF) and/or semiclassical transport models[91,167,168] shall open a new chapter on the quantum transport of SCLC in the few-atom limit. The discussion above is strictly for 1D model, where some
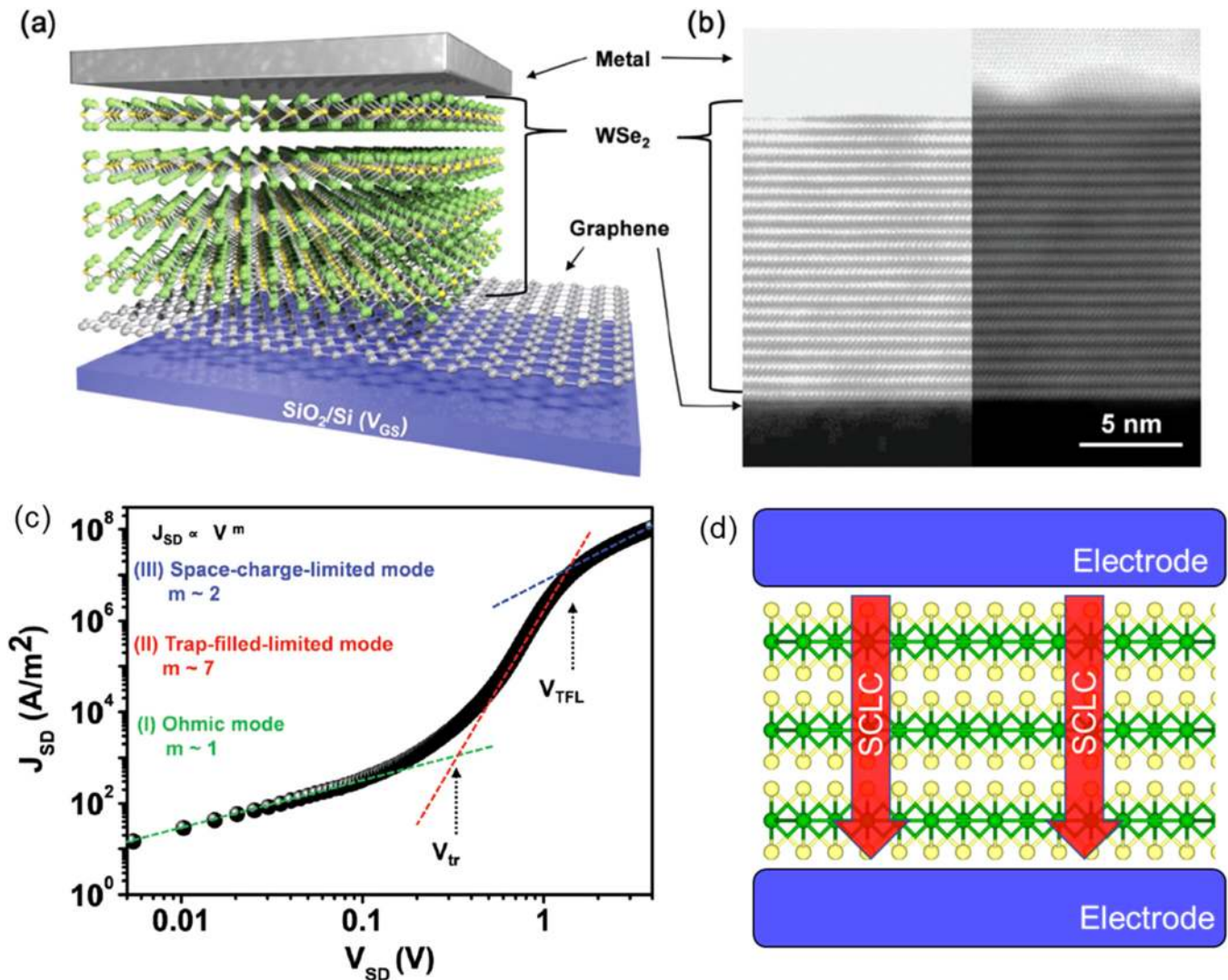
FIG. 5. Vertical SCLC in the 2D-material-based van der Waals (VDW) heterostructure. (a) Schematic drawing of the VDW tunneling diode;[164] (b) Cross-sectional image of the device;[162] (c) current–voltage characteristics showing the transition from Ohmic to trap-filled-limit and the trap-free MG SCLC regime;[164] (d) schematic drawing of the vertical SCLC in 2D layered heterostructures.[164] (a), (b) and (c) reproduced with permission from Y. S. Shin et al, Adv. Mater. 30, 1704435 (2018). Copyright 2018 Wiley.

geometrical effects of SCLC in both bulk and 2D materials can be found in Sec. IV.

F. Thermal-field electron emission from 2D materials to space–charge limited current

It is found that current–temperature–voltage scaling of the electron emission from 2D materials also exhibit unconventional as compared to the traditional models.[169] For instance, the *thermionic emission* of electrons from 2D materials—in which thermally excited electrons undergo flyover across the surface confining barrier—follows the semiclassical transport equation,[170–173]

$$J_{TE}^{(2D)}(T) = A_{2D}^{*} T^{\beta} \exp\left(-\frac{\Phi_B}{k_B T}\right), \tag{19}$$

where A_{2D}^{*} is a material-and device-dependent parameter, Φ_B is the work function of the 2D materials, and β is a scaling constant, which depends on the direction of the electrons emitted from the 2D materials and electron scattering effects in the 2D materials. For one-dimensional (1D) classical thermionic emission from bulk materials, also known as the Richardson–Dushman (RD) law,[174,175]

$A^\star$ is a constant derived from a parabolic dispersion and $\beta = 2$. For thermionic emission vertically out from a 2D planar material, β varies from 2 to 3 where carrier scattering effects are nearly absent[173] and able to provide agreement with thermionic emission from a suspended graphene sample.[176] Intriguingly, in the presence of carrier scattering effects, the scaling exponent is pinned to a universal value of $\beta = 1$ for a large variety of 2D materials.[170] A recent experiment of charge carriers across a graphene–silicon Schottky junction has confirmed this $\beta = 1$ scaling.[177] For thermionic emission laterally from the edge of the 2D-material, we have another universal scaling exponent of $\beta = 3/2$.[170,178] It should be noted that such *scaling universality* of the current–temperature dependence is not found in 3D bulk materials, and it is a direct consequence of the reduced dimensionality of 2D materials.

Using the same concept, a preliminary study[179] has predicted a *universal* thermal-field emission current–voltage scaling law of

$$J_{TFE}^{(2D)}(V, T) = A_{2D}^{\star\star} \frac{\pi d_F}{c \sin(\pi/c)} \exp\left(-\frac{B}{V}\right), \qquad (20)$$

where $A_{2D}^{\star\star}$ and B are material-and device-dependent parameters, $d_F \propto V$ is a voltage-dependent parameter, and $c = d_F/k_B T$. Equation (20) is in stark contrast to the classic Murphy–Good scaling law derived under the Fowler–Nordheim (FN) framework, which is given by[180,181]

$$J_{TFE}^{(3D)}(V, T) = A_{3D}^{\star\star} \frac{\pi d_F^2}{c \sin(\pi/c)} \exp\left(-\frac{B}{V}\right). \qquad (21)$$

Note the field (or voltage) dependence in Eq. (21) for traditional FN law is d_F^2, which differs from d_F in Eq. (20) for 2D materials. The constants $A_{3D}^{\star\star}$ and $A_{2D}^{\star\star}$ are also different. Despite a growing number of experimental studies focusing on the physics of vacuum-based electron emission from graphene and other 2D materials,[182–187] the transition from the various electron emission mechanisms, such as field, thermal-field, or thermionic emission from 2D materials to SCLC remains elusive thus far. In fact, due to the ultrathin-body nature of 2D materials, the number of electrons available for emission is much more limited when compared to 3D bulk materials. For example, the thermionic emission current from 2D graphene is several orders of magnitude lower than that from bulk 3D metals[188] [see Fig. 6(a)]. Because the emission current density is inevitably limited by the low availability of electrons in 2D materials, it is predicted[189] that the field emission current undergoes a rapid transition from normal field-thermal emission to *source-limited* emission without entering the SCLC regime [Fig. 6(b)] for $D = 100$ nm to $1\,\mu$m.

Despite being studied immediately after the discovery of graphene,[182] the physics of field and thermal-field emission remains largely incomplete. Because 2D materials are atomically thin and typically fabricated on a substrate, the unambiguous isolation of 2D field-based electron emission physics without the influence of the substrate remains a major challenge. Furthermore, the generalization of the universal electron emission theory developed by Jensen[190] covering field, thermal-field, and thermionic and photoinduced emissions into the new domain of 2D materials remains unexplored. It
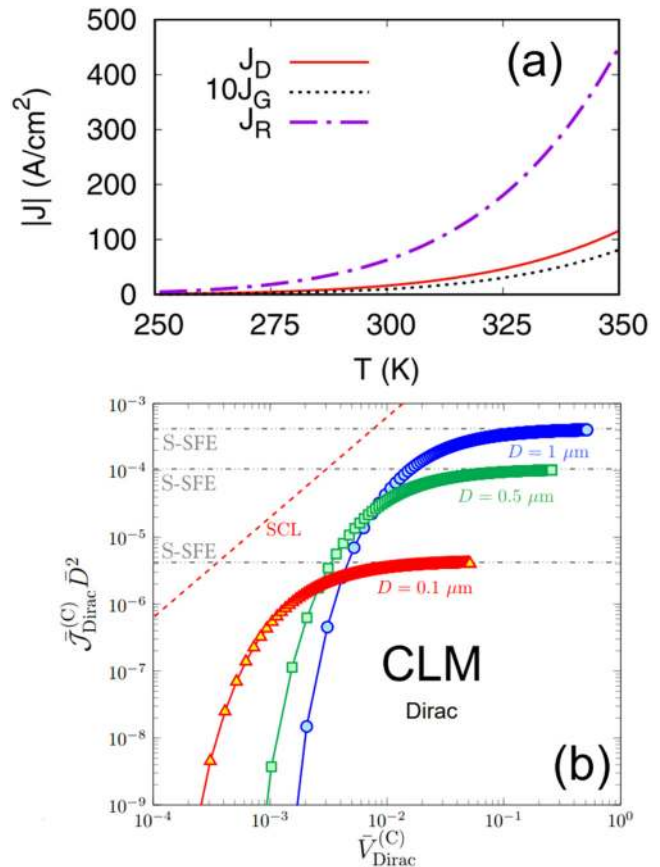

FIG. 6. Source-limited electron emission and the absence of SCLC in graphene. (a) The thermionic emission current from graphene (J_G) is orders of magnitude lower than that of the 3D metals (J_R).[188] (b) Source-limited electron emission leads to the absence of SCLC in 2D materials. The emission current transits from field emission to source-limited saturated emission (denoted by gray dashed-dotted horizontal lines) without entering the SCLC regime (denoted by red dashed line). The term "CLM" denotes the electron field emission model of 2D Dirac materials in which the lateral momentum of the emitted electrons are assumed to be conserved. (a) Reproduced with the permission from Huang *et al.*, Appl. Phys. Lett. **111**, 183902 (2017). Copyright 2017 AIP Publishing LLC.

should be noted that the current model of single-electron field emission from the bulk material interface is based on matching or coupling the electronic wave function at the bulk metal/vacuum interface, which is based heavily on matching the Bloch wavefunction in the metal with that of the free-electron wavefunctions propagating perpendicularly to the metal/vacuum interface.[181] Such a model seems to fail for the 2D-metal/vacuum interface, where there are no propagating electronic states perpendicular to the 2D-metal/vacuum interface due to the lack of out-of-plane crystal periodicity in the 2D atomic layer. Whether the standard Sommerfeld transport theory, such as the Fowler–Nordheim (FN) law or Murphy–Good models, remains microscopically valid for 2D materials remains an open question. We suggest that DFT-based transport simulations shall be a necessary tool to elucidate the microscopic electron field

emission physics at the 2D-metal/vacuum interface. The extension to consistent photon-emission for 2D-materials is also less explored due to the complexity of light-matter interaction at atomistic limits. For example, extremely nonlinear strong-field photo-emission from carbon nanotubes (CNTs) has been observed experimentally[191] that space charge effects may be critical. The physical situations of 2D materials make it difficult to understand exactly what we mean by a steady state, especially in the context of the photon–electron interaction. In this spirit, we note that time-dependent electron emission from quantum materials is an interesting application for newer "beyond DFT" techniques, such as Time-Dependent Density Functional Theory (TDDFT).[192–194] One may refer to Ref. 193 for a review of TDDFT and Ref. 192 for applications to transport in electromagnetic fields. We turn now to a more general consideration of these time-dependent effects in Sec. III.

III. TIME-DEPENDENT EFFECTS OF SPACE–CHARGE LIMITED CURRENT

A. Discrete particle effects

In nano- and microscale vacuum diodes, the discrete nature of the charge plays an important role. This can be seen from several different vantage points. First of all, we recognize that in a diode of such small dimensions, an upper limit, set by space–charge considerations, to the number of electrons present in the gap, N_e, can be roughly estimated to be $N_e = CV_g/q$, where C is the capacitance of the diode, V_g is the voltage applied across the diode, and q is the fundamental charge. In the case where electrons are injected into the gap via field emission, this number can be significantly smaller (by orders of magnitude). Using this estimate of the upper limit, we can find an upper bound for the estimated plasma parameter Λ_e in terms of the gap spacing D, electron temperature T_e, and plasma parameter,

$$\Lambda_e \approx n_e \lambda_e^3 \approx D \frac{\varepsilon_0}{q} \frac{(kT_e/q)^{3/2}}{V_g^{1/2}}, \tag{22}$$

where n_e is the electron density and λ_e is the electron Debye length. The plasma parameter is small for typical nano- and microscale diodes, indicating that scattering processes are important. Indeed, molecular dynamics based simulations have indicated that Coulomb scattering near the point of field emission from a hyperbolic-spheroid shaped emitting tip can lead to significant changes in the energy spread of electrons within hundreds of nanometers from the tip.[14] Discrete electron effects are also important with regard to electron emission. In determining emission from a certain point on the cathode the local electric field at the surface plays a critical role. The distance Δr over which a single electron can effectively influence the electric field by ΔE is given by

$$\Delta r \lesssim \sqrt{\frac{q}{\pi \varepsilon_0 \Delta E}}. \tag{23}$$

This shows that a ΔE ranging from 1 MV/m to 100 MV/m will cause Δr to range approximately from 100 nm to 10 nm, respectively. From this, it follows that the lateral spacing between

emitted electrons in nano- and microdiodes is typically on the order of tens of nanometers, as has been observed in simulations.[14,32,195] This represents a significant distance with respect to the important length scales of the emitter in the systems under consideration and thus must be taken into account. More broadly, this suggests that aspects of strongly coupled plasma physics may be necessary to understand even single-species electron plasmas in micro/nano-gaps as at the point of emission, the density can be high while the kinetic energy and temperature of the electron population are modest, leading naturally to a situation where the potential energy is greater than the kinetic energy. This ratio of potential to kinetic energy exceeding unity is the signature for strongly coupled plasma physics.

Even in macroscopic systems, the importance of discreteness cannot be neglected. Electron emission is typically non-uniform across the cathode, whether by design, as in the case of field emitter arrays, or due to inhomogeneity of the cathode surface, e.g., surface contaminants, grain boundaries, or morphological variance at the microscale. For field emitter arrays, the effects of three-dimensional charge distribution and discreteness should be taken into account within a distance from the cathode corresponding to the pitch of the array.[196] Similarly, cathode inhomogeneity at the microscale can have a significant effect on the quality of electron beams on the macroscale due to variability in emission and scattering near the cathode surface.[197–200] Therefore, discrete particle effects must be accounted for to establish appropriate boundary conditions to accurately model electron beams in macroscale systems. For this purpose, it might be useful to consider *virtual* diodes where the "anode" corresponds to the boundary of the computational cell that demarcates the boundary between the region where discrete electrons are important and the region where particle-in-cell or continuum models are fully applicable.

The discrete nature of electric charge may lead to shot noise in electronics.[201] As the discrete particle effects become important when the dimension of the diode decreases,[202,203] future research may also consider shot noise effects in SCLC in nanodiodes with different electron emission mechanisms, which is beyond the scope of this paper.

B. Temporal (short pulse) effects and AC beam loading

Another characteristic parameter of nano- and microdiodes is the transit time of electrons through the gap, which is given by $\tau = C_\tau D \sqrt{m/qV}$, where C_τ is a constant on the order of unity that depends on the exact diode geometry and distribution of space–charge in the diode gap. A typical nano- or microdiode will typically exhibit transit times from tens of femtoseconds to several picoseconds. It is possible to understand the relevance of the transit time for different situations.

Let us begin by considering a regime where current is generated over a period that is comparatively long compared to the transit time. For a vacuum nanodiode with space–charge limited emission from a spot of finite size on the cathode, simulations indicate that electrons will be injected into the diode gap in distinct bunches. This is due to space–charge forces and the discrete nature of the current at this scale,[32–34] somewhat akin to a Coulomb blockade. These bunches can induce a time-varying current in the

diode with a characteristic frequency ranging from hundreds of GHz to several THz. For suitably low voltage in a nanodiode, it is even possible to extend the Child–Langmuir law to a true Coulomb blockade regime where there is only one electron present in the gap at a time.[38] Both situations described cause a modulation in the diode current with a period comparable to the transit time. Next, we may turn our attention to a different regime, namely, where the current pulse is short compared to the characteristic transit time across the diode. This case is relevant for ultrafast emission, where the pulse length may be on the order of 10 fs.[204–209] In this case, we typically encounter a hybrid of multiphoton emission and strong-field emission, or even Schottky emission, where the goal is to produce a tight bunch of coherent electrons for applications such as ultrafast transmission microscopy.[208] For these applications, understanding and controlling space–charge effects are imperative to maintain the coherence of the electron bunch. In some instances, a nanostructured surface is used to guide the laser field to a point of emission,[207–209] with the result that the near field is of such strength that electrons can be accelerated into the much weaker far-field region in less than half a laser oscillation period, and thus an even shorter characteristic time scale is introduced that must be taken into account.

In a typical nano- or microscale diode the current is so miniscule, and the electrons of such low energy, that one might anticipate any electromagnetic effects to be safely ignored. On the other hand, the rapid variation of current is often characteristic of the behavior of systems at this length scale. For instance, in strong-field emission, the laser pulse length may be on the order of 10's of femtoseconds, and the rise time of the current pulse even shorter than that.[209] Similarly, electrostatic beam loading (or the Coulomb blockade) can give rise to current variations with a period close to the transit time for electrons to cross the diode gap, which may be on the order of a picosecond.[32,38] Thus, inductive loading of the gap, whether due to parasitic inductance or a designed inductance, may be important. Luginsland et al.[29] showed that a persistent virtual cathode may be formed in a drift tube due to electromagnetic transients even when the self-magnetic field is negligible. This occurs due to an inductive potential and illustrates how rapid changes in current may be important, even when a cursory examination of system parameters would suggest otherwise.

An additional feature of emission under AC loading can be seen by assuming that the structure has an electromagnetic mode associated with the structure, as described in Ref. 30. It is then possible to write a lumped circuit model where the electromagnetic mode is characterized by a frequency ω_0, a quality factor Q, and an impedance of that RF mode designated by R. In this case, one can write the following for the evolution of the time-dependent voltage:

$$\left(\frac{d^2}{dt^2} + \frac{\omega_0}{Q}\frac{d}{dt} + \omega_0^2\right)V_{rf}(t) = -\omega_0\frac{R}{Q}\frac{dI}{dt}. \qquad (24)$$

In a one-dimensional limit, this equation contains both displacement and convection current.

In the small signal limit, assuming that the time-dependent, fast time scale electromagnetic signal is small compared to the applied "DC" voltage ($V_{rf} \ll V_{DC}$) and assuming that the diode is

emitting as a space–charge limited diode such that $I = AP(D^\gamma)V^\beta$ and $Z_D = V/I = 1/[AP(D^\gamma)V^{\beta-1}]$ consistent with our generalized scaling law of $J_{SCL} \propto V^\beta/D^\gamma$, where A is the area of the diode, P is a perveance that functionally depends on the details of the geometry including the gap spacing D, and V is the applied voltage linearizing Eq. (24) yields

$$\left(\frac{d^2}{dt^2} + \frac{\omega_0}{Q}\left[1 - \beta\frac{R}{Z_D}\right] + \omega_0^2\right)V_{rf}(t) = 0. \qquad (25)$$

This equation is a simple second-order differential equation that gives the condition for the growth of the time-dependent electromagnetic signal as a function of the characteristics of the space–charge limited emission, be it classical CL, quantum, MG, or any of the other conditions described above in this article, and the impedance of the electromagnetic mode. This condition is simply $Z_D < \beta R$.

While it has been shown that this scaling works well for classical Child–Langmuir macroscopic gaps, it would be interesting to also study the validity of this model in nanogaps under quantum space–charge limited emission or thermo-field emission. The exponential dependence of Fowler–Nordheim to the surface electric field raises interesting questions on the role of convection and displacement current in nanogaps.

As can be seen from this analysis, the role of the electromagnetic mode supported by an RF circuit is critical in describing the full time evolution of the flow. One can imagine similar critical details, such as a return current path, where the image current encounters an inductor, in effect, as providing important details to fully describe the evolution of the time-dependent flow.[29] The full behavior can be very complicated—for example, a change in the transit time for the same electromagnetic circuit results in highly different beam wave interaction.[30] In this Perspective, we have chosen to focus our attention on the gap itself and determine threshold conditions where more complex behavior comes into play [see, e.g., the threshold of instability due to transit time oscillations as shown in Eq. (25)]. Beyond this critical point, we point the reader to the literature,[210–213] where self-consistent numerical tools such as density functional theory[192] and particle-in-cell methods[214,215] are needed to understand the detailed nuances of the time-dependent flow.[212,213,216,217]

C. Time-dependent photoemission from metal nanotips to space–charge limited current

Photoelectron emission from metal nanotips driven by ultrafast lasers offers an attractive route to generate high brightness, low emittance, and spatiotemporally coherent electron bunches, which are central to time resolved electron microscopy,[218,219] free-electron lasers,[220] carrier-envelope-phase (CEP) detection,[221] and novel nanoelectronic devices.[222–225] To extract as much current as possible from a photoemitter, the space–charge effect would become important. Due to the oscillating nature of the laser fields, photoemission is intrinsically a time-dependent process.

The modern treatment of nonlinear photoemission started with the seminal work of Keldysh,[226] who distinguished different intensity-dependent photoemission mechanisms through the Keldysh parameter $\gamma = \sqrt{W/2U_p}$ with W being the cathode work function and $U_p = e^2F^2/(4m_e\omega^2)$ the ponderomotive energy, where

e is the elementary charge, m_e is the electron mass, and F and ω are the optical electric field strength and frequency, respectively. When $\gamma \gg 1$, the optical field strength is relatively small and multiphoton absorption induced electron emission dominates; whereas, when $\gamma \ll 1$, the optical field is sufficiently strong such that photoemission approaches quasi-static tunneling, with emission current following the Fowler–Nordheim equation.[227] Since Keldysh, strong-field nonlinear photoemission has been extensively studied both theoretically and experimentally by many groups across the world. For a comprehensive overview of the literature, one may refer to recent review articles[209,228–230] and references therein. Some recent studies may be found in Refs. 221,231–236,204,237,238. It is shown that the photoelectric scaling breaks down when the optical fields approach a few cycles (sub-10 fs),[235] or when the photon energy approaches the work function at increased optical intensity.[239] Non-equilibrium heating is also important for metals for sub-100 fs pulses.[234]

Recently, analytical quantum mechanical models have been developed to study the highly nonlinear photoemission induced by continuous wave (CW) lasers by solving the time-dependent Schrödinger equation (TDSE) exactly.[77,204,205,233,239–241] Various emission mechanisms, such as multiphoton absorption or emission, optical, or DC field emission, and the transition among them, are all included in a single formulation.[204] The model was later extended to study ultrafast strong-field photoelectron emission due to two-color laser fields, which is predicted to be able to modulate not only the electron energy spectra but also the emission current up to 99% due to the interference effects between the two lasers,[205,240] in excellent agreement with experimental measurements.[242] The interference modulation of photoemission driven by two lasers of the same frequency was also examined.[241] The quantum model predicts that quantum efficiency (QE) increases with the laser field strength in the longer laser wavelength range due to the increased contributions from multiphoton absorption processes.[239] Plasmonic resonant photoemission from dielectric coated metal emitters was also investigated to increase QE,[77] where optical field tunneling can be accessed at a significantly reduced incident laser intensity. The effect of thin-film coating on field emission was also studied.[243] Most recently, an exact quantum theory is developed for ultrafast photoelectron emission from a DC-biased surface induced by laser pulses of arbitrary duration, ranging from sub-cycle to continuous wave, which is valid from photon-driven electron emission in low intensity optical fields to field-driven emission in high intensity optical fields.[244]

While these models give a precise description of the time-dependent dynamics of photoemission based on the exact solution of the TSDE, they do not take into account the space–charge effect, which is expected to play an important role, especially during high current electron emission. Further work is needed to study the space–charge effect in the time-dependent photoemission process and to determine the conditions under which the above models become invalid. The transition from time-dependent photoemission to time-dependent SCL emission also requires future studies.

In addition to photoemission from nanotips, there has been strong recent interest in electron transport in nanoscale gaps triggered by ultrafast lasers.[27,206,209,230,245–250] The tunneling current in the nanogaps depends on the applied electric field and on the gap distance with high nonlinearity, where the shape of the tunneling potential barrier is modulated by the applied electric fields, which may consist of both the DC-biased field and the time-varying optical field due to the ultrafast laser. Direct control of ultrafast electron transport in nanoscale gaps has been demonstrated in recent proof-of-concept experiments,[246,247] as shown in Fig. 7. It is clear that the tunneling current depends strongly on the laser intensity, carrier-envelope phase of the laser, and bias voltage, which offers strong flexibility to precisely control the electron dynamics in nanoscale condensed matter systems. The optically rectified tunneling current is envisioned to open new ways to petahertz electronics operating at optical frequencies, and strong-field nano-optics.[209]

Increasing the efficiency requires extracting as much tunneling current as possible in such ultrafast tunneling junctions. Currently, the effect of space charge, which is expected to become increasingly important for higher current, is rarely studied in these devices. It would be interesting to test if space-charge could cause the saturation behavior of current under strong fields [e.g., Fig. 7(b)] and if it is possible to achieve SCL operation[26,28] in such ultrafast nanodiodes. Recently, spatially confined THz electric fields exceeding 10 V/nm in a nanogap in a scanning tunneling microscope (STM) were achieved to drive the electron emission current into the nonlinear SCL saturation regime (Fig. 8),[26,251] confirming the theoretical predictions.[26]

Another important aspect of SCLC with oscillating gap voltage is the possibility to overcome the time-averaged CL law.[36,37,252,253] It would be interesting to see if such theoretical predictions can be realized in ultrafast laser triggered nanogaps.

D. Time-dependent space–charge limited current in air and liquid

While space–charge limited current (SCLC) is less well studied in gases and liquids than in vacuum, we may provide some initial thoughts based on the comparison of the electron force laws that may be used to derive SCLC from single-particle trajectories in vacuum[55] and in gases[56] and liquids.[117] In general, we may write the electron force law as[56,117]

$$m\frac{dv}{dt} = e\frac{d\phi}{dx} - \frac{ev}{\mu}, \tag{26}$$

where m is the electron mass, v is the electron velocity, e is the electron charge, v is velocity, t is time, and μ is electron mobility, which is, in general, a function of the electric field and pressure and varies from medium to medium (gas to gas, liquid to liquid, or phase to phase). Typical calculations assume constant μ for first order approximations.[56,115,117] In the limit of $\mu \to \infty$, one recovers the vacuum condition.[56] Equation (26) shows the physically obvious effect that reducing μ reduces v due to collisions. Although studies on time dependence have yet to be carried out for collisional gases or liquids, we may anticipate that these added collisions will provide a "lag" in time-dependent effects compared to vacuum. The situation may become more complicated when compared to vacuum due to the complicated behavior of μ as a function of pressure and electric field for liquids and gases. Future studies examining such phenomena are increasingly important for air (and other gases) due to the increasing importance of short-duration electric pulses for microscale and smaller
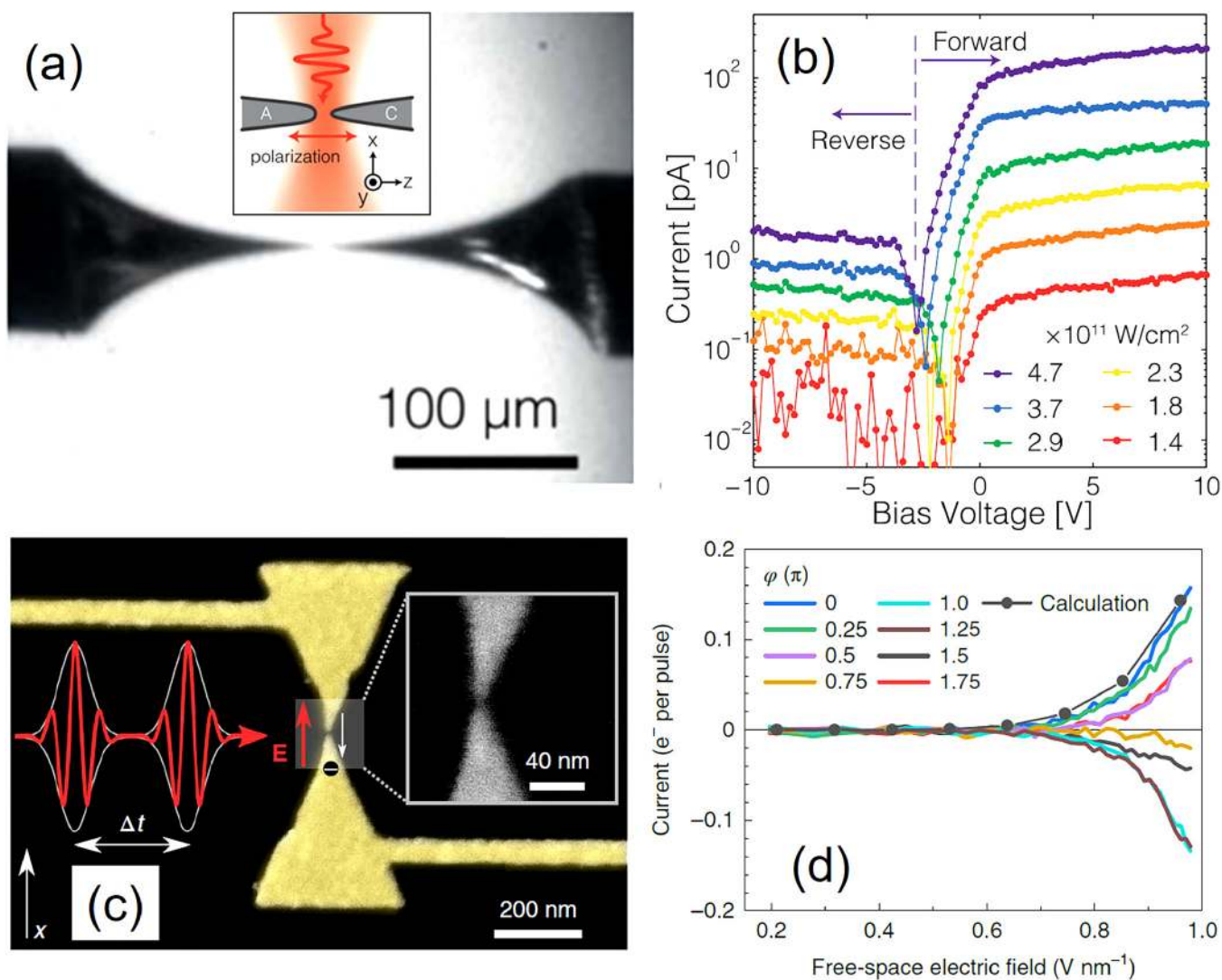
FIG. 7. Nanoscale vacuum-tube diode triggered by ultrafast lasers. (a) Optical microscopic image of the two metal nanotips facing each other. Inset: schematic of the two tips in the focus of a few-cycle laser pulse. (b) Laser-induced current between the two tips as a function of the bias voltage with different laser intensity. (c) Two single-cycle light pulses focused on a nanocircuit of Au optical antenna with electrical leads on a fused-silica substrate. Inset: an enlarged view into the gap region. (d) The pulse-averaged current as a function of the free-space amplitude of the electric field of the laser pulse. The phase φ is directly related to the far-field carrier-envelope-phase (CEP) of the driving pulse. The line with dots is for the theoretical calculation using the time-dependent density functional theory (TDDFT). (a) and (b) Reproduced with the permission from Higuchi *et al.*, Appl. Phys. Lett. **106**, 051109 (2015). Copyright 2015 AIP Publishing LLC. (c) and (d) Reproduced with permission from Ludwig *et al.*, Nat. Phys. **16**, 341 (2020). Copyright 2020 Springer Nature.

gaps[100,101,254] and microwave microscale breakdown, which remains incompletely understood due to the added complexity of frequency effects[255,256] on avalanche and on electron emission, which plays a pivotal role in DC microscale gas breakdown.[100,101,254] Future theoretical work could involve deriving analytic scaling laws to characterize the relative importance of the AC frequency, pressure, gap distance, and electrode characteristics (work function and field enhancement) on gas breakdown for microwave fields and further determine the temporal behavior under these conditions, which would likely be equally relevant for liquids for emission behavior.

IV. MULTI-DIMENSIONAL AND HIGHER-DIMENSIONAL EFFECTS

A. Finite emitter area effects

The classic form of the Child–Langmuir law is derived for a planar diode of infinite extent.[1] Later work extended this to
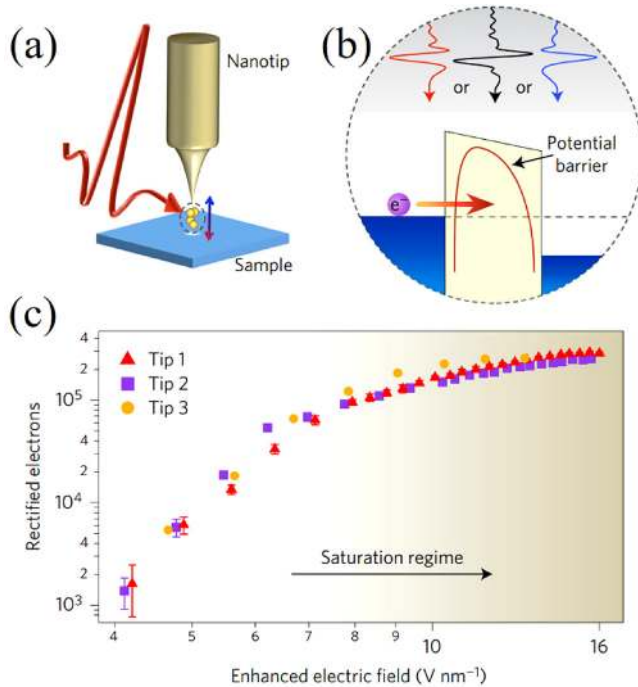
FIG. 8. (a) Schematic of the experimental setup for THz STM, (b) electron tunneling between a nanotip and a sample under the influence of an electric field, (c) gap current saturation under strong electric fields without DC bias for different tips. Reproduced with permission from Yoshioka *et al.*, Nat. Photonics **10**, 762 (2016). Copyright 2016 Springer Nature.

FIG. 9. Current from an emitting area of finite radius for an applied field of 1 MV/m and different aspect ratios (α). Solid curves are obtained from simulation. Dashed lines labeled as I_{2d} are calculated from Eq. (28). The dotted line is obtained from the point emitter Coulomb blockade model. The horizontal solid line is obtained from the multiple electron point emitter model. Reproduced with permission from Gunnarsson *et al.*, IEEE Trans. Electron Dev. **68**, 342 (2021). Copyright 2021 IEEE.

different geometries, but assuming uniform current density over the cathode.[257,258] For most practical cathodes, current is drawn from a finite area outside of which there is no space–charge. Significantly, the limiting current may be markedly affected by the absence of space–charge beyond the emitting region,[8,9] and the current density may be considerably higher at the edge of the emitter than it is in the central region.[12] An elegant analysis showed that the space–charge limited current from an emitter of finite area, J_{2DCL}, has the form,[8,9,11]

$$J_{2DCL} = J_{CL}(1 + G), \qquad (27)$$

where G is a geometrical factor determined by the shape of the emitting area, the gap spacing of the diode, and the characteristic width of the emitting area, and J_{CL} is the Child–Langmuir current density. Importantly, Eq. (27) assumes that the current density is uniform over the emitting area and that the beam does not spread laterally. Although Eq. (27) generally agrees with simulation, it is not expected to be applicable to emitting areas of microscopic length scale or if the ratio of the diode gap spacing to the characteristic width is very large. Recent simulations and analysis by Gunnarsson *et al.* has shown the deviation of the SCLC from Eq. (27) for microscopic emitters.[259] The main results of that work may be summarized as follows. For a finite emitting
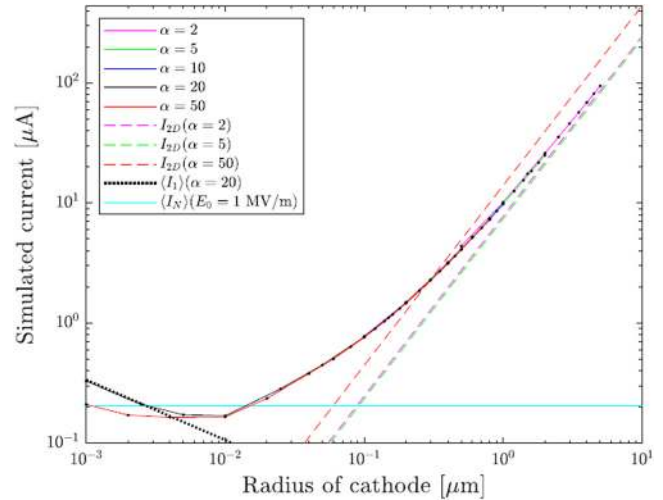
area of radius R embedded in the cathode of an infinite, planar, diode of gap spacing D, the conventional theory predicts the space–charge limited current to be

$$I_{2D} = \frac{\pi}{9}\varepsilon_0\sqrt{\frac{2q}{m}}E_0^{3/2}\left(\frac{4}{\sqrt{\alpha}} + \sqrt{\alpha}\right)R^{3/2}, \qquad (28)$$

where E_0 is the electric field in the absence of space–charge and $\alpha = D/R$ is the aspect ratio of the system. Gunnarsson *et al.* found that the actual current transitions from a point emitter regime, for very small emitter areas, through an intermediate regime where the current is generally higher than predicted by Eq. (28), to asymptotically scaling with emitter radius as predicted by Eq. (28) as shown in Fig. 9.

Note that the minimum value of current is very close to that predicted by a model where there are a number of electrons present in the diode gap emitted from the same point emitter. The predicted minimum is given by

$$I_N = \left(\frac{q^5\pi\varepsilon_0}{2m^2}\right)^{1/4}E_0^{3/2}, \qquad (29)$$

which is independent of radius and gap spacing. If the diode gap is small enough that it can only accommodate one electron, the point emitter model must be adjusted to reflect that and the average

current in the diode becomes

$$I_N = \sqrt{\frac{q^3 E_0}{2m\alpha R}}. \tag{30}$$

Figure 9 shows how the simulated current agrees with Eq. (30) at very small radii. Finally, it is of interest to note that the current obtained from simulation is generally higher than that predicted by Eq. (28), the exception being for large aspect ratios and greater values of the emitter radius. On a related note, it can be seen that the current curves for large aspect ratios converge asymptotically with those of lower aspect ratio. This is most likely due to transverse expansion of the beam near the cathode resulting in an "effectively lower" aspect ratio for a given gap spacing.

Similarly, the equilibrium current density for space–charge influenced field emission increases with decreasing emitter dimension and shows enhanced emission at the boundary of the emitting area,[195] although this has not been investigated thoroughly for such small emitter sizes that the point emitter model applies.

As will be discussed later in the context of inhomogeneous cathodes, the physics of the two-dimensional Child–Langmuir law can be used to explain the performance characteristics of diodes with a heterogeneous work function on the cathode, whether they are subject to field emission or thermionic emission.[198–200]

B. Analytical protrusive CL law

While calculating space–charge limited current (SCLC) is well established for planar geometries by the Child–Langmuir law,[1,2,70] most practical devices are not simply planar diodes. This issue was recognized over a century ago, motivating research by Langmuir and Blodgett to derive equations describing SCLC for 1D concentric cylinders[257] and spheres;[258] however, these equations require a series expansion whose accuracy deteriorates as the ratio of the anode radius to cathode radius diverges from unity. Subsequent studies have attempted to improve upon these theories by applying numerical methods,[260–265] deriving transit time models,[6,266] or deriving analytical approximations assuming no space–charge.[267,268] Even then, such approaches are often limited when dealing with other geometries, such as the simple case of a pin-to-plate geometry, or, thought another way, a diode comprised of a flat, planar cathode and an anode with a surface protrusion, which has been solved numerically.[13] Another example is a recent study examining SCLC for two curved electrodes that applied the nonlinear line charge model to show that $J_{SCL} \propto \gamma_a V^{3/2}/D^2$, where γ_a is the apex field enhancement factor of the curved emitter.[269] The lack of exact, analytic solutions from first-principles for these relatively simple deviations from planar geometries demonstrate the need for a standard means of calculating SCLC for non-planar diodes in general.

One approach undertaken to address this challenge applied variational calculus to derive exact, closed-form solutions for SCLC in 1D planar, cylindrical, and spherical coordinate systems by starting from a coordinate system invariant representation obtained from first-principles.[270] This required writing an appropriate Euler–Lagrange equation and selecting an appropriate parameter to minimize, which was selected to be the energy deposited into the system as represented by determining the average current with respect to

the path length across the gap. Coupling this with the conservation of electron energy, Poisson's equation, and continuity yields

$$\nabla^2 \phi = \frac{|\nabla \phi|^2}{4\phi}, \tag{31}$$

where ϕ is the electric potential across the gap, which is a function of position. Using this approach gives

$$J_{SCL} = \frac{4V_g^{3/2}\epsilon_0 \sqrt{2e/m}}{9\bar{D}^2}, \tag{32}$$

where $\bar{D} = D$, $R_C \ln(\bar{a})$, and $a_b|R_a - R_c|$ for planar, concentric cylinder, and concentric spherical geometries, respectively, $\bar{a} = R_c/R_a$, R_c is the cathode radius, and R_a is the anode radius.[270] This approach has recently been applied to a pin-to-plate geometry to obtain[271]

$$\frac{J_{SCL}^{tip}}{J_{CL}} = \frac{\beta(1+\beta)}{(\ln(\sqrt{1+\beta} + \sqrt{\beta}))^2}, \tag{33}$$

where $\beta = (D/R)^{1/2}$, with R the radius of the pin (or protrusion) in a pin-to-plate (or plate to protrusion) geometry.

Note that variational calculus will fail when one cannot write expressions for $\nabla\phi$ or $\nabla^2\phi$, which may occur for curvilinear electron flows, for which few analytic solutions exist,[272,273] or more complicated geometries.[274] To address this, one may apply conformal mapping, which has been used to model electron emission for non-planar geometries,[80,275] but not systematically to derive SCLC for such scenarios. A recent study demonstrated that conformal mapping can recover J_{SCL} for concentric cylinders by mapping to a planar geometry.[276] More complicated 1D geometries were then derived based on using conformal mapping to translate them either to a planar or cylindrical geometry.[276] Ongoing studies are applying conformal mapping to generalize the pin-to-plate geometry described above to pin-to-pin, which may be subsequently modified to address curved electrodes,[269] and the effects of tilted pins (e.g., misalignment), which would be challenging using variational calculus due to the complications involved in determining $\nabla\phi$ and $\nabla^2\phi$. Conformal mapping is also used often for 2D geometries, as demonstrated by prior work deriving an approximate solution of ϕ in 2D.[277] This may suggest the potential feasibility of using conformal mapping to derive SCLC in 2D geometries, starting from planar geometries[8,9] and potentially extending this approach to more complicated geometries as described above for 1D.

C. Fractional models of CL law, FN law, and MG law

Most revised CL laws, such as the 2D or 3D CL law[8–13] or the well-defined sharp tip—protrusive CL law,[70] have focused on a flat electrode with the finite emission area. For practical cathodes, the roughness of cathode is difficult or computationally expensive to simulate. Using the techniques of fractional calculus, a fractional CL law[278] has been recently formulated. In the model, the roughness of the cathode is modeled as a "fractional slab" with a parameter α (≤ 1) and the specific values of α can be determined by the box-counting method for a given image of the cathode's roughness. Here, $\alpha = 1$ is the limiting case for a perfect flat cathode, and the

roughness increases with small values of $0 < \alpha < 1$. Figure 10 shows that for a rough cathode[272] with $\alpha = 0.934$, the SCLC $J(\alpha)$ is enhanced over the CL law J (at $\alpha = 1$), and the enhancement is larger for small gap spacing D. This implies that the scaling of gap spacing $J_{CL} \propto D^{-2}$ from the classical 1D CL law no longer holds for a rough cathode if the degree of roughness is not eligible as compared to the gap spacing D. The model compares well with the experimental results at $D = 4$ mm and $D = 8$ mm, which gives enhancement factors of 1.5 and 1.25, respectively.[279]

At low voltage (where the SCL condition is not reached), a rough cathode may operate at the field emission regime. However, the traditional field emission formulated by the Fowler–Nordheim (FN) law[227] is valid for a flat cathode and an arbitrary field enhancement factor is assigned to enhance the surface electric field to account for the roughness. To resolve this inconsistency, a fractional FN law has been formulated[280] as

$$J_{FN}(\alpha) = A \times \frac{F^{2\alpha}}{\Phi^{2\alpha-1}} \exp\left(-\frac{B \times \Phi^{0.5+\alpha}}{F^{\alpha}}\right), \quad (34)$$

where A and B are constants are FN-like coefficients that depend on $0 < \alpha \leq 1$ to account for the degree of roughness. At $\alpha = 1$ (zero roughness), it will converge to the normal FN law. To characterize the measured field emitted current I (instead of J) as a function of applied voltage V (instead of the electric field), it is suggested to use a fractional FN law in the form of

$$I = CV^{2\alpha}\exp(-D/V^{\alpha}), \quad (35)$$

where α is determined by the y-intercept of $d[\ln(I/V^2)]/d[\ln(V)] = 2\alpha - 2$. From the obtained values of α, the corresponding electric potential (and its electric field) near the emitting surface can be calculated, as shown in Fig. 11 for $\alpha = 1$ (flat surface) and $\alpha < 1$ (rough surface). Thus, the *average* electric field enhancement for the entire rough surface is self-consistently determined once the values of α are determined by using the newly suggested FN plotting in Eq. (35).

With the fractional CL and FN laws,[278,280] it is now possible to construct a smooth transition model from field emission (at low voltage) to CL law (at high voltage) for a rough cathode, which is similar to a prior paper[55] developed for a flat cathode. Such an analytical or semi-analytical universal model will be extremely useful to be included as a fast emission algorithm to be used in any PIC simulation or gun codes to avoid the computationally expensive fine-meshes required near to the electrode surface. The results of such a transition model will be published in a separate paper.

For SCLC transport in a solid like organic material having disordered properties, a fractional SCLC model is developed recently for both trap-free and trap-filled porous solids.[281] For a trap-free solid, the 1D fractional MG law is

$$J_{MG} = \frac{9}{8}\mu\varepsilon\left[\frac{\alpha \times \Gamma(\alpha/2)}{\pi^{\alpha/2}}\right]^3 \frac{V^2}{D^{3\alpha}}, \quad (36)$$

where $\Gamma(\alpha)$ is the gamma function. At $\alpha = 1$, Eq. (36) recovers the classical MG law. The MG law is inversely proportional to $D^{3\alpha} = D^3$ with $\alpha = 1$ for a perfect solid. However, in using the newly developed fractional MG law to compare with various experimental results of SCLC measurements in organic materials, we have $\alpha = 0.83$–0.97, thus confirming that the D^{-3} scaling of the MG law is no longer valid of porous solids. Using the correct values of α, the models also give better agreement for the carrier mobility.[281] Note that any errors occurring in the mobility would greatly affect the design of organic
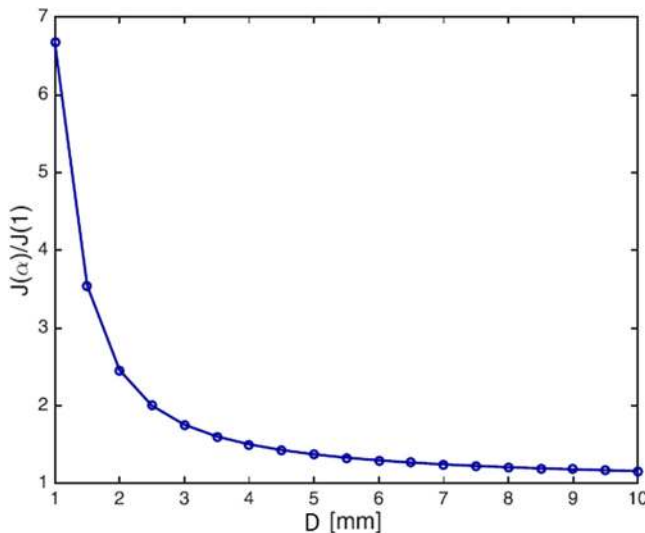

FIG. 10. The enhancement of the fractional CL law (over the 1D classical CL law) at 1 kV. Reproduced with permission from Zubair and Ang, Phys. Plasmas **23**, 072118 (2016). Copyright 2016 AIP Publishing LLC.
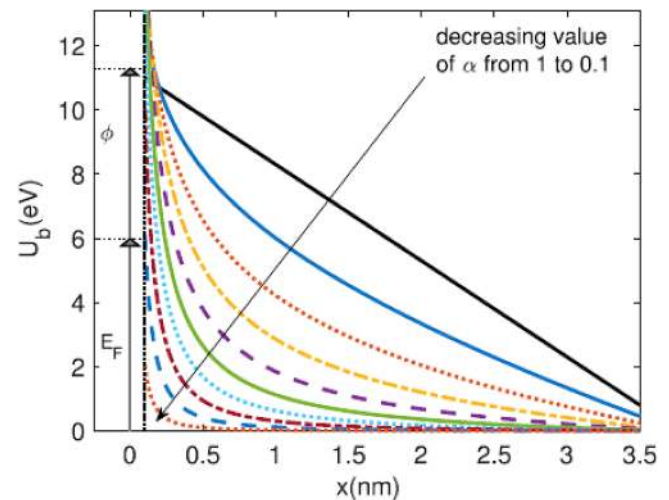

FIG. 11. Electric potential for a surface of the work function of $\Phi = 5.3$ eV, E_F (Fermi energy) = 6 eV, and applied field $F = 3$ V/nm (at a flat surface with $\alpha = 1$). Reproduced with permission from Zubair *et al.*, IEEE Trans. Electron Device **65**, 2089 (2018). Copyright 2018 IEEE.

materials-based devices, such as organic light emitting diodes (OLEDs), organic transistors, and other SCL solid-state devices.

This section has introduced some recent studies in using fractional calculus in modeling charge injection and electron emission such as the fractional CL law,[278] fractional FN law[280] and fractional MG law.[281] Such approaches can be applied to account for the interface roughness in 2D-material's contact with electrodes for which the nano-scale roughness cannot be ignored due to the "atomic-scale" thickness of the 2D Dirac based materials. Thus, fractional modeling is ready to be used for the recent Dirac materials-based electrical contact and others.[91,167,170] In fact, a fractional model to calculate the exciton binding energy of 2D materials has been shown to have good agreements with prior results.[282] A fractional Fresnel model for light absorption on a rough metallic surface also agrees with experimental results.[283] In the future, it is also of interest to apply this concept to expand the classical photocurrent SCLC model[40,41] to a fractional model for organic materials.

D. Multi-dimensional SCLC in solids and interfaces

Based on the concept of the 2D and 3D CL laws developed,[8,9] their enhancement over the 1D models can be written in a general form[11,45] of $J_{SCL}/J_{SCL}[1D] = 1 + F \times G$, where F is a parameter measuring the normalized average position of the electron charge density inside a diode of spacing D at the SCLC condition. For example, we have $F = 1/4$ for the classical CL law[11] and $F = 1/3$ for the classical MG law (trap-free solid), and $F = 1/(l+1)$ for a trap-filled solid, where the value of $l > 1$ characterizes the energy distribution of the traps.[45] Here, G is a geometrical parameter to characterize the size and shape of the emitting areas on a *flat* cathode. For an infinitely long strip of the emitting patch of width W, we have $G = (4/\pi)/(W/D)$. Other forms of G can be referred to a prior paper.[11]

An extension of the SCLC model for a diode in a thin-film geometry (using 2D materials) has been performed by Grinberg *et al.* using a Green's function approach.[284] In the thin-film limit, the classical trap-free SCLC becomes

$$J_{thin\text{-}film}(V, L) = \xi_{2D}\epsilon\mu\left(\frac{V}{D}\right)^2, \tag{37}$$

where ξ_{2D} is a contact-geometry-dependent parameter that is numerically equal to 0.57, 0.70, and 1.0 for three different settings: edge, coplanar, and perpendicular plane contacts, respectively. Here, the thickness scaling of the SCLC is modified to $J_{thin\text{-}film} \propto D^{-2}$, in contrast to that of the classic MG law, i.e., $J_{MG} \propto D^{-3}$. Using a similar theoretical framework, the SCLC model of an ultrathin-body 2D Dirac semiconductor has also been developed,[161] yielding an *equal* scaling of $\beta = \alpha$ (see, Sec. II E, too),

$$J_{Dirac}^{(2D)}(V, L) \propto \left(\frac{V}{D}\right)^{\alpha}. \tag{38}$$

Here, the voltage and length scaling of the SCLC varies synchronously between $\alpha = 3/2$ and 2. The *equal* scaling of SCLC with respect to bias voltage and device length represents another signature of SCLC in 2D Dirac materials that is unfound in bulk solids.

There are relatively few studies[46] examining the transition of SCLC in a solid for a finite emission area at the interface between the metallic injecting electrode and the dielectric slab. Such an interface property is expected to play an important role for a nano-size diode where the scale of roughness cannot be ignored compared to the thickness D. Depending on contact properties, various charge injection mechanisms such as the Ohmic contact and Schottky contact for an imperfect interface should be developed to study such transition to SCLC. One way is to use the fractional modeling approach that has been discussed above. By combining the approach of the fractional MG law[280] for the issue of a geometrically imperfect interface, one may be able to develop a consistent model to study the source-limited injection (at low voltage) to SCLC (at high voltage) for a metal–dielectric interface. Note the effects of finite particles and Coulomb blockade will be important for a nano-scale diode too, as shown in the transition of field emission to the CL law.[14,32,38,195] Thus, it is of interest to extend such finite particle effects for SCLC models of solids.

As mentioned above, the degree of the surface or interface roughness would become comparable to or even larger than the thickness of the solid when its thickness decreases to a few atomic layers, and thus the effects of roughness will become increasingly important. It is found that the presence of contact interface roughness, in the form of fluctuating Schottky barrier heights in the contact region, can significantly reduce the contact resistance of MoS$_2$/metal Schottky 2D/3D contacts.[91] It is important to examine if such benefits of interface roughness for reducing contact resistance can still exist if the electrical contacts are operated under the SCLC injection condition. For nanoscale diodes, the geometry of the contacting electrodes plays an important role.[90–93] Current injection at material contact interfaces and the associated current crowding effects due to current constriction or current spreading near the electrical contacts have been characterized using various models, such as simple transmission line models (TLMs)[285,286] and field solutions.[90,95,287–292] By solving a two-dimensional TLM coupled with the local interface current injection consistently, we have examined the nonuniform current distribution in nanoscale electrical contacts for both Cartesian parallel contacts[90,91] and circular contacts.[92] It is also proposed to mitigate current crowding effects by designing contact interfaces with spatially varying contact resistivity.[93] Significant future research is needed to investigate SCLC transport in these higher-dimensional diode configurations, along with the impact of electrode surface morphology,[80] electrode geometry irregularity,[293,294] and different contact setups.[295] These geometrical effects will inevitably influence the SCLC properties in solid and interfaces. Finally, the dynamics of time-dependent SCLC in solid is less explored that we speculate that it will be an interesting topic for future studies. For example, a recent paper just reported the probing of metastable space–charge potential in a wide bandgap semiconductor.[296]

E. Inhomogeneous cathodes and Miram curves

As described previously in this paper, the magnitude and distribution of current drawn from a bounded area on the cathode can be substantially different from that of a boundless emitter.[8,9,11,195,259] Current density is generally higher at the edge of the emitting area

than for the interior region of the emitter. Nonetheless, the current density from the interior of the bounded emitter will exceed that from a boundless emitter with the same operating parameters. Another important fact is that separate, bounded, emitters will interact via mutual space–charge interaction if they are not too far apart.[297,298] In essence, if we consider two emitters that we may call A and B, then the space–charge that is due to current drawn from emitter A will affect the local electric field on emitter B and vice versa.

If we consider a macroscopic cathode that has a microstructure, such that the work function varies across the cathode surface, it may be construed to be an assembly of individual emitters that interact via mutual space–charge effects. This viewpoint has been used to explain the physics of transition from source-limited flow to space–charge limited flow in thermionic cathodes, e.g., the shape of the so-called Miram curve that describes current as a function of temperature in thermionic cathodes. We may look at this problem in some more detail.

A one-dimensional model of a thermionic diode assumes that the current density across the cathode is uniform and can be described by the Richardson–Dushman law for thermionic emission until it reaches the limit set by the Child–Langmuir current density. From this, one would expect a sharp transition between the two emission regimes. For real thermionic cathodes, this is not the case as they exhibit a much smoother transition from source-limited to space–charge limited emission as is shown schematically in Fig. 12.

Longo[299] introduced a simple transition model that was later modified by Vaughan[300] to describe the observed current density, J, in terms of the Richardson–Dushman current, J_{RD}, the Child–Langmuir current density, J_{CL}, and an empirical parameter, α,

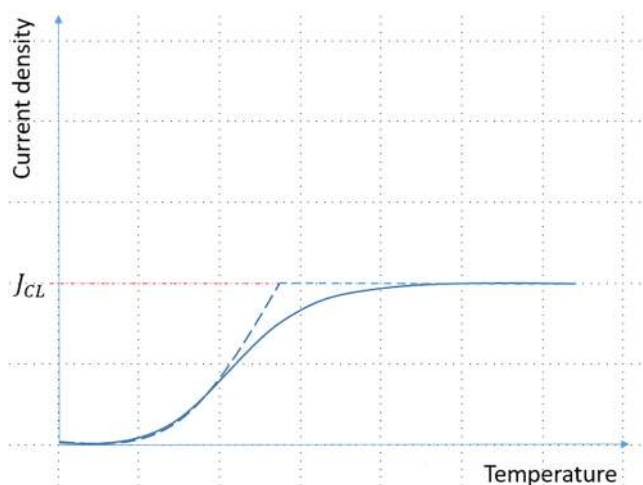$$J^{-\alpha} = J_{RD}^{-\alpha} + J_{CL}^{-\alpha}. \tag{39}$$

FIG. 12. Schematic diagram of Miram curve. The dashed blue line shows the Miram curve expected by the one-dimensional model, the solid blue line shows the "realistic" Miram curve, and the red dotted line shows one-dimensional Child–Langmuir limiting current density.

Longo later postulated that parameter α was related to the surface uniformity of the cathode and that it could be used to explain cathode aging in terms of changing uniformity.[301]

Chernin et al.[200] constructed a 1½ dimensional model of a thermionic diode consisting of an infinite planar diode constructed of a periodic array of parallel strips of finite width with varying work function. They used this model to solve Poisson's equation numerically and showed how current is initially drawn preferentially from the strips with low work function as if they were separate emitters of finite width. As the temperature increases the current density from those strips with higher work function increases and the resulting space–charge affects emission from the low work function strips in such a manner that the current density across the cathode becomes uniformly equal to the Child–Langmuir current density and the Miram curve exhibits a smooth transition region. It is noteworthy that even if some of the strips were non-emitting, the average current density would eventually be equal to the Child–Langmuir current density when the cathode temperature was high enough. This model fit simulations using the code MICHELLE very well. A follow-up paper[302] has extended this work to a 2 ½ dimensional model of an infinite planar diode where the regions of different work functions are comprised of finite squares rather than semi-infinite strips of finite width.

Sitek et al. used a molecular dynamics approach, with a self-consistent thermal-field emission mechanism based on the work of Jensen[181] to simulate thermionic emission from a finite, yet inhomogeneous, area embedded into a planar cathode.[198] These simulations exhibited much of the same physics observed by Chernin et al., namely, how the microstructure in the cathode causes rounding of the Miram curve; how the initially nonuniform current density becomes more uniform with rising temperature; and how the ultimate current limit is set by the Child–Langmuir limit (though in this case it is determined by the *two-dimensional* Child–Langmuir law rather than the one-dimensional Child–Langmuir limit). Sitek et al. also showed that for a bounded emitter area, the Miram curve will be rounded for a uniform work function. This is presumably because such a diode has a higher current density at the emitter edge than at the interior. Sitek et al. also investigated beam quality in terms of *emittance* and *brightness*. They showed that a fine grained cathode is superior to a coarse grained one in terms of the beam quality and that a given cathode has an optimal temperature for maximum beam brightness that is in the transition region of the Miram curve.

Chen et al.[303] have examined a checkerboard model similar to that studied by Sitek et al. This work shows the same effect of space–charge and inhomogeneous work function on the Miram function as is observed by Chernin et al. and Sitek et al., but Chen et al. also provides a more extended study of the effect of Schottky lowering of the surface barrier. The Schottky effect is of minimal importance when considering the Miram curve for a fixed temperature, but is important when looking at the effect of increasing the applied potential for a fixed cathode temperature. It should be kept in mind that the emission model used by Chen et al. is an over-barrier emission model, and tunneling effects that are incorporated in Jensen's emission model incorporated by Sitek et al. could lead to higher current, though that is by no means certain.

The effects of an inhomogeneous work function on the cathode under field emission can also be investigated in a similar manner. Torfason *et al.* have conducted molecular dynamics based simulations similar to those of Sitek *et al.* for a planar diode with an emitting area of finite size and inhomogeneous work function.[199] The focus in this work was on how the disorder of the cathode affected current, emittance, and brightness of the beam drawn from the cathode for fixed diode spacing and voltage. They observed that a fine grained cathode gives a superior beam compared to a coarse grained one in terms of current and brightness; that the brightness and current characteristics of a low work function cathode can be improved by introducing a small fraction of non-emitting or high work function spots spread out over the cathode; that if the beam originates primarily from a few low work function *hot spots* it will have higher brightness, albeit with a lower current, if the low work function regions are closely spaced rather than spread out. Torfason *et al.* did not consider the *I–V* curves for the diode in this work to examine how inhomogeneity affects the transition from Fowler–Nordheim emission to Child–Langmuir Law emission, but previous work by Haraldsson *et al.*[298] on field emitting patches showed that mutual space–charge effects between them can be pronounced if they are closely spaced and that this effect becomes stronger as the applied field is increased. This suggests that work function inhomogeneity should influence the transition from Fowler–Nordheim to Child–Langmuir current in field emitting cathodes, although this has not been investigated thoroughly. Similar examination of how cathode inhomogeneity affects photoemission is also incomplete.

V. SELECTED APPLICATIONS OF SPACE–CHARGE LIMITED CURRENT

A. Nanodiodes and nano-transistors: From vacuum to air

Vacuum is intrinsically a better carrier transport medium than a solid because particles travel ballistically with minimum collisions in vacuum, whereas the carriers suffer from optical and acoustic phonon scattering in a solid, resulting in local heating and degradation in both signal quality and the physical device. Nanoscale vacuum gaps have been used as a conducting channel in nanodiodes and nano-transistors.[224,304–307] In particular, a nanoscale vacuum-channel transistor (NVCT) is a transistor in which the electron transport medium is vacuum. Instead of having a semiconductor channel between the source and the drain as in a traditional solid-state transistor, a NVCT has no material between the source and the drain; therefore, the current flows through vacuum. It is an emerging field due to the advantages of having vacuum condition (instead of materials) for application in space or other environments, where the radiation damages on materials are critical. Theoretically, a NVCT is expected to operate at fast speed (with the same feature size), but fabricating smaller dimensions and scaling to larger areas is challenging. The development has focused on using different types of field emitters or electron sources (comparable to nano-fabrication technology) such as silicon field emitters[306,308,309] and metal–oxide–semiconductor field-effect transistors with a vacuum channel of 20 nm.[310] While most of such NVCTs are designed to operate at low voltage

(field emission regime), it is interesting to note that SCLC operation has also been reported with a current output to the 3/2-power of the forward bias [see Fig. 3(b) in Ref. 310].

Reducing the device size to nanoscale causes the gap distance to approach the electron mean free path, which may vary from tens of nm to hundreds of nm depending upon gas pressure and other assumptions.[58,254,304,311] Thus, nanodiodes at atmospheric pressure may behave essentially as vacuum nano-transistors.[304,309] Han *et al.* fabricated a planar lateral air transistor that could be shrunk to ~10 nm, making it shorter than the electron mean free path so that it did not require vacuum and could achieve a cut-off frequency of 0.46 THz at an operating voltage below 10 V.[309] Another such device demonstrated a metal–oxide–semiconductor field-effect transistor (MOSFET) with an integrated vacuum chamber,[310] which combines the scalability and low cost of ballistic transport through vacuum with the reliability of conventional silicon transistor technology, while operating at atmospheric pressure.[304] Jones *et al.* addressed the challenges with achieving the high electric fields required for electron emission for these nanogaps by constructing CMOS compatible, integrable two- and three-terminal devices that operate near atmospheric pressure with single tip currents of hundreds of nA below 10 V.[312] Nikoo *et al.* demonstrated nanoplasma-enabled picosecond switches operating at atmospheric air.[313] Given the lack of material for electron transport, these vacuum-based circuits should be inherently "hard" to radiation, in addition to the obvious benefits in terms of speed of operation, suggesting the potential to develop electronics suitable for space and other radiation filled environments.

Driven by the recent advancements of nanofabrication and material synthesis techniques, 2D materials, such as graphene[184,185,314–316] and MoS_2,[317,318] hold enormous potential for designing nanoscale ultracompact emitters (compact, robust, chemical-inertness, and low work function) for NVCTs. Successful experimental demonstrations of graphene-based vacuum transistor devices have elucidated the role of 2D materials as a promising building block in NVCTs. Both surface-type[185] and edge-type[184,314–316] emitter geometries, where electrons are emitted from atomically sharp edges and the flat planar surface, respectively, are commonly employed in designing graphene-based vacuum transistors (see Fig. 13). An exceptional ON/OFF ratio of 10^6 with a low operating voltage range < 10 V and a subthreshold swing of 120 mV/dec has been demonstrated in a graphene surface-emission-type transistor device,[185] suggesting the potential of graphene-based NVCTs in electronics applications. Phototransistors capable of efficient 633 nm light sensing have also been demonstrated based on a sidewall electron emission in graphene/SiO_2[315] and graphene/Si[316] heterostructures. More recently, NVCTs based on 2D materials beyond graphene have also been actively explored. A recent proof-of-concept demonstration of 2D tin selenide (SnSe) in NVCT without being limited by SCL condition[319] further reveals the potential of the 2D-material family as a high-performance nanoscale emitter for NVCT applications.

Ideally, space charge is the major limiting factor for the operation of vacuum-channel conduction and requires systematic evaluation to optimize the design of vacuum-channel devices. The nanoscale vacuum-channel devices are found to be robust against high temperature and ionizing radiation, which hold promises for potential applications in high frequency devices, THz electronics, radiation tolerant space electronic circuits, and deep space communications.[306]
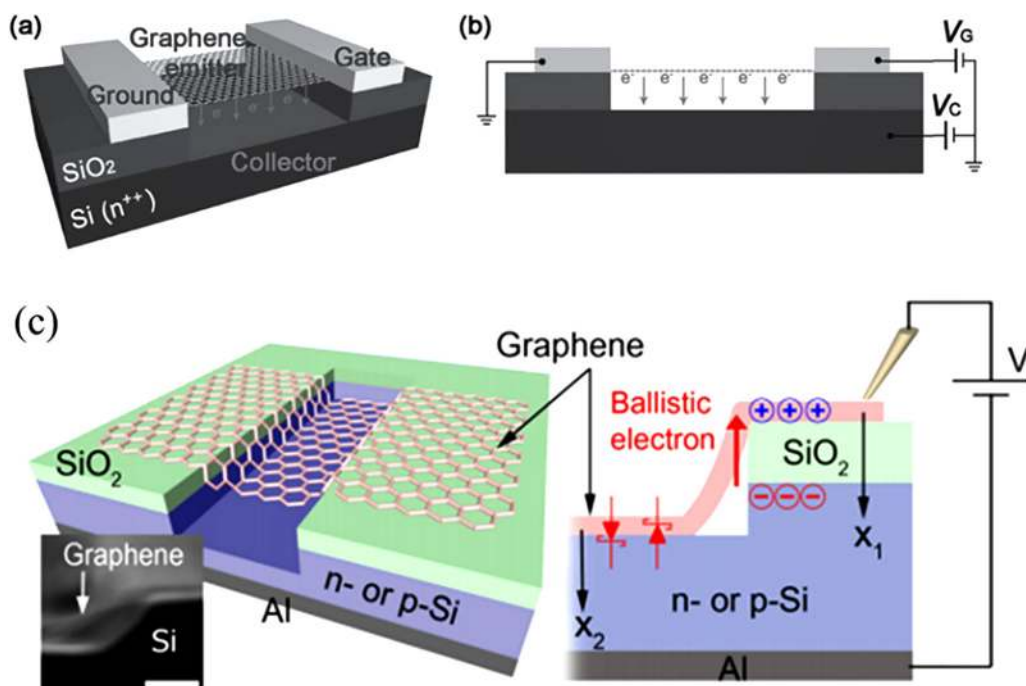
FIG. 13. Schematic drawings of graphene-based nanoscale vacuum-channel transistors (NVCTs). (a) and (b) A graphene-based vacuum transistor based on the planar surface-emission geometry. (c) Phototransistor based on the graphene/SiO₂ heterostructure. (a) and (b) Reproduced with permission from Wu *et al.*, Adv. Funct. Mater. **25**, 5972 (2015). Copyright 2015 Wiley. (c) Reproduced with permission from S. Srisonphan, ACS Photonics **3**, 1799 (2016). Copyright 2016 American Chemical Society.

In nanoscale gaps, as the applied voltage is concentrated in the very small space between electrodes, the resulting very high electric field would lead to ultrafast electron transfer, leading to extremely short time responses. Recent experiments demonstrated that nanogap based switches could achieve an ultrafast switching speed, higher than 10 V/ps, which is approximately two orders of magnitude larger than field-effect transistors and more than ten times faster than conventional electronic switches.[313] These emerging ultrahigh speed electronics based on nanoscale gaps would enable the broad applications of ultra-wideband signals and terahertz waves in quantum measurements,[320] imaging and sensing,[321] and high-data-rate communications.[322] Because of the absence of energy dissipation mechanisms (e.g., collisions and scattering) during carrier transport and the ultrafast response, these vacuum nanodevices may be designed to fulfill the hardware requirements of future data-centric computing with dramatically improved throughput and energy efficiency for artificial intelligence and machine learning.[323]

B. Microplasma transistors and beyond

Microplasma devices are very attractive because they can operate in harsh environments, have large off-to-on resistance ratios, can conduct large currents, operate under extreme environments (high temperature and in the presence of ionizing radiation), and can serve as reconfigurable antennas due to the tunability of

their electrically conducting paths.[324] These devices typically operate in the sub-Paschen regime, where plasma formation is no longer governed by the Townsend avalanche and Paschen's law but by ion-enhanced field emission.[49–51] One microplasma system developed metal oxide plasma field-effect transistors (MOPFETs) that used electric fields (gate voltage) to modulate the plasma current.[324] Applying a voltage on the gate modifies the charge density in the plasma to modulate the drain–source current.[324] Microwave excitation (up to a few GHz) of the plasma increased device lifetime by mitigating ion-sputtering that occurs during DC excitation. Additional studies have explored the development of microplasma transistors. Chen and Eden integrated a controllable solid-state electron emitter with a microcavity plasma to develop a three-terminal current-controlled device to modulate the microplasma's conduction current and light intensity.[325] The resulting system resembled an *n–p–n* transistor with the microplasma sheath analogous to the base of the transistor.[325] Another system leveraged the similarity between low temperature, weakly ionized plasmas in the gas phase and electron–hole (e⁻–h⁺) plasmas in semiconductors to develop an *n–p–n* plasma bipolar junction phototransistor.[326]

As gap distances decrease, electron emission will eventually transition from field emission to space–charge limited, whether at vacuum[55] or with collisions.[56,57] Theoretical studies indicate that emission at non-vacuum pressure transitions from field emission to space–charge limited emission with collisions (Mott–Gurney) to space–charge limited emission at vacuum (Child–Langmuir) with

reducing gap distance.[56–58] In fact, this theory showed that even with collisions, electron emission asymptotically approaches Child–Langmuir at a sufficiently small gap distance.[56] Recent experiments at atmospheric pressure with gaps from tens to hundreds of nanometers showed that electron emission may begin to exhibit space–charge effects prior to undergoing breakdown, unlike microscale gaps, which go directly from field emission to breakdown.[57,327] Thus, one may achieve "vacuum" behavior at the nanoscale, essentially achieving an atmospheric nanodiode, although challenges, such as the altering of emission properties due to gas adsorption on emission and collection surfaces at non-vacuum pressures,[304] remain.

As with the vacuum case, these devices should also be quite resilient to radiation environments. In principle, the radiation fields may allow even lower power operation by providing a natural source of free energy to partially ionize the gas in the micro-gaps.

C. Thermionic energy converters

Thermionic energy converters (TECs)[328] are devices that convert heat energy directly into electricity by driving hot electrons across a vacuum gap between two metallic electrodes, where one is the hot electrode (or cathode), which has a higher temperature than anode. Thermionic electrons are emitted from the cathode at a temperature T into the vacuum gap of spacing D. The heat energy carried by these electrons collected on the anode (colder electrode) is converted to electrical energy with an external load. The injected electron current density J follows the Richardson–Dushman (RD) law for bulk materials.[174,175] The theoretical efficiency of TECs (including energy loss, such as joule heating, radiation loss, etc.) can be high (>30%) at a power of approximately 100 W/cm^2. It is also required to have a difference of 1 eV or more between the work functions of the two electrodes for high efficiency.

However, such performance is difficult to realize, especially at lower operating temperature, due primarily to two effects: (a) relatively high work function of the robust cathode, which allows $T > 1500$ K and (b) space–charge effects within the gap. The first issue has been approached by using new materials with low work function (<2 eV), such as barium oxide (BaO), but the stability of such new materials at high temperature remains an issue. The problem of the space–charge effect is generally minimized by using three approaches: (a) neutralize the space–charge effects by introducing positive ions, such as cesium ions, into the vacuum gap; (b) reduce the gap spacing D (since $J_{CL} \propto D^{-2}$); and (c) employ a third electrode (gate or grid) to accelerate the electrons (since $J_{CL} \propto F^{3/2}$, where F is the electric field).

High efficiency TEC development remains an active topic,[329,330] which may provide significant potential for various applications, in particular, the solar thermionic space power technology.[331] Photon-enhanced thermionic emission (PETE) from semiconducting cathodes[332] is promising for increasing the emitted current density at relatively low cathode temperatures (500–1100 K). The field emission heat engine (FEHE) is another novel thermionic converter to directly convert heat into electricity with high efficiency.[333–335] However, particle-in-cell (PIC) simulations showed that the high emitted current density is still limited by space–charge effects, motivating the

proposal of Cs plasma for neutralization.[336] Using the hybrid concepts of TEC and PETE, near-field thermionic-thermophotovoltaic energy converters have been studied.[337,338] Due to the recent advances in new quantum materials, it was predicted that the classical RD law is no longer valid for 2D[169,170,173] and 3D[188] Dirac materials. In comparison to well-studied traditional materials-based TEC, Dirac materials-based TEC have been studied only recently.[339,340] This new direction will require better understanding of SCLC in such systems so that space–charge effects may be avoided in a micrometer-scale or smaller spacing.[189] Other effects such as gas-induced ions, finite particles, dynamical and multi-dimensional effects of SCLC discussed in this paper can be readily extended to future TEC design.

D. Multipactor

Multipactor discharge is an ac discharge in which a high frequency rf field creates an electron avalanche sustained through secondary electron emission from a metal or dielectric surface.[341–348] It threatens telecommunication systems, high-power microwave sources,[61,64,349,350] and accelerator structures. Under certain conditions, multipactor may dissipate power, degrade performance, increase system noise, cause degradation of the microwave components, and, in the worst scenario, lead to the complete destruction of the microwave circuits. In space-based communications, the restricted frequency spectrum and the cluttered satellite orbits require a single satellite or spacecraft to perform multiple functions which previously required several satellites. This necessitates complex multi-frequency operation for a much enlarged orbital capacity and mission. The required high-power RF payload significantly increases the threat of multipactor. As a result, multipactor discharge and breakdown received substantial attention in recent years.[351,352] Besides threatening the integration of microwave components, the degradation of the signal quality due to multipactor has become a major concern.[353–355]

The effects of multipactor on the quality of a complex signal propagating in a transmission line have been recently analyzed.[353] Multipactor under multifrequency operation[354,356–360] is shown to have different dynamics and susceptibility boundaries. Using a recently developed multiparticle Monte Carlo model with adaptive time steps,[359] it is found that the trajectory of multipactor electrons can be steered to migrate to certain directions for different configurations of two-frequency rf fields.[360] This can be of interest in applications such as local surface cleaning of a structure to reduce further susceptibility to multipactor or directing multipacting electrons to a specific desirable location in the geometry.[360,361] The generation of intermodulation products, higher harmonics, and the attempts to mitigate multipactor using non-sinusoidal waveforms have also been investigated.[354,355,362,363]

However, the effects of space charge are not adequately characterized in these recent efforts, though it is known that space charge effects play an important role in the time-dependent dynamics and the saturation mechanisms of mulitpactor. Previously, the space charge shielding effect on multipactor on a dielectric was analyzed to estimate the power deposition and saturation level.[344,346,364] The effects of desorption or background gas[348,365] on multipactor discharge and the transition from vacuum

multipactor to rf plasmas[366] were also studied. The secondary electron avalanche at electrically stressed insulator–vacuum interfaces was analyzed theoretically at SCL condition charge.[367] As space charge influences the trajectories of mulitpactor electrons, it would be necessary to examine its impact on the signal distortion of the multipactor and multicarrier operation, which are particularly important to space-based communication systems. The impact of SCLC in secondary electron emission,[367] especially from artificially roughened or micro- or nano-scale porous surfaces with suppressed SEY,[88,89,368–371] would be a new direction in better understanding the physics of the multipactor. For higher frequency operation, the size of the devices shrinks to mm or microscale,[372] multipactor discharge and their connection to the physics of SCLC diodes, as well as multipactor induced noises,[353–358] would represent new challenges for space communications and beyond.

VI. CONCLUSION

This Perspective article gives an overview of the fundamental physics of the space–charge limited current (SCLC), with focus on recent advances in the SCLC transport in nanodiodes of different media, including vacuum, air, liquids, and solids. We have discussed new developments on the understanding of SCLC phenomena when the size of the medium (diode) is reduced to sub-micrometer dimensions including using novel 2D materials, the dynamical and transient behaviors far from the steady-state condition, and multi-dimensional and higher-dimensional effects with transitions between different regimes with various emission mechanisms and material properties. We have identified unanswered questions in these areas. A few selected applications of SCLC in nanodiodes were also discussed.

Understanding steady-state SCLC in nanodiodes remains a critical direction for future research. While there have been extensive studies on quantum mechanical modeling of SCLC in nanoscale vacuum and dielectric tunneling gaps, the effects of collisional effects and material defects, and their possible impact on the electron emission processes requires significant future research. Recent SCLC studies in air gaps have led to a nexus theory that demonstrates the transition and linkage between electron emission mechanisms, gas breakdown, and SCLC transport in either vacuum (no collisions) or solid (with collisions). Future modeling efforts require consistent quantum mechanical modeling of these behaviors, especially when the size of the gaps reduces to the sub-micrometer scale. Experimental verification of the theory is also needed. SCLC in liquids is largely unexplored, which necessitates substantial future research in both theory and experiments. SCLC models in bulk solids would provide a useful tool to characterize the properties of complicated solids (e.g., mobility). SCLC in 2D Dirac materials shows distinctive behaviors due to the reduced dimensionality and the unique energy-momentum dispersion of the 2D materials. The study of SCLC in 2D materials and van der Waals heterostructures is still in its infancy and would open a new chapter on the physics of SCLC in the few-atom limit, which may be important for future 2D materials-based nanoelectronics. An important open question is whether the standard Sommerfeld transport theory is microscopically valid for 2D materials, where first-principle calculations, such as DFT-based simulations, may be needed to address the electron emission physics, in particular, the scaling of photoemission models for 2D materials remains unknown.

Compared to the steady-state condition, time-dependent effects of SCLC in nanodiodes are relatively less explored. In particular, discrete particle effects require significant attention, especially when the size of the gap reduces to the micro- or nano-scale, the number of electrons present in the gap can be very limited even under the SCL condition. Coulomb scattering will become important in such systems with limited particles. Space–charge forces and Coulomb blockade effects can induce rapid time-varying current injection in micro- and nanodiodes. Electrostatics and possible inductive beam loading effects may give rise to current variations with a period close to the transit time of electrons across the diode gap. Novel susceptibility to electromagnetic oscillation may be possible as surface fields couple emission physics to electromagnetic modes. The rapid development of ultrafast lasers has offered unprecedented opportunities to drive ultrashort pulse photoemission from nanotips and to trigger ultrafast electron transport in nanoscale gaps. The effects of SCLC in these setups, along with the effects of different medium, remain largely unexplored. Accurate theoretical modeling and simulations are needed to address these unanswered questions regarding time-dependent SCLC.

Multi-dimensional and higher-dimensional effects become increasingly important when the gap size of the diodes decreases. This is especially so when the gap size becomes comparable to the scale of the electrodes, surface, or interface structures either by design or due to imperfections (e.g., roughness). The validity of macroscopic 2D and 3D Child–Langmuir law requires further examination in diodes with microscopic emitters. There have been ongoing studies of developing new methods to characterize the multi-dimensional and higher-dimensional physics, including variational calculus, conformal mapping, and fractional models of CL law, FN law, and MG law. These studies require significant extensions to apply to more sophisticated geometries of practical importance. Recent studies on inhomogeneous cathodes of varying work function have demonstrated the outstanding theoretical problem of smooth transition from thermionic emission to SCLC in Miram curves. It would be important to extend such studies in nanodiodes for different emission mechanisms. By combining the higher-dimensional models (including fractional models) of SCLC and accounting for the effects of surface or interface imperfection, together with the nonuniform current injection due to electrical contact geometries, one may be able to develop consistent higher-dimensional SCLC models to study current injection at material interfaces across different regimes. Such models are aided for simple scaling laws in order to avoid expensive computational resources.

As scaling laws of SCLC represent the fundamental constraints imposed by the Maxwell equations, they govern the operations of countless applications and devices involving diodes. The emerging nanodiodes and nano-transistors using nanoscale vacuum or air gaps as conducting channels have demonstrated superior properties with significantly higher switching speed compared to conventional solid-state devices. Microplasma transistors have shown promise for operating under extreme environments of high temperature and in the presence of ionizing radiation. SCLC studies would further push the operational limits of these devices to higher current and

higher speed. Understanding of SCLC in thermionic energy converters and field emission heat engine along with novel emitters based on 2D or 3D Dirac materials would help increase their efficiency and optimize their future design. As the key saturation mechanisms for multipactor, developing multipactor mitigation strategies with SCLC physics would become important for space-based communication systems. The physics of SCLC in nanodiodes will play a critical role in numerous applications and may even ultimately dictate some of the devices' operation and performance.

ACKNOWLEDGMENTS

DATA AVAILABILITY

The data that support the findings of this study are available from the corresponding author upon reasonable request.

REFERENCES

[1]C. D. Child, "Discharge from hot CaO," Phys. Rev. Ser. I 32, 492 (1911).
[2]I. Langmuir, "The effect of space charge and residual gases on thermionic currents in high vacuum," Phys. Rev. 2, 450 (1913).
[3]N. F. Mott and R. W. Gurney, Electronic Processes in Ionic Crystals (Oxford University Press, New York, 1940).
[4]M. A. Lampert and P. Mark, Current Injection in Solids (Academic Press, New York, 1970).
[5]R. J. Umstattd, C. G. Carr, C. L. Frenzen, J. W. Luginsland, and Y. Y. Lau, Am. J. Phys. 73, 160 (2005).
[6]Y. B. Zhu, P. Zhang, A. Valfells, L. K. Ang, and Y. Y. Lau, "Novel scaling laws for the Langmuir-Blodgett solutions in cylindrical and spherical diodes," Phys. Rev. Lett. 110, 265007 (2013).
[7]Y. B. Zhu and L. K. Ang, "Analytical re-derivation of space charge limited current in solids using capacitor model," J. Appl. Phys. 110, 094514 (2011).
[8]J. W. Luginsland, Y. Y. Lau, and R. M. Gilgenbach, "Two-dimensional Child-Langmuir law," Phys. Rev. Lett. 77, 4668 (1996).
[9]Y. Y. Lau, "Simple theory for the two-dimensional Child-Langmuir law," Phys. Rev. Lett. 87, 278301 (2001).
[10]J. W. Luginsland, Y. Y. Lau, R. J. Umstattd, and J. J. Watrous, "Beyond the Child–Langmuir law: A review of recent results on multidimensional space-charge-limited flow," Phys. Plasmas 9, 2371 (2002).
[11]W. S. Koh, L. K. Ang, and T. J. T. Kwan, "Three-dimensional Child–Langmuir law for uniform hot electron emission," Phys. Plasmas 12, 053107 (2005).
[12]R. J. Umstattd and J. W. Luginsland, "Two-dimensional space-charge-limited emission: Beam-edge characteristics and applications," Phys. Rev. Lett. 87, 145002 (2001).
[13]Y. B. Zhu and L. K. Ang, "Space charge limited current emission for a sharp tip," Phys. Plasmas 22, 052106 (2015).
[14]K. Torfason, A. Valfells, and A. Manolescu, "Molecular dynamics simulations of field emission from a prolate spheroidal tip," Phys. Plasmas 23, 123119 (2016).
[15]F. Hegeler, M. Friedman, M. C. Myers, J. D. Sethian, and S. B. Swanekamp, "Reduction of edge emission in electron beam diodes," Phys. Plasmas 9, 4309 (2002).
[16]M. D. Haworth, K. L. Cartwright, J. W. Luginsland, D. A. Shiffler, and R. J. Umstattd, "Improved electrostatic design for MILO cathodes," IEEE Trans. Plasma Sci. 30, 992 (2002).
[17]Y. Y. Lau, D. Chernin, D. G. Colombant, and P.-T. Ho, "Quantum extension of Child-Langmuir law," Phys. Rev. Lett. 66, 1446 (1991).
[18]L. K. Ang, T. J. T. Kwan, and Y. Y. Lau, "New scaling of Child-Langmuir law in the quantum regime," Phys. Rev. Lett. 91, 208303 (2003).
[19]L. K. Ang, Y. Y. Lau, and T. J. T. Kwan, "Simple derivation of quantum scaling in Child-Langmuir law," IEEE Trans. Plasma Sci. 32, 410 (2004).
[20]S. Bhattacharjee, A. Vartak, and V. Mukherjee, "Experimental study of space-charge-limited flows in a nanogap," Appl. Phys. Lett. 92, 191503 (2008).
[21]S. Bhattacharjee and T. Chowdhury, "Experimental investigation of transition from Fowler–Nordheim field emission to space-charge-limited flows in a nanogap," Appl. Phys. Lett. 95, 061501 (2009).
[22]L. K. Ang and P. Zhang, "Ultrashort-pulse Child-Langmuir law in the quantum and relativistic regimes," Phys. Rev. Lett. 98, 164802 (2007).
[23]W. S. Koh and L. K. Ang, "Transition of field emission to space-charge-limited emission in a nanogap," Appl. Phys. Lett. 89, 183107 (2006).
[24]W. S. Koh and L. K. Ang, "Quantum model of space-charge-limited field emission in a nanogap," Nanotechnology 19, 235402 (2008).
[25]L. K. Ang, W. S. Koh, Y. Y. Lau, and T. J. T. Kwan, "Space-charge-limited flows in the quantum regime," Phys. Plasmas 13, 056701 (2006).
[26]P. Zhang, "Scaling for quantum tunneling current in nano- and subnano-scale plasmonic junctions," Sci. Rep. 5, 9826 (2015).
[27]P. Zhang and Y. Y. Lau, "Ultrafast and nanoscale diodes," J. Plasma Phys. 82, 595820505 (2016).
[28]S. Banerjee and P. Zhang, "A generalized self-consistent model for quantum tunneling current in dissimilar metal-insulator-metal junction," AIP Adv. 9, 085302 (2019).
[29]J. W. Luginsland, S. McGee, and Y. Y. Lau, "Virtual cathode formation due to electromagnetic transients," IEEE Trans. Plasma Sci. 26, 901 (1998).
[30]J. W. Luginsland, M. J. Arman, and Y. Y. Lau, "High-power transit-time oscillator: Onset of oscillation and saturation," Phys. Plasmas 4, 4404 (1997).
[31]Á. Valfells, D. W. Feldman, M. Virgo, P. G. O'Shea, and Y. Y. Lau, "Effects of pulse-length and emitter area on virtual cathode formation in electron guns," Phys. Plasmas 9, 2377 (2002).
[32]A. Pedersen, A. Manolescu, and Á. Valfells, "Space-charge modulation in vacuum microdiodes at THz frequencies," Phys. Rev. Lett. 104, 175002 (2010).
[33]P. Jonsson, M. Ilkov, A. Manolescu, A. Pedersen, and A. Valfells, "Tunability of the terahertz space-charge modulation in a vacuum microdiode," Phys. Plasmas 20, 023107 (2013).
[34]M. Ilkov, K. Torfason, A. Manolescu, and Á. Valfells, "Terahertz pulsed photo-generated current in microdiodes at room temperature," Appl. Phys. Lett. 107, 203508 (2015).
[35]M. E. Griswold, N. J. Fisch, and J. S. Wurtele, "An upper bound to time-averaged space-charge limited diode currents," Phys. Plasmas 17, 114503 (2010).
[36]M. E. Griswold, N. J. Fisch, and J. S. Wurtele, "Amended conjecture on an upper bound to time-dependent space-charge limited current," Phys. Plasmas 19, 024502 (2012).
[37]R. E. Caflisch and M. S. Rosin, "Beyond the Child-Langmuir limit," Phys. Rev. E 85, 056408 (2012).
[38]Y. Zhu and L. K. Ang, "Child–Langmuir law in the Coulomb blockade regime," Appl. Phys. Lett. 98, 051502 (2011).
[39]S. H. Chen, L. C. Tai, Y. L. Liu, L. K. Ang, and W. S. Koh, "Two-dimensional electromagnetic Child–Langmuir law of a short-pulse electron flow," Phys. Plasmas 18, 023105 (2011).

[40]A. Rose, "Space-charge-limited currents in solids," Phys. Rev. 97, 1538 (1955).

[41]M. A. Lampert, "Simplified theory of space-charge-limited currents in an insulator with traps," Phys. Rev. 103, 1648 (1956).

[42]A. M. Goodman and A. Rose, "Double extraction of uniformly generated electron-hole pairs from insulators with noninjecting contacts," J. Appl. Phys. 42, 2823 (1971).

[43]V. D. Mihailetchi, J. Wildeman, and P. W. M. Blom, "Space-charge limited photocurrent," Phys. Rev. Lett. 94, 126602 (2005).

[44]M. S. Shur, "Ballistic transport in a semiconductor with collisions," IEEE Trans. Electron Devices 28, 1120 (1981).

[45]W. Chandra, L. K. Ang, K. L. Pey, and C. M. Ng, "Two-dimensional analytical Mott-Gurney law for a trap-filled solid," Appl. Phys. Lett. 90, 153505 (2007).

[46]W. Chandra, L. K. Ang, and W. S. Koh, "Two-dimensional model of space charge limited electron injection into a diode with Schottky contact," J. Phys. D: Appl. Phys. 42, 055504 (2009).

[47]A. A. Talin, F. Léonard, B. S. Swartzentruber, X. Wang, and S. D. Hersee, "Unusually strong space-charge-limited current in thin wires," Phys. Rev. Lett. 101, 076802 (2008).

[48]W. Chandra and L. K. Ang, "Space charge limited current in a gap combined of free space and solid," Appl. Phys. Lett. 96, 183501 (2010).

[49]D. B. Go and A. Venkattraman, "Microscale gas breakdown: Ion-enhanced field emission and the modified Paschen's curve," J. Phys. D: Appl. Phys. 47, 503001 (2014).

[50]Y. Fu, P. Zhang, J. P. Verboncoeur, and X. Wang, "Electrical breakdown from macro to micro/nano scales: A tutorial and a review of the state of the art," Plasma Res. Express 2, 013001 (2020).

[51]A. L. Garner, A. M. Loveless, J. N. Dahal, and A. Venkattraman, "A tutorial on theoretical and computational techniques for gas breakdown in microscale gaps," IEEE Trans. Plasma Sci. 48, 808 (2020).

[52]F. Paschen, "Ueber die zum Funkenübergang in Luft, Wasserstoff und Kohlensäure bei verschiedenen Drucken erforderliche Potentialdifferenz," Ann. Phys. 273, 69 (1889).

[53]Y. P. Raizer, Gas Discharge Physics (Springer-Verlag, Berlin, 1991).

[54]A. Venkattraman and A. A. Alexeenko, "Scaling law for direct current field emission-driven microscale gas breakdown," Phys. Plasmas 19, 123515 (2012).

[55]Y. Y. Lau, Y. Liu, and R. K. Parker, "Electron emission: From the Fowler–Nordheim relation to the Child–Langmuir law," Phys. Plasmas 1, 2082 (1994).

[56]A. M. Darr, A. M. Loveless, and A. L. Garner, "Unification of field emission and space charge limited emission with collisions," Appl. Phys. Lett. 114, 014103 (2019).

[57]A. L. Garner, G. Meng, Y. Fu, A. M. Loveless, R. S. Brayfield II, and A. M. Darr, "Transitions between electron emission and gas breakdown mechanisms across length and pressure scales," J. Appl. Phys. 128, 210903 (2020).

[58]S. D. Dynako, A. M. Darr, and A. L. Garner, "Incorporating resistance into the transition from field emission to space charge limited emission with collisions," IEEE J. Electron Devices Soc. 7, 650 (2019).

[59]A. M. Darr, C. R. Darr, and A. L. Garner, "Theoretical assessment of transitions across thermionic, field, and space-charge-limited emission," Phys. Rev. Res. 2, 033137 (2020).

[60]High-Power Microwave Sources and Technologies, 1st ed., edited by R. J. Barker, and E. Schamiloglu (Wiley/IEEE Press, New York, 2001).

[61]J. H. Booske, "Plasma physics and related challenges of millimeter-wave-to-terahertz and high power microwave generation," Phys. Plasmas 15, 055502 (2008).

[62]R. J. Barker, N. C. Luhmann, J. H. Booske, and G. S. Nusinovich, Modern Microwave and Millimeter Wave Power Electronics (IEEE Press, Piscataway, NJ, 2004).

[63]J. W. Luginsland, T. Antonsen, J. P. Verboncoeur, R. W. Lemke, L. Ludeking, P. Mardahl, A. T. Lin, Y. Y. Lau, and J. D. Blahovec, High-Power Microw. Sources Technol., edited by E. Schamiloglu, and R. J. Bark (Wiley/IEEE Press, New York, 2001), p. 376.

[64]D. Shiffler, T. K. Statum, T. W. Hussey, O. Zhou, and P. Mardahl, Modern Microwave and Millimeter-Wave Power Electronics (IEEE Press, Piscataway, NJ, 2005), p. 691.

[65]P. Wong, P. Zhang, and J. Luginsland, "Recent theory of traveling-wave tubes: A tutorial-review," Plasma Res. Express 2, 023001 (2020).

[66]M. Franzi, R. Gilgenbach, Y. Y. Lau, B. Hoff, G. Greening, and P. Zhang, "Passive mode control in the recirculating planar magnetron," Phys. Plasmas 20, 033108 (2013).

[67]B. Hoff, W. Tang, R. Seviour, and P. Zhang, "Guest editorial The eighteenth special issue on high-power microwave and millimeter-wave generation," IEEE Trans. Plasma Sci. 48, 1858 (2020).

[68]H. T. Nicolai, M. Kuik, G. a, H. Wetzelaer, B. de Boer, C. Campbell, C. Risko, J. L. Brédas, and P. W. M. Blom, "Unification of trap-limited electron transport in semiconducting polymers," Nat. Mater. 11, 882 (2012).

[69]M. Sajedi Alvar, P. W. M. Blom, and G.-J. A. H. Wetzelaer, "Space-charge-limited electron and hole currents in hybrid organic-inorganic perovskites," Nat. Commun. 11, 4023 (2020).

[70]P. Zhang, A. Valfells, L. K. Ang, J. W. Luginsland, and Y. Y. Lau, "100 years of the physics of diodes," Appl. Phys. Rev. 4, 011304 (2017).

[71]D. Gall, "Electron mean free path in elemental metals," J. Appl. Phys. 119, 085101 (2016).

[72]B. Qiu, Z. Tian, A. Vallabhaneni, B. Liao, J. M. Mendoza, O. D. Restrepo, X. Ruan, and G. Chen, "First-principles simulation of electron mean-free-path spectra and thermoelectric properties in silicon," Europhys. Lett. 109, 57006 (2015).

[73]C.-W. Lee, Y. Ikematsu, and D. Shindo, "Measurement of mean free paths for inelastic electron scattering of Si and SiO_2," J. Electron Microsc. 51, 143 (2002).

[74]J. G. Simmons, "Conduction in thin dielectric films," J. Phys. D: Appl. Phys. 4, 613 (1971).

[75]J. G. Simmons, "Generalized formula for the electric tunnel effect between similar electrodes separated by a thin insulating film," J. Appl. Phys. 34, 1793 (1963).

[76]J. G. Simmons, "Electric tunnel effect between dissimilar electrodes separated by a thin insulating film," J. Appl. Phys. 34, 2581 (1963).

[77]X. Xiong, Y. Zhou, Y. Luo, X. Li, M. Bosman, L. K. Ang, P. Zhang, and L. Wu, "Plasmon-enhanced resonant photoemission using atomically thick dielectric coatings," ACS Nano 14, 8806 (2020).

[78]F. Antoulinakis, D. Chernin, P. Zhang, and Y. Y. Lau, "Effects of temperature dependence of electrical and thermal conductivities on the joule heating of a one dimensional conductor," J. Appl. Phys. 120, 135105 (2016).

[79]P. Zhang, J. Park, S. B. Fairchild, N. P. Lockwood, Y. Y. Lau, J. Ferguson, and T. Back, "Temperature comparison of looped and vertical carbon nanotube fibers during field emission," Appl. Sci. 8, 1175 (2018).

[80]J. Lin, P. Y. Wong, P. Yang, Y. Y. Lau, W. Tang, and P. Zhang, "Electric field distribution and current emission in a miniaturized geometrical diode," J. Appl. Phys. 121, 244301 (2017).

[81]Y. Fu, P. Zhang, and J. P. Verboncoeur, "Gas breakdown in atmospheric pressure microgaps with a surface protrusion on the cathode," Appl. Phys. Lett. 112, 254102 (2018).

[82]J. R. Harris, K. L. Jensen, J. J. Petillo, S. Maestas, W. Tang, and D. A. Shiffler, "Practical considerations in the modeling of field emitter arrays with line charge distributions," J. Appl. Phys. 121, 203303 (2017).

[83]P. Zhang, S. B. Fairchild, T. C. Back, and Y. Luo, "Field emission from carbon nanotube fibers in varying anode-cathode gap with the consideration of contact resistance," AIP Adv. 7, 125203 (2017).

[84]S. B. Fairchild, P. Zhang, J. Park, T. C. Back, D. Marincel, Z. Huang, and M. Pasquali, "Carbon nanotube fiber field emission array cathodes," IEEE Trans. Plasma Sci. 47, 2032 (2019).

[85]W. Tang, D. Shiffler, and K. L. Cartwright, "Analysis of electric field screening by the proximity of two knife-edge field emitters," J. Appl. Phys. 110, 034905 (2011).

[86]S. S. Baturin, T. Nikhar, and S. V. Baryshev, "Field electron emission induced glow discharge in a nanodiamond vacuum diode," J. Phys. D: Appl. Phys. 52, 325301 (2019).

[87]T. Schuelke and T. A. Grotjohn, "Diamond polishing," Diam. Relat. Mater. 32, 17 (2013).

[88]A. Iqbal, J. Ludwick, S. Fairchild, M. Cahay, D. Gortat, M. Sparkes, W. O'Neill, T. C. Back, and P. Zhang, "Empirical modeling and Monte Carlo simulation of secondary electron yield reduction of laser drilled microporous gold surfaces," J. Vac. Sci. Technol. B **38**, 013801 (2019).

[89]J. Ludwick, A. Iqbal, D. Gortat, J. D. Cook, M. Cahay, P. Zhang, T. C. Back, S. Fairchild, M. Sparkes, and W. O'Neill, "Angular dependence of secondary electron yield from microporous gold surfaces," J. Vac. Sci. Technol. B **38**, 054001 (2020).

[90]S. Banerjee, J. Luginsland, and P. Zhang, "A two dimensional tunneling resistance transmission line model for nanoscale parallel electrical contacts," Sci. Rep. **9**, 14484 (2019).

[91]S. Banerjee, L. Cao, Y. S. Ang, L. K. Ang, and P. Zhang, "Reducing contact resistance in two-dimensional-material-based electrical contacts by roughness engineering," Phys. Rev. Appl. **13**, 064021 (2020).

[92]S. Banerjee, P. Y. Wong, and P. Zhang, "Contact resistance and current crowding in tunneling type circular nano-contacts," J. Phys. D: Appl. Phys. **53**, 355301 (2020).

[93]P. Zhang, S. Banerjee, and J. Luginsland, U.S. Patent 10,755,975B2 (25 August 2020).

[94]P. Zhang, D. M. H. Hung, and Y. Y. Lau, "Current flow in a 3-terminal thin film contact with dissimilar materials and general geometric aspect ratios," J. Phys. D: Appl. Phys. **46**, 065502 (2013).

[95]P. Zhang, Y. Y. Lau, and R. M. Gilgenbach, "Minimization of thin film contact resistance," Appl. Phys. Lett. **97**, 204103 (2010).

[96]P. Zhang and D. M. H. Hung, "An analytical model for ballistic diode based on asymmetric geometry," J. Appl. Phys. **115**, 204908 (2014).

[97]J. P. Custer, J. D. Low, D. J. Hill, T. S. Teitsworth, J. D. Christesen, C. J. McKinney, J. R. McBride, M. A. Brooke, S. C. Warren, and J. F. Cahoon, "Ratcheting quasi-ballistic electrons in silicon geometric diodes at room temperature," Science **368**, 177 (2020).

[98]W. S. Boyle and P. Kisliuk, "Departure from Paschen's law of breakdown in gases," Phys. Rev. **97**, 255 (1955).

[99]A. M. Loveless and A. L. Garner, "A universal theory for gas breakdown from microscale to the classical Paschen law," Phys. Plasmas **24**, 113522 (2017).

[100]G. Meng, X. Gao, A. M. Loveless, C. Dong, D. Zhang, K. Wang, B. Zhu, Y. Cheng, and A. L. Garner, "Demonstration of field emission driven microscale gas breakdown for pulsed voltages using in-situ optical imaging," Phys. Plasmas **25**, 082116 (2018).

[101]A. M. Loveless, G. Meng, Q. Ying, F. Wu, K. Wang, Y. Cheng, and A. L. Garner, "The transition to Paschen's law for microscale gas breakdown at subatmospheric pressure," Sci. Rep. **9**, 5669 (2019).

[102]K. H. Schoenbach and K. Becker, "20 years of microplasma research: A status report," Eur. Phys. J. D **70**, 29 (2016).

[103]T. Gotszalk, *MEMS Field Models and Optimal Design* (Springer, Cham, 2020), pp. 115–141.

[104]R. Bogue, "MEMS sensors: Past, present and future," Sens. Rev. **27**, 7 (2007).

[105]C. B. Ru, Y. H. Ye, C. L. Wang, P. Zhu, R. Q. Shen, Y. Hu, and L. Z. Wu, "Design and fabrication of MEMS-based solid propellant microthrusters array," Appl. Mech. Mater. **490 and 491**, 1042–1046 (2014).

[106]H. Gensler, R. Sheybani, P.-Y. Li, R. L. Mann, and E. Meng, "An implantable MEMS micropump system for drug delivery in small animals," Biomed. Microdevices **14**, 483 (2012).

[107]L. Boodhoo, L. Crudgington, H. M. H. Chong, Y. Tsuchiya, Z. Moktadir, T. Hasegawa, and H. Mizuta, "Fabrication and characterisation of suspended narrow silicon nanowire channels for low-power nano-electro-mechanical (NEM) switch applications," Microelectron. Eng. **145**, 66 (2015).

[108]D. Lev, R. M. Myers, K. M. Lemmer, J. Kolbeck, H. Koizumi, and K. Polzin, "The technological and commercial expansion of electric propulsion," Acta Astronaut. **159**, 213 (2019).

[109]O. O. Baranov, S. Xu, L. Xu, S. Huang, J. W. M. Lim, U. Cvelbar, I. Levchenko, and K. Bazaka, "Miniaturized plasma sources: Can technological solutions help electric micropropulsion?," IEEE Trans. Plasma Sci. **46**, 230 (2018).

[110]G. Shivkumar, L. Qiao, and A. A. Alexeenko, "Plasma-flow interactions in field-emission discharges with applications in microcombustion," J. Phys. D: Appl. Phys. **52**, 384001 (2019).

[111]T. Takahashi, D. Mori, T. Kawanabe, Y. Takao, K. Eriguchi, and K. Ono, "Microplasma thruster powered by X-band microwaves," J. Appl. Phys. **125**, 083301 (2019).

[112]W.-H. Chiang, D. Mariotti, R. M. Sankaran, J. G. Eden, and K. (Ken) Ostrikov, "Microplasmas for advanced materials and devices," Adv. Mater. **32**, 1905508 (2020).

[113]M. G. Kong, G. Kroesen, G. Morfill, T. Nosenko, T. Shimizu, J. van Dijk, and J. L. Zimmermann, "Plasma medicine: An introductory review," New J. Phys. **11**, 115012 (2009).

[114]M. Laroussi, "Low-temperature plasma jet for biomedical applications: A review," IEEE Trans. Plasma Sci. **43**, 703 (2015).

[115]M. S. Benilov, "The Child–Langmuir law and analytical theory of collisionless to collision-dominated sheaths," Plasma Sources Sci. Technol. **18**, 014005 (2008).

[116]A. M. Loveless, A. M. Darr, R. S. B. Ii, J. R. Malayter, S. A. Lang, and A. L. Garner, "Nanoscale feature implications on electron emission and gas breakdown," Trans. Am. Nucl. Soc. **121**, 399 (2019).

[117]S. A. Lang, A. M. Darr, and A. L. Garner, "Theoretical analysis of the transition from field emission to space-charge-limited emission in liquids and gases," J. Appl. Phys. **128**, 185104 (2020).

[118]J. K. Bragg, A. H. Sharbaugh, and R. W. Crowe, "Cathode effects in the dielectric breakdown of liquids," J. Appl. Phys. **25**, 382 (1954).

[119]B. Halpern and R. Gomer, "Field emission in liquids," J. Chem. Phys. **43**, 1069 (1965).

[120]B. Halpern and R. Gomer, "Field emission in liquids," J. Chem. Phys. **51**, 1031 (1969).

[121]B. Halpern and R. Gomer, "Field ionization in liquids," J. Chem. Phys. **51**, 1048 (1969).

[122]A. H. Sharbaugh, J. C. Devins, and S. J. Rzad, "Progress in the field of electric breakdown in dielectric liquids," IEEE Trans. Electr. Insul. **EI-13**, 249 (1978).

[123]W. F. Schmidt, "Electronic conduction processes in dielectric liquids," IEEE Trans. Electr. Insul. **EI-19**, 389 (1984).

[124]P. V. E. McClintock, "Field emission in liquid helium," Phys. Lett. A **29**, 453 (1969).

[125]J. Qian, R. P. Joshi, J. Kolb, K. H. Schoenbach, J. Dickens, A. Neuber, M. Butcher, M. Cevallos, H. Krompholz, E. Schamiloglu, and J. Gaudet, "Microbubble-based model analysis of liquid breakdown initiation by a submicrosecond pulse," J. Appl. Phys. **97**, 113304 (2005).

[126]N. S. Phan, W. Wei, B. Beaumont, N. Bouman, S. M. Clayton, S. A. Currie, T. M. Ito, J. C. Ramsey, and G. M. Seidel, "A study of DC electrical breakdown in liquid helium through analysis of the empirical breakdown field distributions," arXiv:2011.08844 (2020).

[127]M. Auger, A. Blatter, A. Ereditato, D. Goeldi, S. Janos, I. Kreslo, M. Luethi, C. R. von Rohr, T. Strauss, and M. S. Weber, "On the electric breakdown in liquid argon at centimeter scale," J. Instrum. **11**, P03017 (2016).

[128]J. E. Foster, "Plasma-based water purification: Challenges and prospects for the future," Phys. Plasmas **24**, 055501 (2017).

[129]L. Xu, A. L. Garner, B. Tao, and K. M. Keener, "Microbial inactivation and quality changes in orange juice treated by high voltage atmospheric cold plasma," Food Bioprocess Technol. **10**, 1778 (2017).

[130]C. P. Bankston, L. H. Back, E. Y. Kwack, and A. J. Kelly, "Experimental investigation of electrostatic dispersion and combustion of diesel fuel jets," J. Eng. Gas Turbines Power **110**, 361 (1988).

[131]S. S.-S. Huang and G. R. Freeman, "Density and temperature effects on electron mobilities in gaseous, critical and liquid n-hexane, cyclohexane, and cyclopentane," Can. J. Chem. **56**, 2388 (1978).

[132]T. Wada and G. R. Freeman, "Density and temperature effects on electron mobilities in gaseous butene isomers," Can. J. Chem. **57**, 2716 (1979).

[133]F. M. Jacobsen, N. Gee, and G. R. Freeman, "Electron mobility in liquid krypton as function of density, temperature, and electric field strength," Phys. Rev. A **34**, 2329 (1986).

[134]F. M. Jacobsen, N. Gee, and G. R. Freeman, "Electron mobility in krypton dense gas as functions of electric field strength, temperature, and density," J. Chem. Phys. **91**, 6943 (1989).

[135]P. Mark and W. Helfrich, "Space-charge-limited currents in organic crystals," J. Appl. Phys. **33**, 205 (1962).

[136]C. Tanase, P. W. M. Blom, and D. M. de Leeuw, "Origin of the enhanced space-charge-limited current in poly(p-phenylene vinylene)," Phys. Rev. B **70**, 193202 (2004).

[137]P. W. M. Blom, C. Tanase, D. M. de Leeuw, and R. Coehoorn, "Thickness scaling of the space-charge-limited current in poly(p-phenylene vinylene)," Appl. Phys. Lett. **86**, 092105 (2005).

[138]P. W. M. Blom, M. J. M. de Jong, and M. G. van Munster, "Electric-field and temperature dependence of the hole mobility in poly(p-phenylene vinylene)," Phys. Rev. B **55**, R656 (1997).

[139]D. M. Pai, "Transient photoconductivity in poly(N-vinylcarbazole)," J. Chem. Phys. **52**, 2285 (1970).

[140]T. N. Ng, W. R. Silveira, and J. A. Marohn, "Dependence of charge injection on temperature, electric field, and energetic disorder in an organic semiconductor," Phys. Rev. Lett. **98**, 066101 (2007).

[141]X.-G. Zhang and S. T. Pantelides, "Theory of space charge limited currents," Phys. Rev. Lett. **108**, 266602 (2012).

[142]C. Tanase, E. J. Meijer, P. W. M. Blom, and D. M. de Leeuw, "Unification of the hole transport in polymeric field-effect transistors and light-emitting diodes," Phys. Rev. Lett. **91**, 216601 (2003).

[143]W. F. Pasveer, J. Cottaar, C. Tanase, R. Coehoorn, P. A. Bobbert, P. W. M. Blom, D. M. de Leeuw, and M. A. J. Michels, "Unified description of charge-carrier mobilities in disordered semiconducting polymers," Phys. Rev. Lett. **94**, 206601 (2005).

[144]H. T. Nicolai, M. M. Mandoc, and P. W. M. Blom, "Electron traps in semiconducting polymers: Exponential versus Gaussian trap distribution," Phys. Rev. B **83**, 195204 (2011).

[145]D. Abbaszadeh, A. Kunz, G. a, H. Wetzelaer, J. J. Michels, N. I. Crăciun, K. Koynov, I. Lieberwirth, and P. W. M. Blom, "Elimination of charge carrier trapping in diluted semiconductors," Nat. Mater. **15**, 628 (2016).

[146]V. Coropceanu, J. Cornil, D. A. da Silva Filho, Y. Olivier, R. Silbey, and J.-L. Brédas, "Charge transport in organic semiconductors," Chem. Rev. **107**, 926 (2007).

[147]H. F. Haneef, A. M. Zeidell, and O. D. Jurchescu, "Charge carrier traps in organic semiconductors: A review on the underlying physics and impact on electronic devices," J. Mater. Chem. C **8**, 759 (2020).

[148]R. W. Smith and A. Rose, "Space-charge-limited currents in single crystals of cadmium sulfide," Phys. Rev. **97**, 1531 (1955).

[149]M. C. J. M. Vissenberg and M. Matters, "Theory of the field-effect mobility in amorphous organic transistors," Phys. Rev. B **57**, 12964 (1998).

[150]P. N. Murgatroyd, "Theory of space-charge-limited current enhanced by Frenkel effect," J. Phys. D: Appl. Phys. **3**, 151 (1970).

[151]S. V. Novikov, D. H. Dunlap, V. M. Kenkre, P. E. Parris, and A. V. Vannikov, "Essential role of correlations in governing charge transport in disordered organic materials," Phys. Rev. Lett. **81**, 4472 (1998).

[152]R. Coehoorn, W. F. Pasveer, P. A. Bobbert, and M. A. J. Michels, "Charge-carrier concentration dependence of the hopping mobility in organic materials with Gaussian disorder," Phys. Rev. B **72**, 155206 (2005).

[153]M. Bouhassoune, S. L. M. van Mensfoort, P. A. Bobbert, and R. Coehoorn, "Carrier-density and field-dependent charge-carrier mobility in organic semiconductors with correlated Gaussian disorder," Org. Electron. **10**, 437 (2009).

[154]A. K. Geim and K. S. Novoselov, "The rise of graphene," Nat. Mater. **6**, 183 (2007).

[155]M. Z. Hasan and C. L. Kane, "*Colloquium*: Topological insulators," Rev. Mod. Phys. **82**, 3045 (2010).

[156]X.-L. Qi and S.-C. Zhang, "Topological insulators and superconductors," Rev. Mod. Phys. **83**, 1057 (2011).

[157]K. F. Mak, C. Lee, J. Hone, J. Shan, and T. F. Heinz, "Atomically thin MoS_2: A new direct-gap semiconductor," Phys. Rev. Lett. **105**, 136805 (2010).

[158]D. Akinwande, C. Huyghebaert, C.-H. Wang, M. I. Serna, S. Goossens, L.-J. Li, H.-S. P. Wong, and F. H. L. Koppens, "Graphene and two-dimensional materials for silicon technology," Nature **573**, 507 (2019).

[159]G. W. Semenoff, "Condensed-matter simulation of a three-dimensional anomaly," Phys. Rev. Lett. **53**, 2449 (1984).

[160]R. M. Ribeiro and N. M. R. Peres, "Stability of boron nitride bilayers: Ground-state energies, interlayer distances, and tight-binding description," Phys. Rev. B **83**, 235312 (2011).

[161]Y. S. Ang, M. Zubair, and L. K. Ang, "Relativistic space-charge-limited current for massive Dirac fermions," Phys. Rev. B **95**, 165409 (2017).

[162]S. Ghatak and A. Ghosh, "Observation of trap-assisted space charge limited conductivity in short channel MoS_2 transistor," Appl. Phys. Lett. **103**, 122103 (2013).

[163]F. Mahvash, E. Paradis, D. Drouin, T. Szkopek, and M. Siaj, "Space-charge limited transport in large-area monolayer hexagonal boron nitride," Nano Lett. **15**, 2263 (2015).

[164]Y. S. Shin, K. Lee, Y. R. Kim, H. Lee, I. M. Lee, W. T. Kang, B. H. Lee, K. Kim, J. Heo, S. Park, Y. H. Lee, and W. J. Yu, "Mobility engineering in vertical field effect transistors based on Van der waals heterostructures," Adv. Mater. **30**, 1704435 (2018).

[165]A. K. Geim and I. V. Grigorieva, "Van der Waals heterostructures," Nature **499**, 419 (2013).

[166]Y. Liu, N. O. Weiss, X. Duan, H.-C. Cheng, Y. Huang, and X. Duan, "Van der Waals heterostructures and devices," Nat. Rev. Mater. **1**, 16042 (2016).

[167]L. Cao, G. Zhou, Q. Wu, S. A. Yang, H. Y. Yang, Y. S. Ang, and L. K. Ang, "Electrical contact between an ultrathin topological Dirac semimetal and a two-dimensional material," Phys. Rev. Appl. **13**, 054030 (2020).

[168]L. Cao, Y. S. Ang, Q. Wu, and L. K. Ang, "Janus PtSSe and graphene heterostructure with tunable Schottky barrier," Appl. Phys. Lett. **115**, 241601 (2019).

[169]Y. S. Ang, S.-J. Liang, and L. K. Ang, "Theoretical modeling of electron emission from graphene," MRS Bull. **42**, 505 (2017).

[170]Y. S. Ang, H. Y. Yang, and L. K. Ang, "Universal scaling laws in Schottky heterostructures based on two-dimensional materials," Phys. Rev. Lett. **121**, 056802 (2018).

[171]Y. S. Ang, Y. Chen, C. Tan, and L. K. Ang, "Generalized high-energy thermionic electron injection at graphene interface," Phys. Rev. Appl. **12**, 014057 (2019).

[172]Y. S. Ang and L. K. Ang, "Current-temperature scaling for a Schottky interface with nonparabolic energy dispersion," Phys. Rev. Appl. **6**, 034013 (2016).

[173]S.-J. Liang and L. K. Ang, "Electron thermionic emission from graphene and a thermionic energy converter," Phys. Rev. Appl. **3**, 014002 (2015).

[174]O. W. Richardson, "LI. Some applications of the electron theory of matter," Lond. Edinb. Dublin Philos. Mag. J. Sci. **23**, 594 (1912).

[175]S. Dushman, "Electron emission from metals as a function of temperature," Phys. Rev. **21**, 623 (1923).

[176]F. Zhu, X. Lin, P. Liu, K. Jiang, Y. Wei, Y. Wu, J. Wang, and S. Fan, "Heating graphene to incandescence and the measurement of its work function by the thermionic emission method," Nano Res. **7**, 553 (2015).

[177]M. Javadi, A. Noroozi, and Y. Abdi, "Kinetics of charge carriers across a graphene-silicon Schottky junction," Phys. Rev. Appl. **14**, 064048 (2020).

[178]A. Anwar, B. Nabet, J. Culp, and F. Castro, "Effects of electron confinement on thermionic emission current in a modulation doped heterostructure," J. Appl. Phys. **85**, 2663 (1999).

[179]Y. S. Ang, C. H. Lee, and L. K. Ang, "Universal scaling and signatures of nodal structures in electron tunneling from two-dimensional semimetals," arXiv:2003.14004 (2020).

[180]E. L. Murphy, R. H. Good, and T. Emission, "Field emission, and the transition region," Phys. Rev. **102**, 1464 (1956).

[181]K. L. Jensen, *Introduction to the Physics of Electron Emission*, 1st ed. (Wiley, Hoboken, NJ, 2017).

[182]Z.-S. Wu, S. Pei, W. Ren, D. Tang, L. Gao, B. Liu, F. Li, C. Liu, and H.-M. Cheng, "Field emission of single-layer graphene films prepared by electrophoretic deposition," Adv. Mater. **21**, 1756 (2009).

[183]X. Wei, Y. Bando, and D. Golberg, "Electron emission from individual graphene nanoribbons driven by internal electric field," ACS Nano **6**, 705 (2012).

[184]S. Kumar, G. S. Duesberg, R. Pratap, and S. Raghavan, "Graphene field emission devices," Appl. Phys. Lett. **105**, 103107 (2014).

[185]G. Wu, X. Wei, Z. Zhang, Q. Chen, and L. Peng, "A graphene-based vacuum transistor with a high ON/OFF current ratio," Adv. Funct. Mater. **25**, 5972 (2015).

[186]G. Wu, X. Wei, S. Gao, Q. Chen, and L. Peng, "Tunable graphene microemitters with fast temporal response and controllable electron emission," Nat. Commun. **7**, 11513 (2016).

[187]A. Di Bartolomeo, F. Giubileo, L. Iemmo, F. Romeo, S. Russo, S. Unal, M. Passacantando, V. Grossi, and A. M. Cucolo, "Leakage and field emission in side-gate graphene field effect transistors," Appl. Phys. Lett. **109**, 023510 (2016).

[188]S. Huang, M. Sanderson, Y. Zhang, and C. Zhang, "High efficiency and non-Richardson thermionics in three dimensional Dirac materials," Appl. Phys. Lett. **111**, 183902 (2017).

[189]Y. S. Ang, M. Zubair, K. J. A. Ooi, and L. K. Ang, "Generalized Fowler-Nordheim field-induced vertical electron emission model for two-dimensional materials," arXiv:1711.05898 (2017).

[190]K. L. Jensen, "General formulation of thermal, field, and photoinduced electron emission," J. Appl. Phys. **102**, 024911 (2007).

[191]C. Li, K. Chen, M. Guan, X. Wang, X. Zhou, F. Zhai, J. Dai, Z. Li, Z. Sun, S. Meng, K. Liu, and Q. Dai, "Extreme nonlinear strong-field photoemission from carbon nanotubes," Nat. Commun. **10**, 4891 (2019).

[192]S. K. Ghosh and A. K. Dhara, "Density-functional theory of many-electron systems subjected to time-dependent electric and magnetic fields," Phys. Rev. A **38**, 1149 (1988).

[193]C. A. Ullrich and Z. Yang, "A brief compendium of time-dependent density functional theory," Braz. J. Phys. **44**, 154 (2014).

[194]N. T. Maitra, "Perspective: Fundamental aspects of time-dependent density functional theory," J. Chem. Phys. **144**, 220901 (2016).

[195]K. Torfason, A. Valfells, and A. Manolescu, "Molecular dynamics simulations of field emission from a planar nanodiode," Phys. Plasmas **22**, 033109 (2015).

[196]K. L. Jensen, D. A. Shiffler, I. M. Rittersdorf, J. L. Lebowitz, J. R. Harris, Y. Y. Lau, J. J. Petillo, W. Tang, and J. W. Luginsland, "Discrete space charge affected field emission: Flat and hemisphere emitters," J. Appl. Phys. **117**, 194902 (2015).

[197]K. L. Jensen, J. J. Petillo, E. J. Montgomery, Z. Pan, D. W. Feldman, P. G. O'Shea, N. A. Moody, M. Cahay, J. E. Yater, and J. L. Shaw, "Application of a general electron emission equation to surface nonuniformity and current density variation," J. Vac. Sci. Technol. B **26**, 831 (2008).

[198]A. Sitek, K. Torfason, A. Manolescu, and A. Valfells, "Space-charge effects in field-assisted thermionic emission from nonuniform cathodes," Phys. Rev. Appl. **15**, 014040 (2020).

[199]K. Torfason, A. Sitek, A. Manolescu, and A. Valfells, Dynamics of a field emitted beam from a microscopic inhomogeneous cathode, IEEE Trans. Electron Devices (unpublished).

[200]D. Chernin, Y. Y. Lau, J. J. Petillo, S. Ovtchinnikov, D. Chen, A. Jassem, R. Jacobs, D. Morgan, and J. H. Booske, "Effect of nonuniform emission on Miram curves," IEEE Trans. Plasma Sci. **48**, 146 (2020).

[201]Y. M. Blanter and M. Büttiker, "Shot noise in mesoscopic conductors," Phys. Rep. **336**, 1 (2000).

[202]L. Wu, L. K. Ang, and W. S. Koh, "Theory of shot noise in high-current space-charge-limited field emission," Phys. Rev. B **77**, 115351 (2008).

[203]W. Chandra, L. K. Ang, and X. Zhou, "Shot noise reduction of space charge limited electron injection through a Schottky contact for a GaN diode," Phys. Rev. B **81**, 125321 (2010).

[204]P. Zhang and Y. Y. Lau, "Ultrafast strong-field photoelectron emission from biased metal surfaces: Exact solution to time-dependent Schrödinger equation," Sci. Rep. **6**, 19894 (2016).

[205]Y. Luo and P. Zhang, "Ultrafast strong-field photoelectron emission due to two-color laser fields," Phys. Rev. B **98**, 165442 (2018).

[206]B. H. Son, D. J. Park, and Y. H. Ahn, "Electronic control of ultrafast field emission in carbon nanotube gaps," Appl. Phys. Lett. **115**, 163102 (2019).

[207]J. Vogelsang, J. Robin, B. J. Nagy, P. Dombi, D. Rosenkranz, M. Schiek, P. Groß, and C. Lienau, "Ultrafast electron emission from a sharp metal nanotaper driven by adiabatic nanofocusing of surface plasmons," Nano Lett. **15**, 4685 (2015).

[208]A. Feist, N. Bach, N. Rubiano da Silva, T. Danz, M. Möller, K. E. Priebe, T. Domröse, J. G. Gatzmann, S. Rost, J. Schauss, S. Strauch, R. Bormann, M. Sivis, S. Schäfer, and C. Ropers, "Ultrafast transmission electron microscopy using a laser-driven field emitter: Femtosecond resolution with a high coherence electron beam," Ultramicroscopy **176**, 63 (2017).

[209]P. Dombi, Z. Pápa, J. Vogelsang, S. V. Yalunin, M. Sivis, G. Herink, S. Schäfer, P. Groß, C. Ropers, and C. Lienau, "Strong-field nano-optics," Rev. Mod. Phys. **92**, 025003 (2020).

[210]C. K. Birdsall and W. B. Bridges, "Space-charge instabilities in electron diodes and plasma converters," J. Appl. Phys. **32**, 2611 (1961).

[211]C. K. Birdsall and W. B. Bridges, *Electron Dynamics of Diode Regions*, 1st ed. (Academic Press, New York, 1966).

[212]K. Schindl, "Space charge," CERN Report 2006-002, 2006.

[213]M. Ferrario, M. Migliorati, and L. Palumbo, "Space charge effects," arXiv:1601.05214 (2014).

[214]C. K. Birdsall and A. B. Langdon, *Plasma Physics via Computer Simulation*, 1st ed. (CRC Press, New York, 2004).

[215]J. P. Verboncoeur, "Particle simulation of plasmas: Review and advances," Plasma Phys. Controlled Fusion **47**, A231 (2005).

[216]M. Siman-Tov, J. G. Leopold, and Y. E. Krasik, "A self-oscillating electron beam experiment," Phys. Plasmas **27**, 023104 (2020).

[217]E. G. Souza, A. Endler, F. B. Rizzato, and R. Pakter, "Adiabatic-nonadiabatic transition in warm long-range interacting systems: The transport of intense inhomogeneous beams," Phys. Rev. Lett. **109**, 075003 (2012).

[218]A. H. Zewail and J. M. Thomas, *4D Electron Microscopy: Imaging in Space and Time*, 1st ed. (Imperial College Press, London, 2009).

[219]S. Sun, X. Sun, D. Bartles, E. Wozniak, J. Williams, P. Zhang, and C.-Y. Ruan, "Direct imaging of plasma waves using ultrafast electron microscopy," Struct. Dyn. **7**, 064301 (2020).

[220]W. A. Barletta, J. Bisognano, J. N. Corlett, P. Emma, Z. Huang, K.-J. Kim, R. Lindberg, J. B. Murphy, G. R. Neil, D. C. Nguyen, C. Pellegrini, R. A. Rimmer, F. Sannibale, G. Stupakov, R. P. Walker, and A. A. Zholents, "Free electron lasers: Present status and future challenges," Nucl. Instrum. Methods Phys. Res., Sect. A **618**, 69 (2010).

[221]B. Piglosiewicz, S. Schmidt, D. J. Park, J. Vogelsang, P. Groß, C. Manzoni, P. Farinello, G. Cerullo, and C. Lienau, "Carrier-envelope phase effects on the strong-field photoemission of electrons from metallic nanostructures," Nat. Photonics **8**, 37 (2014).

[222]F. Rezaeifar, R. Ahsan, Q. Lin, H. U. Chae, and R. Kapadia, "Hot-electron emission processes in waveguide-integrated graphene," Nat. Photonics **13**, 843 (2019).

[223]H. U. Chae, R. Ahsan, Q. Lin, D. Sarkar, F. Rezaeifar, S. B. Cronin, and R. Kapadia, "High quantum efficiency hot electron electrochemistry," Nano Lett. **19**, 6227 (2019).

[224]E. Forati, T. J. Dill, A. R. Tao, and D. Sievenpiper, "Photoemission-based microelectronic devices," Nat. Commun. **7**, 13399 (2016).

[225]S. Piltan and D. Sievenpiper, "Plasmonic nano-arrays for enhanced photoemission and photodetection," J. Opt. Soc. Am. B **35**, 208 (2018).

[226]L. V. Keldysh, "Ionization in the field of a strong electromagnetic wave," Sov. Phys. JETP **20**, 1307 (1965).

[227]R. H. Fowler and L. Nordheim, "Electron emission in intense electric fields," Proc. R. Soc. Lond. Ser. A **119**, 173 (1928).

[228]X. Zhou, S. He, G. Liu, L. Zhao, L. Yu, and W. Zhang, "New developments in laser-based photoemission spectroscopy and its scientific applications: A key issues review," Rep. Prog. Phys. **81**, 062101 (2018).

[229]S. Zhou, K. Chen, M. T. Cole, Z. Li, J. Chen, C. Li, and Q. Dai, "Ultrafast field-emission electron sources based on nanomaterials," Adv. Mater. **31**, 1805845 (2019).

[230]D. J. Park and Y. H. Ahn, "Ultrashort field emission in metallic nanostructures and low-dimensional carbon materials," Adv. Phys. X **5**, 1726207 (2020).

[231]R. Bormann, M. Gulde, A. Weismann, S. V. Yalunin, and C. Ropers, "Tip-enhanced strong-field photoemission," Phys. Rev. Lett. **105**, 147601 (2010).

[232]H. Yanagisawa, M. Hengsberger, D. Leuenberger, M. Klöckner, C. Hafner, T. Greber, and J. Osterwalder, "Energy distribution curves of ultrafast laser-induced field emission and their implications for electron dynamics," Phys. Rev. Lett. **107**, 087601 (2011).

[233]S. V. Yalunin, M. Gulde, and C. Ropers, "Strong-field photoemission from surfaces: Theoretical approaches," Phys. Rev. B **84**, 195426 (2011).

[234]L. Wu and L. K. Ang, "Nonequilibrium model of ultrafast laser-induced electron photofield emission from a dc-biased metallic surface," Phys. Rev. B **78**, 224112 (2008).

[235]M. Pant and L. K. Ang, "Ultrafast laser-induced electron emission from multiphoton to optical tunneling," Phys. Rev. B **86**, 045423 (2012).

[236]M. Pant and L. K. Ang, "Time-dependent quantum tunneling and nonequilibrium heating model for the generalized Einstein photoelectric effect," Phys. Rev. B **88**, 195434 (2013).

[237]M. Krüger, C. Lemell, G. Wachter, J. Burgdörfer, and P. Hommelhoff, "Attosecond physics phenomena at nanometric tips," J. Phys. B At. Mol. Opt. Phys. **51**, 172001 (2018).

[238]M. Reutzel, A. Li, and H. Petek, "Coherent two-dimensional multiphoton photoelectron spectroscopy of metal surfaces," Phys. Rev. X **9**, 011044 (2019).

[239]Y. Zhou and P. Zhang, "A quantum model for photoemission from metal surfaces and its comparison with the three-step model and Fowler–DuBridge model," J. Appl. Phys. **127**, 164903 (2020).

[240]Y. Luo and P. Zhang, "Analysis of two-color laser-induced electron emission from a biased metal surface using an exact quantum mechanical solution," Phys. Rev. Appl. **12**, 044056 (2019).

[241]Y. Luo, J. Luginsland, and P. Zhang, "Interference modulation of photoemission from biased metal cathodes driven by two lasers of the same frequency," AIP Adv. **10**, 075301 (2020).

[242]M. Förster, T. Paschen, M. Krüger, C. Lemell, G. Wachter, F. Libisch, T. Madlener, J. Burgdörfer, and P. Hommelhoff, "Two-color coherent control of femtosecond above-threshold photoemission from a tungsten nanotip," Phys. Rev. Lett. **117**, 217601 (2016).

[243]Y. Zhou and P. Zhang, "Theory of field emission from dielectric coated surfaces," Phys. Rev. Res. **2**, 043439 (2020).

[244]Y. Luo, Y. Zhou, and P. Zhang, "Few-cycle optical-field induced photoemission from biased surfaces: An exact quantum theory," Phys. Rev. B **103**, 085410 (2021).

[245]P. Zimmermann, A. Hötger, N. Fernandez, A. Nolinder, K. Müller, J. J. Finley, and A. W. Holleitner, "Toward plasmonic tunnel gaps for nanoscale photoemission currents by on-chip laser ablation," Nano Lett. **19**, 1172 (2019).

[246]T. Higuchi, L. Maisenbacher, A. Liehl, P. Dombi, and P. Hommelhoff, "A nanoscale vacuum-tube diode triggered by few-cycle laser pulses," Appl. Phys. Lett. **106**, 051109 (2015).

[247]M. Ludwig, G. Aguirregabiria, F. Ritzkowsky, T. Rybka, D. C. Marinica, J. Aizpurua, A. G. Borisov, A. Leitenstorfer, and D. Brida, "Sub-femtosecond electron transport in a nanoscale gap," Nat. Phys. **16**, 341 (2020).

[248]M. Ludwig, A. K. Kazansky, G. Aguirregabiria, D. C. Marinica, M. Falk, A. Leitenstorfer, D. Brida, J. Aizpurua, and A. G. Borisov, "Active control of ultrafast electron dynamics in plasmonic gaps using an applied bias," Phys. Rev. B **101**, 241412 (2020).

[249]J. Heimerl, T. Higuchi, M. Ammon, M. A. Schneider, and P. Hommelhoff, "Gap-size dependence of optical near fields in a variable nanoscale two-tip junction," Phys. Rev. B **101**, 125403 (2020).

[250]T. L. Cocker, V. Jelic, M. Gupta, S. J. Molesky, J. A. J. Burgess, G. D. L. Reyes, L. V. Titova, Y. Y. Tsui, M. R. Freeman, and F. A. Hegmann, "An ultrafast terahertz scanning tunnelling microscope," Nat. Photonics **7**, 620 (2013).

[251]K. Yoshioka, I. Katayama, Y. Minami, M. Kitajima, S. Yoshida, H. Shigekawa, and J. Takeda, "Real-space coherent manipulation of electrons in a single tunnel junction by single-cycle terahertz electric fields," Nat. Photonics **10**, 762 (2016).

[252]A. Rokhlenko, "Child–Langmuir flow with periodically varying anode voltage," Phys. Plasmas **22**, 022126 (2015).

[253]M. E. Griswold and N. J. Fisch, "Maximum time-dependent space-charge limited diode currents," Phys. Plasmas **23**, 014502 (2016).

[254]G. Meng, Q. Ying, A. M. Loveless, F. Wu, K. Wang, Y. Fu, A. L. Garner, and Y. Cheng, "Spatio-temporal dynamics of pulsed gas breakdown in microgaps," Phys. Plasmas **26**, 014506 (2019).

[255]M. U. Lee, J. Lee, J. K. Lee, and G. S. Yun, "Extended scaling and Paschen law for micro-sized radiofrequency plasma breakdown," Plasma Sources Sci. Technol. **26**, 034003 (2017).

[256]M. U. Lee, J. Lee, G. S. Yun, and J. K. Lee, "Scalings and universality for high-frequency excited high-pressure argon microplasma," Eur. Phys. J. D **71**, 94 (2017).

[257]I. Langmuir and K. B. Blodgett, "Currents limited by space charge between coaxial cylinders," Phys. Rev. **22**, 347 (1923).

[258]I. Langmuir and K. B. Blodgett, "Currents limited by space charge between concentric spheres," Phys. Rev. **24**, 49 (1924).

[259]J. B. Gunnarsson, K. Torfason, A. Manolescu, and Á. Valfells, "Space-charge limited current from a finite emitter in nano- and microdiodes," IEEE Trans. Electron Devices **68**, 342 (2021).

[260]R. Torres-Cordoba and E. Martinez-Garcia, "Analytical and exact solutions of the spherical and cylindrical diodes of Langmuir–Blodgett law," Phys. Plasmas **24**, 103113 (2017).

[261]C. B. Wheeler, "The approach to space charge limited current flow between coaxial cylinders," J. Phys. A: Math. Gen. **8**, 555 (1975).

[262]C. B. Wheeler, "The approach to space charge limited current flow between concentric spheres," J. Phys. A: Math. Gen. **8**, 1159 (1975).

[263]C. B. Wheeler, "Space charge limited current flow between coaxial cylinders at potentials up to 15 MV," J. Phys. A: Math. Gen. **10**, 631 (1977).

[264]C. B. Wheeler, "Space charge limited current flow between concentric spheres at potentials up to 15 MV," J. Phys. A: Math. Gen. **10**, 1645 (1977).

[265]L. Gold, "Transit time and space-charge for the cylindrical diode," J. Electron. Control **3**, 567 (1957).

[266]X. Chen, J. Dickens, L. L. Hatfield, E.-H. Choi, and M. Kristiansen, "Approximate analytical solutions for the space-charge-limited current in one-dimensional and two-dimensional cylindrical diodes," Phys. Plasmas **11**, 3278 (2004).

[267]D. Anderson and M. Desaix, "Introduction to direct variational and moment methods and an application to the Child–Langmuir law," Eur. J. Phys. **36**, 065032 (2015).

[268]A. Rokhlenko, "Minimum current principle and variational method in theory of space charge limited flow," J. Appl. Phys. **118**, 153303 (2015).

[269]G. Singh, R. Kumar, and D. Biswas, "Enhanced space charge limited current for curved electron emitters," Phys. Plasmas **27**, 104501 (2020).

[270]A. M. Darr and A. L. Garner, "A coordinate system invariant formulation for space-charge limited current in vacuum," Appl. Phys. Lett. **115**, 054101 (2019).

[271]N. R. Sree Harsha and A. L. Garner, in *Proceedings of IEEE International Vacuum Electronics Conference, Monterrey, CA* (IEEE Press, New York, 2020), pp. 395–396.

[272]G. B. Walker, "Congruent space charge flow," Proc. Phys. Soc. Sect. B **63**, 1017 (1950).

[273]H. F. Ivey, "Space charge limited currents between inclined plane electrodes. Approximate solutions," J. Appl. Phys. **24**, 227 (1953).

[274]H. F. Ivey, "Approximate solutions of the space-charge problem for some unusual electrode geometries," J. Appl. Phys. **24**, 1466 (1953).

[275]R. Miller, Y. Y. Lau, and J. H. Booske, "Electric field distribution on knife-edge field emitters," Appl. Phys. Lett. **91**, 074105 (2007).

[276]N. R. Sree Harsha and A. L. Garner, IEEE Trans. Electron Devices **68**, 264 (2020).

[277]A. Rokhlenko and J. L. Lebowitz, "Space-charge-limited 2D electron flow between two flat electrodes in a strong magnetic field," Phys. Rev. Lett. **91**, 085002 (2003).

[278]M. Zubair and L. K. Ang, "Fractional-dimensional Child-Langmuir law for a rough cathode," Phys. Plasmas **23**, 072118 (2016).

[279]L. Martina, V. Nassisi, G. Raganato, and A. Pedone, "Electron beam propagation in a space-charge regime," Nucl. Instrum. Methods Phys. Res., Sect. B **188**, 272 (2002).

[280]M. Zubair, Y. S. Ang, and L. K. Ang, "Fractional Fowler–Nordheim law for field emission from rough surface with nonparabolic energy dispersion," IEEE Trans. Electron Devices **65**, 2089 (2018).

[281]M. Zubair, Y. S. Ang, and L. K. Ang, "Thickness dependence of space-charge-limited current in spatially disordered organic semiconductors," IEEE Trans. Electron Devices **65**, 3421 (2018).

[282]S. Ahmad, M. Zubair, O. Jalil, M. Q. Mehmood, U. Younis, X. Liu, K. W. Ang, and L. K. Ang, "Generalized scaling law for exciton binding energy in two-dimensional materials," Phys. Rev. Appl. **13**, 064062 (2020).

[283]M. Zubair, Y. S. Ang, K. J. A. Ooi, and L. K. Ang, "Fractional Fresnel coefficients for optical absorption in femtosecond laser-induced rough metal surfaces," J. Appl. Phys. **124**, 163101 (2018).

[284]A. A. Grinberg, S. Luryi, M. R. Pinto, and N. L. Schryer, "Space-charge-limited current in a film," IEEE Trans. Electron Devices **36**, 1162 (1989).

[285]D. K. Schroder, *Semiconductor Material and Device Characterization*, 3rd ed. (Wiley–IEEE Press, Piscataway, NJ, 2015).

[286]P. Zhang and Y. Y. Lau, "An exact field solution of contact resistance and comparison with the transmission line model," Appl. Phys. Lett. **104**, 204102 (2014).

[287]R. Holm, *Electric Contacts: Theory and Application*, 4th ed. (Springer, Berlin, 1967).

[288]P. Zhang and Y. Y. Lau, "Scaling laws for electrical contact resistance with dissimilar materials," J. Appl. Phys. **108**, 044914 (2010).

[289]P. Zhang, Y. Y. Lau, and R. M. Gilgenbach, "Thin film contact resistance with dissimilar materials," J. Appl. Phys. **109**, 124910 (2011).

[290]P. Zhang, Y. Y. Lau, and R. S. Timsit, "On the spreading resistance of thin-film contacts," IEEE Trans. Electron Devices **59**, 1936 (2012).

[291]P. Zhang, Y. Y. Lau, and R. M. Gilgenbach, "Analysis of current crowding in thin film contacts from exact field solution," J. Phys. D: Appl. Phys. **48**, 475501 (2015).

[292]M. R. Gomez, D. M. French, W. Tang, P. Zhang, Y. Y. Lau, and R. M. Gilgenbach, "Experimental validation of a higher dimensional theory of electrical contact resistance," Appl. Phys. Lett. **95**, 072103 (2009).

[293]P. Yang, S. Banerjee, W. Kuang, Y. Ding, Q. Ma, and P. Zhang, "Current crowding and spreading resistance of electrical contacts with irregular contact edges," J. Phys. D: Appl. Phys. **53**, 485303 (2020).

[294]P. Zhang, Q. Gu, Y. Y. Lau, and Y. Fainman, "Constriction resistance and current crowding in electrically pumped semiconductor nanolasers with the presence of undercut and sidewall tilt," IEEE J. Quantum Electron. **52**, 2000207 (2016).

[295]P. Zhang and Y. Y. Lau, "Constriction resistance and current crowding in vertical thin film contact," IEEE J. Electron Devices Soc. **1**, 83 (2013).

[296]A. Lozovoi, H. Jayakumar, D. Daw, A. Lakra, and C. A. Meriles, "Probing metastable space-charge potentials in a wide band gap semiconductor," Phys. Rev. Lett. **125**, 256602 (2020).

[297]M. Ilkov, K. Torfason, A. Manolescu, and Á. Valfells, "Synchronization in arrays of vacuum microdiodes," IEEE Trans. Electron Devices **62**, 200 (2015).

[298]H. V. Haraldsson, K. Torfason, A. Manolescu, and Á. Valfells, "Molecular dynamics simulations of mutual space-charge effect between planar field emitters," IEEE Trans. Plasma Sci. **48**, 1967 (2020).

[299]R. T. Longo, *International Electron Devices Meeting* (1980), pp. 467–470.

[300]R. Vaughan, "A synthesis of the Longo and Eng cathode emission models," IEEE Trans. Electron Devices **33**, 1925 (1986).

[301]R. T. Longo, "Physics of thermionic dispenser cathode aging," J. Appl. Phys. **94**, 6966 (2003).

[302]A. Jassem, D. Chernin, J. J. Petillo *et al.*, "Analysis of anode current from a thermionic cathode with a two-dimensional work function distribution," IEEE Trans. Plasma Sci. (published online, 2020).

[303]D. Chen, R. Jacobs, D. Morgan, and J. Booske, "Modeling thermionic electron emission from heterogeneous surfaces," arXiv:2010.01053 (2020).

[304]B. R. Stoner and J. T. Glass, "Nanoelectronics: Nothing is like a vacuum," Nat. Nanotechnol. **7**, 485 (2012).

[305]J.-W. Han and M. Meyyappan, "Introducing the vacuum transistor: A device made of nothing," IEEE Spectr. **35**, 31 (2014).

[306]J.-W. Han, D.-I. Moon, and M. Meyyappan, "Nanoscale vacuum channel transistor," Nano Lett. **17**, 2146 (2017).

[307]S. Nirantar, T. Ahmed, G. Ren, P. Gutruf, C. Xu, M. Bhaskaran, S. Walia, and S. Sriram, "Metal–air transistors: Semiconductor-free field-emission air-channel nanoelectronics," Nano Lett. **18**, 7478 (2018).

[308]H. F. Gray, G. J. Campisi, and R. F. Greene, *International Electron Devices Meeting* (IEEE Press, New York, 1986), pp. 776–779.

[309]J.-W. Han, J. S. Oh, and M. Meyyappan, "Vacuum nanoelectronics: Back to the future?—Gate insulated nanoscale vacuum channel transistor," Appl. Phys. Lett. **100**, 213505 (2012).

[310]S. Srisonphan, Y. S. Jung, and H. K. Kim, "Metal-oxide-semiconductor field-effect transistor with a vacuum channel," Nat. Nanotechnol. **7**, 504 (2012).

[311]S. G. Jennings, "The mean free path in air," J. Aerosol Sci. **19**, 159 (1988).

[312]W. M. Jones, D. Lukin, and A. Scherer, "Practical nanoscale field emission devices for integrated circuits," Appl. Phys. Lett. **110**, 263101 (2017).

[313]M. Samizadeh Nikoo, A. Jafari, N. Perera, M. Zhu, G. Santoruvo, and E. Matioli, "Nanoplasma-enabled picosecond switches for ultrafast electronics," Nature **579**, 534 (2020).

[314]J. Xu, Z. Gu, W. Yang, Q. Wang, and X. Zhang, "Graphene-based nanoscale vacuum channel transistor," Nanoscale Res. Lett. **13**, 311 (2018).

[315]M. Kim and H. K. Kim, "Ultraviolet-enhanced photodetection in a graphene/SiO$_2$/Si capacitor structure with a vacuum channel," J. Appl. Phys. **118**, 104504 (2015).

[316]S. Srisonphan, "Hybrid graphene–Si-based nanoscale vacuum field effect phototransistors," ACS Photonics **3**, 1799 (2016).

[317]F. Giubileo, L. Iemmo, M. Passacantando, F. Urban, G. Luongo, L. Sun, G. Amato, E. Enrico, and A. Di Bartolomeo, "Effect of electron irradiation on the transport and field emission properties of few-layer MoS$_2$ field-effect transistors," J. Phys. Chem. C **123**, 1454 (2019).

[318]F. Urban, M. Passacantando, F. Giubileo, L. Iemmo, and A. Di Bartolomeo, "Transport and field emission properties of MoS$_2$ bilayers," Nanomaterials **8**, 151 (2018).

[319]H. D. Nguyen, J. S. Kang, M. Li, and Y. Hu, "High-performance field emission based on nanostructured tin selenide for nanoscale vacuum transistors," Nanoscale **11**, 3129 (2019).

[320]I.-C. Benea-Chelmus, F. F. Settembrini, G. Scalari, and J. Faist, "Electric field correlation measurements on the electromagnetic vacuum state," Nature **568**, 202 (2019).

[321]T. L. Cocker, D. Peller, P. Yu, J. Repp, and R. Huber, "Tracking the ultrafast motion of a single molecule by femtosecond orbital imaging," Nature **539**, 263 (2016).

[322]S. Koenig, D. Lopez-Diaz, J. Antes, F. Boes, R. Henneberger, A. Leuther, A. Tessmann, R. Schmogrow, D. Hillerkuss, R. Palmer, T. Zwick, C. Koos, W. Freude, O. Ambacher, J. Leuthold, and I. Kallfass, "Wireless sub-THz communication system with high data rate," Nat. Photonics **7**, 977 (2013).

[323]K. K. Berggren, Q. Xia, K. Likharev, D. B. Strukov, H. Jiang, T. Mikolajick, D. Querlioz, M. Salinga, J. Erickson, S. Pi, F. Xiong, P. Lin, C. Li, S. Xiong, B. Hoskins, M. Daniels, A. Madhavan, J. Liddle, J. McClelland, Y. Yang, J. Rupp, S. Nonnenmann, N. Gong, K.-T. (Tim) Cheng, M. A. L. Montaño, A. A. Talin, A. Salleo, B. J. Shastri, T. F. de Lima, A. N. Tait, Y. Shen, H. Meng, C. Roques-Carmes, Z. Cheng, H. Bhaskaran, D. Jariwala, H. Wang, K. Segall, J. Shainline, J. J. Yang, K. Roy, S. Datta, and A. Raychowdhury, "Roadmap on emerging hardware and technology for machine learning," Nanotechnology **32**, 012002 (2020).

[324]M. Tabib-Azar and P. Pai, "Microplasma field effect transistors," Micromachines **8**, 117 (2017).

[325]K.-F. Chen and J. G. Eden, "The plasma transistor: A microcavity plasma device coupled with a low voltage, controllable electron emitter," Appl. Phys. Lett. **93**, 161501 (2008).

[326]C. J. Wagner, P. A. Tchertchian, and J. G. Eden, "Coupling electron-hole and electron-ion plasmas: Realization of an npn plasma bipolar junction phototransistor," Appl. Phys. Lett. **97**, 134102 (2010).

[327]R. S. Brayfield, "Electrode effects on electron emission and Gas breakdown from nano to microscale," PhD thesis (Purdue University, 2020).

[328]G. N. Hatsopoulos E. P. Gyftopoulos, *Thermionic Energy Conversion—Vol. 2: Theory, Technology, and Application* (The MIT Press, 1979).

[329]K. A. Abdul Khalid, T. J. Leong, K. Mohamed, IEEE T. Electron Dev. 2016, 63, 6 2231.

[330]D. B. Go, J. R. Haase, J. George, J. Mannhart, R. Wanke, A. Nojeh, and R. Nemanich, "Thermionic energy conversion in the twenty-first century: Advances and opportunities for space and terrestrial applications," Front. Mech. Eng. **3**, 13 (2017).

[331]S. F. Adams, "Solar thermionic space power technology testing: A historical perspective," AIP Conf. Proc. **813**, 590 (2006).

[332]J. W. Schwede, I. Bargatin, D. C. Riley, B. E. Hardin, S. J. Rosenthal, Y. Sun, F. Schmitt, P. Pianetta, R. T. Howe, Z.-X. Shen, and N. A. Melosh, "Photon-enhanced thermionic emission for solar concentrator systems," Nat. Mater. **9**, 762 (2010).

[333]R. A. Hyde, J. T. Kare, N. P. Myhrvold, T. S. Pan, and L. L. Wood, Jr, U.S. patent 8,575,842 B2 (5 November 2013).

[334]T. Pan, H. Busta, R. Gorski, and B. Rozansky, in *27th International Vacuum Nanoelectronics Conference, IVNC 2014* (IEEE Press, New York, 2014), pp. 147–148.

[335]P. Zhang and T. Pan, "Exact analytical theory for inverse tunneling of free vacuum electrons into a solid," AIP Adv. **7**, 065307 (2017).

[336]T. Ito and M. A. Cappelli, "Optically pumped cesium plasma neutralization of space charge in photon-enhanced thermionic energy converters," Appl. Phys. Lett. **101**, 213901 (2012).

[337]A. Datas, "Hybrid thermionic-photovoltaic converter," Appl. Phys. Lett. **108**, 143503 (2016).

[338]T. Liao, X. Zhang, X. Chen, and J. Chen, "Near-field thermionic-thermophotovoltaic energy converters," J. Appl. Phys. **125**, 203103 (2019).

[339]X. Zhang, W. Peng, G. Su, S. Su, and J. Chen, "Thermionic energy conversion based on 3D Dirac semimetals," J. Phys. D: Appl. Phys. **51**, 405501 (2018).

[340]X. Zhang, Y. S. Ang, J.-Y. Du, J. Chen, and L. K. Ang, "Graphene-based thermionic-thermoradiative solar cells: Concept, efficiency limit, and optimum design," J. Cleaner Prod. **242**, 118444 (2020).

[341]J. R. M. Vaughan, "Multipactor," IEEE Trans. Electron Devices **35**, 1172 (1988).

[342]R. Kishek and Y. Y. Lau, "Interaction of multipactor discharge and rf circuit," Phys. Rev. Lett. **75**, 1218 (1995).

[343]R. Kishek and Y. Y. Lau, "Multipactor discharge on a dielectric," Phys. Rev. Lett. **80**, 193 (1998).

[344]L.-K. Ang, Y. Y. Lau, R. A. Kishek, and R. M. Gilgenbach, "Power deposited on a dielectric by multipactor," IEEE Trans. Plasma Sci. **26**, 290 (1998).

[345]R. A. Kishek, Y. Y. Lau, L. K. Ang, A. Valfells, and R. M. Gilgenbach, "Multipactor discharge on metals and dielectrics: Historical review and recent theories," Phys. Plasmas **5**, 2120 (1998).

[346]A. Valfells, J. P. Verboncoeur, and Y. Y. Lau, "Space-charge effects on multipactor on a dielectric," IEEE Trans. Plasma Sci. **28**, 529 (2000).

[347]A. Valfells, L. K. Ang, Y. Y. Lau, and R. M. Gilgenbach, "Effects of an external magnetic field, and of oblique radio-frequency electric fields on multipactor discharge on a dielectric," Phys. Plasmas **7**, 750 (2000).

[348]P. Zhang, Y. Y. Lau, M. Franzi, and R. M. Gilgenbach, "Multipactor susceptibility on a dielectric with a bias dc electric field and a background gas," Phys. Plasmas **18**, 053508 (2011).

[349]J. Benford, J. A. Swegle, and E. Schamiloglu, *High Power Microwaves*, 2nd ed. (Taylor and Francis, New York, 2007).

[350]B. W. Hoff, P. J. Mardahl, R. M. Gilgenbach, M. D. Haworth, D. M. French, Y. Y. Lau, and M. Franzi, "Microwave window breakdown experiments and simulations on the UM/L-3 relativistic magnetron," Rev. Sci. Instrum. **80**, 094702 (2009).

[351]F. Piro and Y. Brand, "PIM and multipactor considerations for future high-RF power space missions," in *8th European Conference on Antennas and Propagation, EuCAP 2014* (IEEE Press, New York, 2014).

[352]Special Sessions on Multipactor, I and II, *IEEE International Conference on Plasma Science, Denver, CO* (IEEE Press, New York, 2018).

[353]P. Y. Wong, Y. Y. Lau, P. Zhang, N. Jordan, R. M. Gilgenbach, and J. Verboncoeur, "The effects of multipactor on the quality of a complex signal propagating in a transmission line," Phys. Plasmas **26**, 112114 (2019).

[354]A. Iqbal, P. Y. Wong, J. P. Verboncoeur, and P. Zhang, "Frequency-domain analysis of single-surface multipactor discharge with single- and dual-tone RF electric fields," IEEE Trans. Plasma Sci. **48**, 1950 (2020).

[355]P. Y. Wong, P. Zhang, and J. P. Verboncoeur, "Harmonic generation in multipactor discharges," IEEE Trans. Plasma Sci. **48**, 1959 (2020).

[356]V. Semenov, A. Kryazhev, D. Anderson, and M. Lisak, "Multipactor suppression in amplitude modulated radio frequency fields," Phys. Plasmas **8**, 5034 (2001).

[357]S. Anza, M. Mattes, C. Vicente, J. Gil, D. Raboso, V. E. Boria, and B. Gimeno, "Multipactor theory for multicarrier signals," Phys. Plasmas **18**, 032105 (2011).

[358]A. Iqbal, J. Verboncoeur, and P. Zhang, "Multipactor susceptibility on a dielectric with two carrier frequencies," Phys. Plasmas **25**, 043501 (2018).

[359]A. Iqbal, J. Verboncoeur, and P. Zhang, "Temporal multiparticle Monte Carlo simulation of dual frequency single surface multipactor," Phys. Plasmas **26**, 024503 (2019).

[360]A. Iqbal, P. Y. Wong, D.-Q. Wen, S. Lin, J. Verboncoeur, and P. Zhang, "Time-dependent physics of single-surface multipactor discharge with two carrier frequencies," Phys. Rev. E **102**, 043201 (2020).

[361]S. A. Rice and J. P. Verboncoeur, "Migration of multipactor trajectories via higher-order mode perturbation," IEEE Trans. Plasma Sci. **45**, 1739 (2017).

[362]D.-Q. Wen, P. Zhang, Y. Fu, J. Krek, and J. P. Verboncoeur, "Temporal single-surface multipactor dynamics under obliquely incident linearly polarized electric field," Phys. Plasmas **26**, 123509 (2019).

[363]D.-Q. Wen, A. Iqbal, P. Zhang, and J. P. Verboncoeur, "Suppression of single-surface multipactor discharges due to non-sinusoidal transverse electric field," Phys. Plasmas **26**, 093503 (2019).

[364]H. C. Kim and J. P. Verboncoeur, "Time-dependent physics of a single-surface multipactor discharge," Phys. Plasmas **12**, 123504 (2005).

[365]C. Chang, G. Liu, C. Tang, C. Chen, S. Qiu, J. Fang, and Q. Hou, "The influence of desorption gas to high power microwave window multipactor," Phys. Plasmas **15**, 093508 (2008).

[366]H. C. Kim and J. P. Verboncoeur, "Transition of window breakdown from vacuum multipactor discharge to rf plasma," Phys. Plasmas **13**, 123506 (2006).

[367]K. D. Bergeron, "Theory of the secondary electron avalanche at electrically stressed insulator-vacuum interfaces," J. Appl. Phys. **48**, 3073 (1977).

[368]M. Ye, Y. N. He, S. G. Hu, R. Wang, T. C. Hu, J. Yang, and W. Z. Cui, "Suppression of secondary electron yield by micro-porous array structure," J. Appl. Phys. **113**, 074904 (2013).

[369]J. M. Sattler, R. A. Coutu, R. Lake, T. Laurvick, T. Back, and S. Fairchild, "Modeling micro-porous surfaces for secondary electron emission control to suppress multipactor," J. Appl. Phys. **122**, 055304 (2017).

[370]C. Chang, G. Z. Liu, H. J. Huang, C. H. Chen, and J. Y. Fang, "Suppressing high-power microwave dielectric multipactor by the sawtooth surface," Phys. Plasmas **16**, 083501 (2009).

[371]C. Watts, M. Gilmore, and E. Schamiloglu, "Effects of laser surface modification on secondary electron emission of copper," IEEE Trans. Plasma Sci. **39**, 836 (2011).

[372]S. C. Schaub, M. A. Shapiro, and R. J. Temkin, "Measurement of dielectric multipactor thresholds at 110GHz," Phys. Rev. Lett. **123**, 175001 (2019).